Synthesis and Adsorption Properties of Large Pore Periodic Mesoporous Organosilicas

by

Na Hao

A Thesis Submitted in Fulfilment of the Requirements for the Degree of Doctor of Philosophy

Department of Chemical Engineering

Monash University, Clayton, Australia

February 2011

Abstract

Periodic mesoporous organosilicas (PMOs) are of scientific and technological interest because of their tunable pore structures as well as their tailored catalytic, sorption and gas storage properties. PMOs therefore present one of the most important families of organic-inorganic functional materials that are hybridized at molecular scale. The last few decades have witnessed extensive research efforts devoted to generating ordered PMOs with different mesostructures, pore sizes, and morphologies by template-directed assembly methods. In order to expand applications of PMOs into the above areas, especially sorption, it is highly desirable to develop porous materials with different compositions, adjustable pore systems and novel properties in versatile synthesis methods.

The current research project is mainly concerned with this issue. In this thesis, we focused on the synthesis of PMOs with different components, structures and pore sizes by using nonionic surfactants as the structure-directing agents. Such materials obtained showed efficient adsorption capacities in different systems, and are of great theoretical and practical significance with potential applications to adsorption.

The thesis is arranged as follows:

Chapters 1 and 2 provide an introduction to the field of mesoporous materials and a detailed literative review on past and present work related to synthesis and characterisation of PMOs. Chapter 3 details the experimental synthesis and characterisation methods employed in this project.

Chapter 4 presents the results from synthesis of large-pore phenyl-bridged PMOs. These materials were facilely synthesized by evaporation-induced self-assembly (EISA) of 1,4-bis(triethoxysily)benzene (BTEB) and triblock copolymer Pluronic F127 ($EO_{106}PO_{70}EO_{106}$) as a template under acid conditions combined with a mixed-solvothermal treatment. The hexagonal ordered PMOs exhibit large uniform mesopores of ~ 9.9 nm in diameter after calcination at 350 °C in a nitrogen atmosphere. N_2 adsorption/desorption isotherms reveal imperfect mesopore channels with high surface areas (up to 1150 $m^2 \cdot g^{-1}$) and thick pore walls (up to 7.7 nm). The mesopores can be expanded with a decrease of acidity, as well as an increase of Pluronic F127 content. A mixed-solvothermal treatment in N,N-dimethylformamide (DMF) and water at 100 °C was first used to improve the periodicity of the mesopore walls, as well as increase the wall thickness. The composites exhibit efficient

adsorption capacities (2.06 $mmol \cdot g^{-1}$) for benzene, suggesting a potential adsorbent for removal of volatile organic compounds.

Inorganic salts were recognized to play an important role in triggering the formation of highly ordered mesostructure. In Chapter 5, we present results from the preparation of well-ordered two-dimensional (2D) hexagonal PMOs with a high content of disulfide groups. These materials were successfully prepared by a simple metal-ion assisted amphiphilic surfactant templating process under strong acid conditions. Long-chain organic bridge silane, bis(triethoxysilylpropyl)disulfide (BTSPDS) was used as a precursor which was co-condensed with tetraethoxysilane (TEOS) to assemble with the triblock copolymer Pluronic P123 ($EO_{20}PO_{70}EO_{20}$) template and construct the mesostructured organic-inorganic frameworks. The content of disulfide functional groups as high as 20 % was incorporated into the framework. The ordered mesoporous DS-PMO materials obtained have relatively high Brunauer-Emmett-Teller (BET) surface area (~ 580 $m^2 \cdot g^{-1}$), large uniform pore size (up to 6.3 nm) and thick pore walls (thickness up to 7.1 nm), because of the long-chain disulfide bridges. The metal ions such as Zn^{2+} formed four-coordination with two sulfides of BTSPDS and ethylene oxide moieties of P123 template, which could enhance the interaction between "soft" long disulfide groups and P123 template, thus improving the mesostructural regularity correspondingly. The disulfide-bridged PMO materials exhibit excellent hydrothermal stability in boiling water for 5 days, probably due to the thick pore walls. Excellent adsorption efficiency (~ 716 $mg \cdot g^{-1}$) for Hg^{2+} ions is observed, suggesting a potential application in removal of heavy metal ions in wastewater.

In chapter 6 we present our results on formation of PMO hollow spheres. Large-pore PMO hollow spheres with controllable pore size and high pore volume (~ 2.5 $cm^3 \cdot g^{-1}$) were successfully synthesized at low temperature (~ 15 °C) by using the triblock copolymer Pluronic F127 as a template and 1, 3, 5-trimethylbenzene (TMB) as a swelling agent in the presence of inorganic salt (KCl). The PMO hollow spheres are uniform and well dispersed, and have a large wall thickness. The pore size (9.8 ~ 15.1 nm) of the hollow spheres can be gradually expanded by increasing the TMB content together with a relatively high acidity. By controlling the content of hexadecyltrimethylammonium bromide (CTAB), successive structural transformation from hollow sphere to wormlike mesostructure and eventually to ordered body-centered cubic (space group of *Im3m*) mesostructure is observed. Our results reveal

that the hydrophobicity of bis(triethoxysilyl)ethane (BTSE) and a low temperature approach lead to the slow hydrolysis rate of silica precursors, which in turn leads to the weak interaction between individual TMB/F127 micelles and silicate oligomers. Furthermore, the salting-out effect of KCl may influence the swelling capacity of individual micelles as well as decrease the critical micelle concentration and critical micelle temperature, resulting in the formation of PMO hollow spheres from the assembly of individual TMB/F127 micelles with silicate oligomers. The composites exhibit efficient adsorption capacity (703 $mg \cdot g^{-1}$) for toluene, suggesting that they are a potentially useful adsorbent for removal of volatile organic compounds. The PMO hollow spheres allow biomolecules with large molecular weight to diffuse in, and showing a superior encapsulation capacity of bovine serum albumin (BSA) molecules (~ 585 $mg \cdot g^{-1}$) over other porous materials.

In chapter 7, ordered mesoporous polymer-organosilica and carbon-silica nanocomposites were synthesized through a triconstituent co-assembly strategy wherein the soluble resol polymer was used as an organic precursor, prehydrolyzed BTSE as another organic precursor, and triblock copolymer F127 as a template. After thermal curing of the resin polymer, the triblock copolymer F127 was removed by calcination at 350 ºC in N_2 atmosphere. The results of characterisations show that the polymer-organosilica nanocomposites have ordered 2D hexagonal mesostructures with uniform pore size (6.2 ~ 7.3 nm), suitable surface areas (619 ~ 794 $m^2 \cdot g^{-1}$) and pore volumes (0.61 ~ 0.88 $cm^3 \cdot g^{-1}$). With increasing BTSE content, the BET surface area and pore volume reduce for the polymer-organosilica composites. The mesoporous polymer-organosilica nanocomposites have homogeneous interpenetrating frameworks, in which both polymer and organosilica synergistically support the ordered mesostructure. Combustion in air or etching in HF solution can remove carbon or silica from the carbon-silica nanocomposites and yield mesoporous pure silica or carbon frameworks. The adsorption performance of the polymer-organosilica hybrid materials for benzene was also measured. Because of the hydrophobic property of phenyl-bridging groups from resin polymer and ethylene groups in the framework, the polymer-organosilica nanocomposite shows adsorption capacity of benzene up to 2.0 $mmol \cdot g^{-1}$, which suggests that they are a potential candidate for adsorption of organic compounds.

Chapter 8 provides the conclusions of this project and gives an outlook for PMOs in some key areas.

Keywords: Periodic mesoporous organosilica, Synthesis, Templating, Evaporation-induced self-assembly, Co-condensation method, Adsorption

Declaration

This thesis contains no material that has been accepted for the award of any other degree or diploma in any university or other institution. To the best knowledge of the author, this thesis contains no material previously published or written by another person except where due reference is made in the text of the thesis.

Na Hao
Department of Chemical Engineering
Monash University
February 2011

To my beloved parents and husband

Acknowledgements

Herein, I would like to express my deepest gratitude to all who have undoubtedly supported me over the course of my Ph.D. candidature.

I would like to sincerely thank my supervisors, Professor Dongyuan Zhao and Paul Webley for their continued support, patient guidance and constant encouragement throughout the entire project. They helped me a lot in project selection, experiment design and result discussion, which are important for my research. And their constructive advices and support have enabled me to go smoothly in this task. Furthermore, it was by their personal examples as well as verbal instruction that made me understand deeply one truth, that is, be a good person before doing anything.

My sincere thanks to Professor Xiaodong Chen, Huanting Wang, Bo Tu (Fudan University), and Yonghui Deng (Fudan University) for their kind help in my project. Thanks to Dr. Haifeng Bao, Yunxia Yang, Xinyi Zhang, Penny Xiao, Ranjeet Singh, Jun Zhang for their support in my experiments. And thanks to Lu Han (Fudan University), Zhangxiong Wu, Gongkui Xiao, Dong Xu, Liying Liu, Jin Shang and Fatin Hasan for communicating their knowledge of various aspects in experiments and giving valuable comments. It's my pleasure to thank my colleagues and friends Dr. Ying Qi, Dr. Dan Li, Dr. Fang Yuan, Li He, and Dr. Duo Wu whose participation made my research life more colourful. All the people at Monash and Fudan Universities have been very supportive and I have enjoyed working in such a friendly environment.

Thanks to the administrative staff in the Monash Chemical Engineering Department: Lilyanne Price, Jill Crisfield, Garry Thunder, Wren Schoppe and Kate Malcolm. Also, thanks to the workshop personnels and technicians in the Department: Ron Graham, Roy Harrip, Gamini Ganegoda, Kim Phu, Ross Ellingham, Daniel, Martin and John Barnard. Many thanks to all staffs of Monash Engineering Faculty and Monash Chemical Engineering Department.

I would like to thank Australian Research Council for providing Discovery Grants (DP0773160 and 0879769). Also thanks to Monash Chemical Engineering Department for providing me the scholarship that made my study possible.

Finally, my sincere gratitude goes to my beloved parents, my husband Peibo Wang, my son Bill Jiaxuan Wang and all my family members who have provided assistance at various occasions. Their love for me is always the power of my life and work.

CHAPTER 1 Introduction

1.1 Introduction to Mesoporous Materials

Porous materials are classified into several kinds by their size. According to the International Union of Pure and Applied Chemistry (IUPAC) notation [1], microporous materials have pore diameters of less than 2 nm, mesoporous materials has pores of size 2 ~ 50 nm, and macroporous materials have pore diameters of greater than 50 nm Typical mesoporous materials include some types of silica and alumina that have similarly-sized fine mesopores. Mesoporous oxides of niobium, tantalum, titanium, and zirconium have also been reported. According to the IUPAC, a mesoporous material can be disordered or ordered in a structure. Much effort has been put into not only the synthesis, but also the applications of these ordered mesoporous materials in catalysis [2-4], drug delivery [5-9], adsorption and separation [10, 11], and biosensors [12, 13].

The first mesoporous material with long range order was reported in the open literature in 1992, by the group of the former Mobil Oil Company [14, 15]. Around that time, the group filed a patent related to these materials [16]. Since then, research in this field has steadily grown.

1.2 Synthesis Mechanism and Pathways of Mesoporous Materials

1.2.1 Synthesis Mechanism of Mesoporous Materials

Ordered mesoporous materials possess large uniform pore sizes (1.5 ~ 10 nm), highly ordered nanochannels, large surface areas (~ 1500 $m^2 \cdot g^{-1}$), attractive liquid-crystal structures and also periodic arrangements of inorganic-organic composite nanoarrays [17].

Several questions arise during the design of mesoporous materials, such as: How can a liquid-crystal structure be formed? What is the role of a “template” in the formation of mesoprous materials? How are the components of a material integrated into an ordered mesostructure? These questions are attractive for researchers, and a large number of studies have been carried out to investigate the formation and assembly of mesostructures. Initially, on the basis of different reaction systems, many modern characterization technologies were applied to study the formation of ordered mesoporous materials, including magic angle spinning nuclear magnetic resonance (MAS-NMR), Electronic spin resonance (EPR), Transition electron microscopy

(TEM), Scanning electron microscopy (SEM), Thermogravimetric analysis (TGA) and N_2 adsorption/desorption *etc.* [18, 19].

1.2.1.1 Liquid-Crystal Templating Mechanism (LCT)

The initial LCT mechanism was first proposed by Mobil's scientists, where an organic surfactant species functions as a central structure, surrounded by inorganic oxides forming a mesopore framework. The two pathways, that is, cooperative self-assembly and "true" liquid-crystal templating processes, play an important role in the synthesis of ordered meostructures, as shown in Figure 1.1 [14, 15, 18-21].

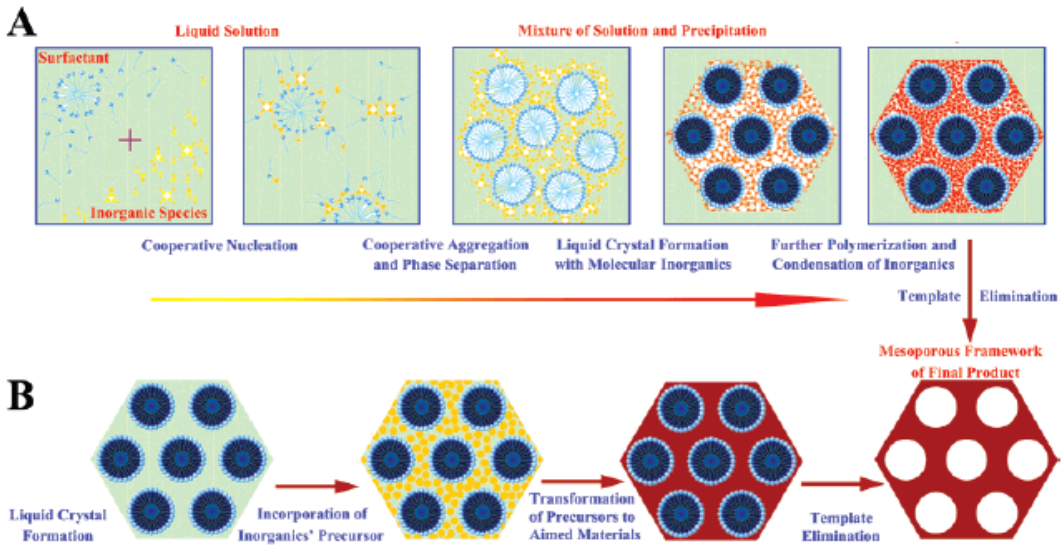

Figure 1.1. Two synthetic strategies of mesoporous materials: (A) cooperative self-assembly; (B) "true" liquid-crystal templating processes, as ref [17].

1.2.1.1A Cooperative Self-Assembly Process

On the one hand, it is impossible for liquid-crystalline phases to form at lower concentrations of surfactant molecules, for example, when there is cooperative self-assembly of the surfactant and the already added inorganic silica species, in which case an organic-inorganic micelle network forms. After hydrothermal treatment of these hybrid 'rods', an organic-inorganic liquid-crystalline phase with hexagonal arrangement can develop (Figure 1.1A) [22]. After the removal of surfactant templates by calcination, extraction, *etc.*, an ordered mesoporous silica material is obtained.

1.2.1.1B "True" Liquid-Crystal Templating Mechanism (TLCT)

On the other hand, as illustrated in Figure 1.1B, the surfactant molecules with long chains arrange themselves anisotropically in water solution, forming a hexagonal liquid-crystalline phase through a micelle self-assembly. The inorganic silicate species hydrolysize and deposite between surfactant 'rods', then condense to form an inorganic-organic network. After removal of the surfactant templates, a mesoporous silica material is obtained from this liquid-crystal scaffold. In this pathway, Attard and co-workers prepared mesoporous silicas by using a high concentration of nonionic surfactants as a template [23].

It should be pointed out that two factors affect the LCT mechanism: (i) the dynamics of surfactant molecules to form assemblies, micelles, and final liquid-crystal structure; and (ii) the ability of the inorganic oxide to hydrolyse and polycondense leading to a network surrounding the surfactant templates [18, 24, 25]. However, the current LCT mechanism does not provide any explanation about the interaction between organic surfactants and inorganic silica species. In general, the LCT mechanism is limited in the synthesis of mesoporous materials.

1.2.1.2 'Silicate Rod Assembly' Mechanism (SRA)

Davis and coworkers [26] proposed the 'silicate rod assembly' mechanism, as they found that the liquid-crystalline phase with hexagonal ordering didn't form during the synthesis process of MCM-41. In this mechanism, the surfactant molecules initially form disordered micellar 'rods', then the micellar 'rods' interact with the inorganic silicate species by Coulomb forces, and the condensed two or three monolayers of silicate species deposit around the isolated micellar 'rods'. Finally these rods aggregate and pack into the ordered hexagonal mesostructure. It is noted that the assembling of such long organic-inorganic rods is difficult so that this mechanism is debatable.

Furthermore, Steel *etc.* [27] pointed out that during the hexagonal mesostructure formation process of MCM-41, it is possibly the silicate species that induce the transformation of the organic-inorganic composite from layer to hexagonal phase, which is called as a 'layer-to-hexagonal' mechanism. It is also known as a 'folded sheets mechanism'. However, it is found that the layered intermediate is unnecessary during the formation of hexagonal mesostructure MCM-41 [17, 28].

1.2.1.3 Cooperative Formation Mechanism (CFM)

The most convincing formation mechanism proposed to date is the cooperative formation mechanism (CFM), which was first proposed by Stucky and co-workers [29-31]. During the formation process of the mesoporous silica, silicate polyanions initially interact with positively charged groups in cationic surfactants driven by Coulomb forces. The silicate species at the interface then polymerize, cross-link and further change the charge density of the inorganic layers. Through the process of nucleation and rapid precipitation of organized arrays by cooperative interactions, the arrangements of surfactants and the charge density between inorganic and organic species influence each other. With the increase of time and temperature, the condensation of the silicate phase proceeds, the silicate framework charge decreases during this process and may lead to liquid-crystal-like phase transitions as the surfactant phase tries to reorganize the changing interface charge density. It is noted that the matching of charge density at the surfactant/inorganic species interfaces governs the assembly process. The cooperative formation mechanism can explain many experimental phenomena in the synthesis of mesoporous materials and also apply in some syntheses of non-silica mesoporous materials. The CFM is therefore widely accepted by most researchers.

1.2.2 Synthesis Pathways of Mesoporous Materials

During the synthesis of mesoporous materials, the interaction between organic and inorganic species is considered to be very important [18, 29, 32]. Adjusting the chemistry of the surfactant headgroups may yield different mesoporous materials. The main synthesis routes are listed as follows:

(1) Four general synthetic routes were proposed by Stucky and co-workers [17, 29, 30]. The routes are S^+I^-, S^-I^+, $S^+X^-I^+$, and $S^-X^+I^-$, where S^+ = surfactant cations, S^- = surfactant anions, I^+ = inorganic precursor cations, I^- = inorganic precursor anions, X^+ = cationic counterions, and X^- = anionic counterions. By Coulomb forces, surfactant cations (S^+) match with silicate anions (I^-) as S^+I^- under basic conditions [14, 33, 34]. The S^-I^+ interaction, by comparision, occurs between cationic Keggin ion (Al_{13}^{7+}) and anionic surfactants, such as dodecyl benzenesulfonate salt [29]. The $S^+X^-I^+$ interaction applies in the syntheses of mesoporous silicates under acidic conditions, where counterions are required [29, 35]. The $S^-N^+I^-$ route can be explained by the successful synthesis of a family of mesoporous silica structures (AMS-*n*) under basic conditions

by using anionic surfactants as structure-directing agents (SDAs) and 3-aminopropyltrimethoxysilane (APS) or N-trimethoxylsilypropyl-*N*, *N*, *N*-trimehylammonium chloride (TMAPS) as co-structure-directing agents (CSDAs) [36]. In this pathway, N^+ are cationic amino groups of organoalkoxysilanes. The negatively charged headgroups of the anionic surfactants (S^-) can interact with the positively charged ammonium sites (N^+) of APS or TMAPS by neutralization [37, 38].

(2) A hydrogen-bonding interaction mechanism for synthesising mesoporous silicates under neutral conditions was reported by Pinnavaia and co-workers. The routes are S^0I^0 or N^0I^0, where S^0 as neutral amines, N^0 as nonionic surfactants, and I^0 as hydrated silicate oligomers from tetraethyl orthosilicate (TEOS) [39-41].

(3) It should be noted that a double-layer hydrogenbonding $S^0H^+X^-I^+$ interaction [42, 43] may lead to the synthesis of mesoporous silica SBA-15 carried out under a strong acidic condition with triblock copolymer P123 ($EO_{20}PO_{70}EO_{20}$) as a template.

(4) The interaction between organic and inorganic species, such as coordination bonds [18, 29] and covalent bonds [44, 45] can also be important for the preparation of mesoporous materials with different mesostructures.

1.3 Mesophases

1.3.1 Mesophases

Till now, various mesoporous silicate structures with different symmetries have been obtained, indicating the synthesis is controllable. The ordered mesophases are included as follows:

1.3.1.1 One-dimensional (1D) Lamellar Mesostructures (*p2* symmetry)

The lamellar mesostructures can be templated by doublechain surfactants, such as $C_{20}H_{41}N(CH_3)_3Br$ [35] and nonionic surfactants with low hydrophilic EO groups as $C_{12}H_{25}EO_3$ [46]. The lamellar mesostructure is important for the study of the synthesis mechanism or phase transformation of mesoporous materials, although most lamellar mesostructures are not stable.

1.3.1.2 Two-dimensional (2D) Hexagonal Mesostructures (Straight channel, *p6mm* symmetry)

The classical products of 2D mesostructured materials with hexagonal symmetry are MCM-41, SBA-15, SBA-3, KSW-2 *etc*. The features for these mesostructures are

hexagonally close packed cylindrical pore channels (*p6mm* space group) and parallel stripes if viewed perpendicular to the channel directions.

MCM-41 is the most extensively investigated mesoporous silica, and can be synthesized with using hexadecyltrimethylammonium bromide (CTAB) as a SDA in a basic solution [47].

The second most widely studied mesoporous silica material is SBA-15, which is prepared using PEO-PPO-PEO triblock copolymer P123 as a SDA under acidic conditions. SBA-15 materials have uniform pore sizes from ~ 6.5 to 10 nm and thick pore walls from 3.1 to 4.8 nm, which results in higher thermal stability and hydrothermal stability. The disordered micropore system exists in the silicate walls [48-50]. The above important features enable the use of SBA-15 for separation and nanocasting, *etc* [51-55].

1.3.1.3 Three-dimensional (**3D) Mesostructures**

Many cubic mesostructures have been synthesized, such as MCM-48 mesostructure [22], SBA-*n* [56-59], FDU-*n* [34, 60-62] KIT-*n* [63-65], AMS-*n*, and IBN-*n* [66, 67] series of silicas.

1.3.1.3.1 3D Cubic Mesostructure (Bicontinuous channels, *Ia3d* symmetry)

MCM-48 is defined by a so-called minimal surface, which divides the space into two enantiomeric separated 3D helical pore systems, forming a cubic uniform bicontinuous structure (*Ia3d*) [22].

The large-pore mesoporous silicas with cubic bicontinuous structure (*Ia*3*d*) can be obtained in the presence of some additives when triblock copolymers are used as templates under acidic conditions, such as using a mixture of triblock copolymer F127 and an anionic surfactant or P123 and sodium dodecyl sulfonate (SDS) as templates [68, 69].

1.3.1.3.2 3D Cubic Mesostructure (Cage-like pore, *Pm3n* symmetry)

The most studied product with cubic *Pm*3*n* mesostructure is SBA-6, in which a B-cage is surrounded by 12 A-cages that are connected through mesopore openings of ~ 2 nm. It can be considered as a packing of spherical cages, distinguished by two kinds of cages with ordered arrangements.

Cubic mesostructures SBA-6 and SBA-1 [56-58] with *Pm*3*n* symmetry can be synthesized using cationic surfactants, for example $C_nH_{2n+1}N(CH_2CH_3)_3Br$ (n = 16, C_{16}TEABr), Gemini and bolaform surfactants as SDAs under acidic and basic conditions, respectively [29, 70-72]. However, such a cubic *Pm*3*n* mesostructure has not been prepared by using triblock copolymers (PEO-PPO-PEO) as templates so far.

1.3.1.3.3 3D Cubic Mesostructure (Cage-like pore, *Im3m* symmetry)

The SBA-16 mesostructure (*Im*3*m*) has a body-centered cubic symmetrical packing of spherical cages [70, 73], and was obtained under acidic conditions [43, 66, 74].

1.3.1.3.4 3D Cubic Mesostructure (Cage-like pore, *Fd3m* symmetry)

AMS-8 was described as a face-centered cubic structure with *Fd*3*m* symmetry, and is composed of a bimodal arrangement of cages, 16 small (5.6 nm) and 8 large (7.6 nm) cages in the unit cell. They are built up via the cage windows of 1.4 ~ 2.5 nm (for connectivity between large cages) and the small windows of less than 5 Å (for large-small and small-small connections) [38].

1.3.1.3.5 3D Cubic Mesostructure (Cage-like pore, *Fm3m* symmetry)

The representive product FDU-12 has a cubic (*Fm*3*m*) mesostructure, which can be thought as a face-centered cubic (*fcc*) close-packing of spherical cages, each connected to 12 nearest neighboring cages [75-77]. The addition of 1,3,5-trimethylenebenzene (TMB) and potassium chloride (KCl) are critical for enlarging the pore sizes during the synthesis of FDU-12 at lower temperatures.

1.3.1.3.6 3D Hexagonal Mesostructure (Cage-like pore, *P*6$_3$/*mmc* and *P*6$_3$/*mcm* symmetry)

SBA-2 may have a 3D hexagonal mesostructure with the space group of P6$_3$/mmc symmetry [35]. SBA-2 was observed as an intergrowth of *hcp* with *ccp* mesostructures viewed along the [110] direction of the cubic phase or the [100] direction of the hexagonal phase from TEM images [72, 78].

IBN-9 presents the first tri-continuous mesoporous silica structure with 3D hexagonal symmetry *P*6$_3$/*mcm* symmetry [67]. IBN-9 is an intermediate phase between the cubic bi-continuous phase and the 2D hexagonal phase, and has the most complex pore structure amongst all reported mesoporous materials. It shows a unique

tri-continuous structure with three congruent interwoven mesoporous channel systems separated by a single continuous silica wall.

1.3.1.4 Disordered Mesostructures

The disordered mesostructures include MSU [39], HMS [40], KIT-1 [79], TUD-1 [80] and Al-MMS [81] mesoporous silicates, which are aften referred to as "foam-like" or "worm-like" mesoporous molecular sieves [82]. The uniform pores and high surface areas favour the use of these materials in adsorption and catalysis. It is not clear whether ordered or disordered structures are beneficial for each application

1.4 Organic-Inorganic Hybrid Mesoporous Silica Materials

Mesoporous organic-inorganic hybrid materials have been obtained through the interaction of inorganic and organic components by surfactant templating. The framework properties can be influenced by the inorganic and organic moieties in the mesostructures. The inorganic components can provide mechanical, thermal, or structural stability, whereas the organic ones can introduce flexibility into the framework, or change the properties of the framework. One pathway to synthesis of functional mesoporous silicates is the incorporation of organic components in the pure silica matrix, either on the surface, or within the channels by grafting or co-condensation method. The disadvantage of the grafting method is that it often leads to nonhomogeneous distribution of the organic groups within the pore walls or pore blocking [83-86].

By comparison, pore blocking is not a problem in the co-condensation method as the organic groups are the direct components of the silica matrix. Furthermore, the organic units are generally more homogeneously distributed in the framework than the materials synthesized by the grafting method. However, the co-condensation method can also lead to the synthesis of disordered products, as the degree of order of the final materials decreases with increasing concentration of organic components $(R'O)_3SiR$ in the reaction mixture. Furthermore, the calcination method is not appropriate for the removal of surfactant as the organic groups will occasionally be broken at high calcination temperatures [83].

In contrast to the two kinds of organic-inorganic hybrid materials described above, which are obtained by grafting or co-condensation methods, the organic units can be incorporated in the silica framework through two covalent bonds with silica atoms

and thus distributed homogeneously in the pore walls. Thus, a new class of mesostructured organic-inorganic hybrid materials - periodic mesoporous organosilicas (PMOs) came into being by self-assembly of surfactants and bissilylated organosilica precursors $(R'O)_3Si\text{-}R\text{-}Si(OR')_3$.

The first PMO was synthesized in 1999 by three research groups independently [87-89]. The double trialkoxysilyl precursors are hydrolyzed and condensed in the presence of amphiphilic surfactant micelles. Then the mesostructured framework can be obtained by removing the surfactant by solvent extraction. Thus, the different organic groups are incorporated in the silicate networks, resulting in higher loadings of organic functional groups and decreasing the possibilities of pore blockage compared with the grafting or co-condensation method. Now, PMOs with a multitude of bridge-bonded organic groups are considered as highly promising candidates for the application of catalysis, adsorption, chromatography, and nanoelectronics [90, 91].

Although much work has been done in the synthesis of PMOs, the adsorption research of large-pore PMO materials is relatively limited. Design of PMOs to make useful adsorbents is therefore unknown. Therefore, one of the challenges undertaken in this project was to extend the adsorption application of the PMO materials.

1.5 Research Motivations and Objectives

PMOs are synthesized by silsesquioxane precursors with organic bridging groups and supermolecules as a template. These materials have attracted much interest in the last decade. Until now, PMOs with different mesostructures, pore sizes and morphologies have been successfully synthesized. The diversity of organic spacers enables modification of bulk properties such as the porosity, thermal stability, optical clarity, refractive index, chemical resistance, hydrophobicity, and dielectric constant. Through these properties, PMOs show great potential in adsorption, catalysis and sensors applications, compared with inorganic mesoporous silica materials.

At present, the synthesis and application of PMOs materials are still at early stage. One important scientific issue in this field is the control of the constitution and pore size of PMOs materials to improve the adsorption properties. As mentioned above, a great deal of study has been carried out in the synthesis of PMOs as M41S structures with small pore sizes. However, the limited pore size of PMOs with functional organic groups may restrict their applications in some areas where large pore PMOs are in demand as substrates from the point of view of sorption, immobilization and

encapsulation of large molecules. Up to now, it is desirable to synthesize PMO materials with a pore size larger than that of M41S structures such as SBA-15, a mesoporous material with pore size in the range of 6 ~ 30 nm. Therefore, the synthesis of large-pore PMOs with functional groups templated by triblock copolymers under acidic conditions *via* the $(S^{\circ}H^{+})(X^{-}I^{+})$ pathway continues to be a challenging objective in this area. On the other hand, inorganic salts have been used to improve the hydrothermal stability, control the morphology, extend the synthesis domain, and tailor the framework porosity during the formation of mesoporous materials. These results can be attributed to the specific effect of inorganic salts on the self-assembly interaction between surfactant headgroups and silica precursors.

Therefore, it is important for both academic investigation and adsorption applications to synthesize large pore PMOs with functional groups and the present work is focused on this project. Much work should be done in two aspects, synthesis and adsorption. To understand the relationship between the properties and the structures of mesoporous organosilica materials, from a synthetic viewpoint, a precondition that should be achieved is that ordered large pore PMOs be synthesized and their structural information clearly identified. Changing reactive systems should be exploited to prepare large-pore PMOs, such as using different surfactants as templates, non-aqueous synthesis conditions *etc.*; at the same time, functional organic groups should be selected as suitable for further modification, or has interaction with target molecules by forming covalent bond, or π-π interaction *etc.*, which will be of benefit for adsorption. Finally, we investigate large-pore PMOs materials with functional groups in targeted areas of sorption application, such as waste water, and air containing toxic constitutents.

References

[1] J. Rouquerol, D. Avnir, C. W. Fairbridge, D. H. Everett, J. M. Haynes, N. Pernicone, J. D. F. Ramsay, K. S. W. Sing, K. K. Unger, "Recommendations for the Characterization of Porous Solids," *Pure Appl. Chem* **1994***, 66*, 1739-1758.

[2] A. Corma, A. Martinez, V. Martinez-Soria, J. B. Monton, "Hydrocracking of Vacuum Gasoil on the Novel Mesoporous MCM-41 Aluminosilicate Catalyst," *J. Catal.* **1995**, *153*, 25-31.

[3] A. Corma, M. T. Navarro, J. P. Pariente, F. Sanchez, *Zeolites and related microporous mateials: State of the art* **1994**, J. Weitkamp, H. G. Karge, H. Pfeifer, W.

Hölderich, *Studies in surface science and catalysis*, Elsevier, Amsterdam, **1994**, *84*, 69.

[4] A. Wingen, N. Anastasievic, A. Hollnagel, D. Werner, F. Schüth, "Fe-MCM-41 as a Catalyst for Sulfur Dioxide Oxidation in Highly Concentrated Gases," *J. Catal.* **2000**, *193*, 248-254.

[5] B. G Trewyn, J. A. Nieweg, Y. N. Zhao, V. S. Y. Lin, "Biocompatible Mesoporous Silica Nanoparticles with Different Morphologies for Animal Cell Membrane Penetration," *Chem. Eng. J.* **2007**, *137*, 23-29.

[6] R. Mellaerts, C. A. Aerts, J. V. Humbeeck, P. Augustijns, M. Den, V. Guy, J. A. Martens, "Enhanced Release of Itraconazole from Ordered Mesoporous SBA-15 Silica Materials," *Chem. Commun.* **2007**, 1375-1377.

[7] T. Heikkila, J. Salonen, J. Tuura, M. Hamdy, G. Mul, N. Kumar, T. Salmi, D. Murzin, "Mesoporous Silica Material TUD-1 as a Drug Delivery System," *Int. J. Pharmace.* **2007**, *331*, 133-138.

[8] A. B. D. Nandiyanto, S. G. Kim, F. Iskandar, K. Okuyama, "Synthesis of Spherical Mesoporous Silica Nanoparticles with Nanometer-size Controllable Pores and Outer Diameters," *Micropor. Mesopor. Mater.* **2009**, *120*, 447-453.

[9] Y. C. Tozuka, A. Wongmekiat, K. Kimura, K. Moribe S. Yamamura, K. J. Yamamoto, "Effect of Pore Size of FSM-16 on the Entrapment of Flurbiprofen in Mesoporous Structures," *Chem. Pharmace. Bull.* **2005**, *53*, 974-977.

[10] A. A. kurganov, K. K. Unger, T. Issaeva, "Packings of An Unidimensional Regular Pore Structure as Model Packings in Size-Exclusion and Inverse Size-Exclusion Chromatography," *J. Chromatogr. A*. **1996**, *753*, 177-190.

[11] T. Martin, D. Brunel, A. Galarneau, F. D. Renzo, F. Fajula, B. Lefevre, P. F. Gobin, G. Vigier, "Dissipative Water Intrusion in Hydrophobic MCM-41 Type Materials," *Chem. Commun.* **2002**, 24-25.

[12] B. G. Trewyn, G. Supratim, I. I. Slowing, V. S. Y. Lin, "Mesoporous Silica Nanoparticle Based Controlled Release, Drug Delivery, and Biosensor Systems," *Chem. Commun.* **2007**, 3236-3245.

[13] D. R. Radu, C. Y. Lai, K. Jeftinija, E. W. Rowe, S. Jeftinija, V. S. Y. Lin, "A Polyamidoamine Dendrimer-Capped Mesoporous Silica Nanosphere-Based Gene Transfection Reagent," *J. Am. Chem. Soc.* **2004**, *126*, 13216-13217.

[14] J. S. Beck, J. C. Vartuli, W. J. Roth, M. E. Leonowicz, C. T. Kresge, K. D. Schmitt, C. T. W. Chu, D. H. Olson, E. W. Sheppard, S. B. McCullen, J. B. Higgins, J.

L. Schlenker, “A New Family of Mesoporous Molecular Sieves Prepared with Liquid Crystal Templates,” *J. Am. Chem. Soc.* **1992**, *114*, 10834-10843.

[15] C. T. Kresge, M. E. Leonowicz, W. J. Roth, J. C. Vartuli, J. S. Beck, “Ordered Mesoporous Molecular Sieves Synthesized by A Liquid-Crystal Template Mechanism,” *Nature* **1992**, *359*, 710-712.

[16] C. T. Kresge, W. C. Pa, M. E. Leonowicz, M. Lakes, W. J. Roth, N. J. Sewell, J. C. Vartuli, “Composition of Synthetic Porous Crystalline Material, Its Synthesis” *U.S. Patent 5,102,643.* **1992**, assigned to Mobil Oil Co.

[17] Y. Wan, D. Y. Zhao, “On the Controllable Soft-Templating Approach to Mesoporous Silicates,” *Chem. Rev.* **2007**, *107*, 2821-2860.

[18] J. Y. Ying, C. P. Mehnert, M. S. Wong, “Synthesis and Applications of Supramolecular-Templated Mesoporous Materials,” *Angew. Chem., Int. Ed.* **1999**, *38*, 56-77.

[19] A. Corma, “From Microporous to Mesoporous Molecular Sieve Materials and Their Use in Catalysis,” *Chem. Rev.* **1997**, *97*, 2373-2420.

[20] F. Schüth, W. Schmidt, “Microporous and Mesoporous Materials,” *Adv. Mater.* **2002**, *14*, 629-638.

[21] F. Schüth, “Non-siliceous Mesostructured and Mesoporous Materials,” *Chem. Mater.* **2001**, *13*, 3184-3195.

[22] A. Monnier, F. Schüth, Q. Huo, D. Kumar, D. Margolese, R. S. Maxwell, G. Stucky, M. Krishnamurty, P. Petroff, A. Firouzi, M. Janicke, B. F. Chmelka, “Cooperative Formation of Inorganic-Organic Interfaces in the Synthesis of Silicate Mesostructures,” *Science* **1993**, *261*, 1299-1303.

[23] G. S. Attard, J. C. Glyde, C. G. Goltner, “Liquid-Crystalline Phases as Templates for the Synthesis of Mesoporous Silica,” *Nature* **1995**, *378*, 366-368.

[24] N. K. Raman, M. T. Anderson, C. J. Brinker, “Template-Based Approaches to the Preparation of Amorphous, Nanoporous Silicas,” *Chem. Mater.* **1996**, *8*, 1682-1701.

[25] I. Soten, G. A. Ozin, (Eds) W. Jones, C. N. R. Rao, *Mesoscale Materials Synthesis and Beyond; Supramolecular Organization and Materials Design* Cambridge University Press, Cambridge **2002**, 34-82.

[26] C. Y. Chen, S. L. Burkett, H. X. Li, M. E. Davis, “Studies on Mesoporous Materials II. Synthesis Mechanism of MCM-41,” *Micropor. Mater.* **1993**, *2*, 27-34.

[27] A. Steel, S. W. Carr, M. W. J. Anderson, "^{14}N NMR Study of Surfactant Mesophases in the Synthesis of Mesoporous Silicates," *J. Chem. Soc., Chem. Commun.* **1994**, 1571-1572.

[28] S. Inagaki, Y. Fukushima, K. Kuroda, "Synthesis of Highly Ordered Mesoporous Materials from A Layered Polysilicate," *J. Chem. Soc., Chem. Commun.* **1993**, 680-681.

[29] Q. S. Huo, D. I. Margolese, U. Ciesla, P. Y. Feng, T. E. Gier, P. Sieger, R. Leon, P. M. Petroff, F. Schüth, G. D. Stucky, "Generalized Synthesis of Periodic Surfactant/Inorganic Composite Materials," *Nature* **1994**, *368*, 317-321.

[30] Q. S. Huo, D. I. Margolese, U. Ciesla, D. G. Demuth, P. Y. Feng, T. E. Gier, P. Sieger, A. Firouzi, B. F. Chmelka, F. Schüth, G. D. Stucky, "Organization of Organic Molecules with Inorganic Molecular Species into Nanocomposite Biphase Arrays," *Chem. Mater.* **1994**, *6*, 1176-1191.

[31] A. Firouzi, D. Kumar, L. M. Bull, T. Besier, P. Sieger, Q. S. Huo, S. A. Walker, J. A. Zasadzinski, C. Glinka, J. Nicol, D. Margolese, G. D. Stucky, B. F. Chmelka, "Cooperative Organization of Inorganic-Surfactant and Biomimetic Assemblies," *Science*, **1995**, *267*, 1138-1143.

[32] G. J. D. Soler-Illia, C. Sanchez, B. Lebeau, J. Patarin, "Chemical Strategies to Design Textured Materials: from Microporous and Mesoporous Oxides to Nanonetworks and Hierarchical Structures," *Chem. Rev.* **2002**, *102*, 4093-4138.

[33] J. M. Kim, S. K. Kim, R. Ryoo, "Synthesis of MCM-48 Single Crystals," *Chem. Commun.* **1998**, 259-260.

[34] S. D. Shen, Y. Q. Li, Z. D. Zhang, J. Fan, B. Tu, W. Z. Zhou, D. Y. Zhao, "A Novel Ordered Cubic Mesoporous Silica Templated with Tri-head Group Quaternary Ammonium Surfactant," *Chem. Commun.* **2002**, 2212-2213.

[35] Q. S. Huo, D. I. Margolese, G. D. Stucky, "Surfactant Control of Phases in the Synthesis of Mesoporous Silica-Based Materials," *Chem. Mater.* **1996**, *8*, 1147-1160.

[36] S. Che, A. E. Garcia-Bennett, T. Yokoi, K. Sakamoto, H. Kunieda, O. Terasaki, T. Tatsumi, "A Novel Anionic Surfactant Templating Route for Synthesizing Mesoporous Silica with Unique Structure," *Nat. Mater.* **2003**, *2*, 801-805.

[37] A. E. Garcia-Bennett, N. Kupferschmidt, Y. Sakamoto, S. Che, O. Terasaki, "Synthesis of Mesocage Structures by Kinetic Control of Self-Assembly in Anionic Surfactants," *Angew. Chem., Int. Ed.* **2005**, *44*, 5317-5322.

[38] A. E. Garcia-Bennett, K. Miyasaka, O. Terasaki, S. N. Che, "Structural Solution of Mesocaged Material AMS-8," *Chem. Mater.* **2004**, *16*, 3597-3605.

[39] S. A. Bagshaw, E. Prouzet, T. J. Pinnavaia, "Templating of Mesoporous Molecular Sieves by Nonionic Polyethylene Oxide Surfactants," *Science* **1995**, *269*, 1242-1244.

[40] P. T. Tanev, T. J. Pinnavaia, "A Neutral Templating Route to Mesoporous Molecular Sieves," *Science* **1995**, *267*, 865-867.

[41] K. Cassiers, P. Van der Voort, T. Linssen, E. F. Vansant, O. Lebedev, J. Van Landuyt, "A Counterion-Catalyzed $(S^{\circ}H^{+})(X^{-}I^{+})$ Pathway toward Heat- and Steam-Stable Mesostructured Silica Assembled from Amines in Acidic Conditions," *J. Phys. Chem. B* **2003**, *107*, 3690-3696.

[42] D. Y. Zhao, J. L. Feng, Q. S. Huo, N. Melosh, G. H. Fredrickson, B. F. Chmelka, G. D. Stucky, "Triblock Copolymer Syntheses of Mesoporous Silica with Periodic 50 to 300 Angstrom Pores," *Science* **1998**, *279*, 548-552.

[43] D. Y. Zhao, Q. S. Huo, J. L. Feng, B. F. Chmelka, G. D. Stucky, "Nonionic Triblock and Star Diblock Copolymer and Oligomeric Surfactant Syntheses of Highly Ordered, Hydrothermally Stable, Mesoporous Silica Structures," *J. Am. Chem. Soc.* **1998**, *120*, 6024-6036.

[44] A. Shimojima, K. Kuroda, "Direct Formation of Mesostructured Silica-Based Hybrids from Novel Siloxane Oligomers with Long Alkyl Chains," *Angew. Chem., Int. Ed.* **2003**, *42*, 4057-4060.

[45] A. Shimojima, Z. Liu, T. Ohsuna, O. Terasaki, K. Kuroda, "Self-Assembly of Designed Oligomeric Siloxanes with Alkyl Chains into Silica-Based Hybrid Mesostructures," *J. Am. Chem. Soc.* **2005**, *127*, 14108-14116.

[46] J. M. Kim, Y. Sakamoto, Y. K. Hwang, Y. U. Kwon, O. Terasaki, S. E. Park, G. D. Stucky, "Structural Design of Mesoporous Silica by Micelle-Packing Control Using Blends of Amphiphilic Block Copolymers," *J. Phys. Chem. B* **2002**, *106*, 2552-2558.

[47] B. P. Feuston, J. B. Higgins, "Model Structures for MCM-41 Materials: A Molecular Dynamics Simulation," *J. Phys. Chem.* **1994**, *98*, 4459-4462.

[48] W. W. Lukens, P. Schmidt-Winkel, D. Y. Zhao, J. L. Feng, G. D. Stucky, "Evaluating Pore Sizes in Mesoporous Materials: A Simplified Standard Adsorption Method and a Simplified Broekhoff-de Boer Method," *Langmuir* **1999**, *15*, 5403-5409.

[49] S. H. Joo, R. Ryoo, M. Kruk, M. Jaroniec, "Evidence for General Nature of Pore Interconnectivity in 2-Dimensional Hexagonal Mesoporous Silicas Prepared Using Block Copolymer Templates," *J. Phys. Chem. B* **2002**, *106*, 4640-4646.

[50] C. G. Spickermann, "Non-Ionic Templating of Silica: Formation Mechanism and Structure," *Curr. Opin. Colloid Interface Sci.* **2002**, *7*, 173-178.

[51] V. T. Hoang, Q. L. Huang, M. Eic, T. O. Do, S. Kaliaguine, "Structure and Diffusion Characterization of SBA-15 Materials," *Langmuir* **2005**, *21*, 2051-2057.

[52] H. Vinh-Thang, Q. L. Huang, M. Eic, T. O. Do, S. Kaliaguine, "Adsorption of C7 Hydrocarbons on Biporous SBA-15 Mesoporous Silica," *Langmuir* **2005**, *21*, 5094-5101.

[53] J. Trebosc, J. W. Wiench, S. Huh, V. S. Y. Lin, M. Pruski, "Solid-State NMR Study of MCM-41-type Mesoporous Silica Nanoparticles," *J. Am. Chem. Soc.* **2005**, *127*, 3057-3068.

[54] S. Takahara, N. Sumiyama, S. Kittaka, T. Yamaguchi, M. C. Bellissent-Funel, "Neutron Scattering Study on Dynamics of Water Molecules in MCM-41. 2. Determination of Translational Diffusion Coefficient," *J. Phys. Chem. B* **2005**, *109*, 11231-11239.

[55] L. Frunza, H. Kosslick, I. Pitsch, S. Frunza, A. Schonhals, "Rotational Fluctuations of Water inside the Nanopores of SBA-Type Molecular Sieves," *J. Phys. Chem. B* **2005**, *109*, 9154-9159.

[56] H. M. Kao, C. C. Cheng, C. C. Ting, L. Y. Hwang, "Phase Control of Cubic SBA-1 Mesostructures *via* Alcohol-Assisted Synthesis," *J. Mater. Chem.* **2005**, *15*, 2989-2992.

[57] H. M. Kao, C. C. Ting, A. S. T. Chiang, C. C. Teng, C. H. Chen, "Facile Synthesis of Stable Cubic Mesoporous Silica SBA-1 Over A Broad Temperature Range with the Aid of D-fructose," *Chem. Commun.* **2005**, 1058-1060.

[58] C. C. Pantazis, P. J. Pomonis, "Mesostructure Design via Poly(acrylic acid)-C_nTAB Complexes: A New Route for SBA-1 Mesoporous Silica," *Chem. Mater.* **2003**, *15*, 2299-2300.

[59] Y. Sakamoto, I. Diaz, O. Terasaki, D. Y. Zhao, J. Perez-Pariente, J. M. Kim, G. D. Stucky, "Three-Dimensional Cubic Mesoporous Structures of SBA-12 and Related Materials by Electron Crystallography," *J. Phys. Chem. B* **2002**, *106*, 3118-3123.

[60] X. Y. Liu, B. Z. Tian, C. Z. Yu, F. Gao, S. H. Xie, B. Tu, R. C. Che, L. M. Peng, D. Y. Zhao, "Room-Temperature Synthesis in Acidic Media of Large-Pore Three-

Dimensional Bicontinuous Mesoporous Silica with *Ia3d* Symmetry," *Angew. Chem., Int. Ed.* **2002**, *41*, 3876-3878.

[61] C. Z. Yu, Y. H. Yu, D. Y. Zhao, "Highly Ordered Large Caged Cubic Mesoporous Silica Structures Templated by Triblock PEO-PBO-PEO Copolymer," *Chem. Commun.* **2000**, 575-576.

[62] J. R. Matos, M. Kruk, L. P. Mercuri, M. Jaroniec, L. Zhao, T. Kamiyama, O. Terasaki, T. J. Pinnavaia, Y. Liu, "Ordered Mesoporous Silica with Large Cage-Like Pores: Structural Identification and Pore Connectivity Design by Controlling the Synthesis Temperature and Time," *J. Am. Chem. Soc.* **2003**, *125*, 821-829.

[63] F. Kleitz, S. H. Choi, R. Ryoo, "Cubic *Ia3d* Large Mesoporous Silica: Synthesis and Replication to Platinum Nanowires, Carbon Nanorods and Carbon Nanotubes," *Chem. Commun.* **2003**, 2136-237.

[64] T. W. Kim, F. Kleitz, B. Paul, R. Ryoo, "MCM-48-like Large Mesoporous Silicas with Tailored Pore Structure: Facile Synthesis Domain in a Ternary Triblock Copolymer-Butanol-Water System," *J. Am. Chem. Soc.* **2005**, *127*, 7601-7610.

[65] F. Kleitz, D. N. Liu, G. M. Anilkumar, I. S. Park, L. A. Solovyov, A. N. Shmakov, R. Ryoo, "Large Cage Face-Centered-Cubic *Fm3m* Mesoporous Silica: Synthesis and Structure," *J. Phys. Chem. B* **2003**, *107*, 14296-14300.

[66] Y. Han, J. Y. Ying, "Generalized Fluorocarbon-Surfactant-Mediated Synthesis of Nanoparticles with Various Mesoporous Structures," *Angew. Chem., Int. Ed.* **2005**, *44*, 288-292.

[67] Y. Han, D. L. Zhang, L. L. Chng, J. L. Sun, L. Zhao, X. D. Zou, J. Y. Ying, A tri-continuous mesoporous material with a silica pore wall following a hexagonal minimal surface, *Nat. Chem.* **2009**, *1*, 123-127.

[68] D. H. Chen, Z. Li, C. Z. Yu, Y. F. Shi, Z. D. Zhang, B. Tu, D. Y. Zhao, "Nonionic Block Copolymer and Anionic Mixed Surfactants Directed Synthesis of Highly Ordered Mesoporous Silica with Bicontinuous Cubic Structure," *Chem. Mater.* **2005**, *17*, 3228-3234.

[69] D. H. Chen, Z. Li, Y. Wan, X. J. Tu, Y. F. Shi, Z. X. Chen, W. Shen, C. Z. Yu, B. Tu, D. Y. Zhao, "Anionic Surfactant Induced Mesophase Transformation to Synthesize Highly Ordered Large-Pore Mesoporous Silica Structures," *J. Mater. Chem.* **2006**, *16*, 1511-1519.

[70] Y. Sakamoto, M. Kaneda, O. Terasaki, D. Y. Zhao, J. M. Kim, G. D. Stucky, H. J. Shim, R. Ryoo, "Direct Imaging of the Pores and Cages of Three-Dimensional Mesoporous Materials," *Nature* **2000**, *408*, 449-453.

[71] M. C. Chao, D. S. Wang, H. P. Lin, C. Y. Mou, "Control of Single Crystal Morphology of SBA-1 Mesoporous Silica," *J. Mater. Chem.* **2003**, *13*, 2853-2854.

[72] A. E. Garcia-Bennett, S. Willliamson, P. A. Wright, I. J. Shannon, "Control of Structure, Pore Size and Morphology of Three-Dimensionally Ordered Mesoporous Silicas Prepared Using the Dicationic Surfactant $[CH_3(CH_2)_{15}N(CH_3)_2(CH_2)_3N(CH_3)_3]Br_2$," *J. Mater. Chem.* **2002**, *12*, 3533-3540.

[73] D. Y. Zhao, P. D. Yang, N. Melosh, J. Feng, B. F. Chmelka, G. D. Stucky, "Continuous Mesoporous Silica Films with Highly Ordered Large Pore Structures," *Adv. Mater.* **1998**, *10*, 1380-1385.

[74] F. Kleitz, T. W. Kim, R. Ryoo, "Phase Domain of the Cubic *Im*3*m* Mesoporous Silica in the $EO_{106}PO_{70}EO_{106}$-Butanol-H_2O System," *Langmuir* **2006**, *22*, 440-445.

[75] J. Fan, C. Z. Yu, T. Gao, J. Lei, B. Z. Tian, L. M. Wang, Q. Luo, B. Tu, W. Z. Zhou, D. Y. Zhao, "Cubic Mesoporous Silica with Large Controllable Entrance Sizes and Advanced Adsorption Properties," *Angew. Chem., Int. Ed.* **2003**, *42*, 3146-3150.

[76] T. Yu, H. Zhang, X. W. Yan, Z. X. Chen, X. D. Zou, P. Oleynikov, D. Y. Zhao, "Pore Structures of Ordered Large Cage-Type Mesoporous Silica FDU-12s," *J. Phys. Chem. B* **2006**, *110*, 21467-21472.

[77] J. Fan, C. Z. Yu, J. Lei, Q. Zhang, T. C. Li, B. Tu, W. Z. Zhou, D. Y. Zhao, "Low-Temperature Strategy to Synthesize Highly Ordered Mesoporous Silicas with Very Large Pores," *J. Am. Chem. Soc.* **2005**, *127*, 10794-10795.

[78] W. Z. Zhou, H. M. A. Hunter, P. A. Wright, Q. F. Ge, J. M. Thomas, "Imaging the Pore Structure and Polytypic Intergrowths in Mesoporous Silica," *J. Phys. Chem. B* **1998**, *102*, 6933-6936.

[79] R. Ryoo, J. M. Kim, C. H. Ko, C. H. Shin, "Disordered Molecular Sieve with Branched Mesoporous Channel Network," *J. Phys. Chem.* **1996**, *100*, 17718-17721.

[80] J. C. Jansen, Z. Shan, L. Marchese, W. Zhou, N. V.D. Puil, T. Maschmeyer, "A New Templating Method for Three-Dimensional Mesopore Networks," *Chem. Commun.* **2001**, 713-714.

[81] R. Mokaya, W. Jones, S. Moreno, G. Poncelet, "n-Heptane Hydroconversion over Aluminosilicate Mesoporous Molecular Sieves," *Catal. Lett.* **1997**, *49*, 87-94.

[82] J. Lee, J. Kim, T. Hyeon, "A Facile Synthesis of Bimodal Mesoporous Silica and Its Replication for Bimodal Mesoporous Carbon," *Chem. Commun.* **2003**, 1138-1139.

[83] F. Hoffmann, M. Cornelius, J. Morell, M. Fröba, "Silica-Based Mesoporous Organic-Inorganic Hybrid Materials," *Angew. Chem. Int. Ed.* **2006**, *45*, 3216-3251.

[84] A. Stein, B. J. Melde, R. C. Schroden, "Hybrid Inorganic-Organic Mesoporous Silicates-Nanoscopic Reactors Coming of Age," *Adv. Mater.* **2000**, *12*, 1403-1419.

[85] K. Moller, T. Bein, "Inclusion Chemistry in Periodic Mesoporous Hosts," *Chem. Mater.* **1998**, *10*, 2950-2963.

[86] G. A. Ozin, E. Chomski, D. Khushalani, M. J. MacLachlan, "Mesochemistry," *Curr. Opin. Colloid Interface Sci.* **1998**, *3*, 181-193.

[87] S. Inagaki, S. Guan, Y. Fukushima, T. Ohsuna, O. Terasaki, "Novel Mesoporous Materials with a Uniform Distribution of Organic Groups and Inorganic Oxide in Their Frameworks," *J. Am. Chem. Soc.* **1999**, *121*, 9611-9614.

[88] B. J. Melde, B. T. Holland, C. F. Blanford, A. Stein, "Mesoporous Sieves with Unified Hybrid Inorganic/Organic Frameworks," *Chem. Mater.* **1999**, *11*, 3302-3308.

[89] T. Asefa, M. J. MacLachlan, N. Coombs, G. A. Ozin, *Nature* **1999**, *402*, 867-871.

[90] W. J. Hunks, G. A. Ozin, "Periodic Mesoporous Phenylene silicas with Ether or Sulfide Hinge Groups-A New Class of PMOs with Ligand Channels," *Chem. Commun.* **2004**, 2426-2427.

[91] J. Alauzun, A. Mehdi, C. Reye, R. J. P. Corriu, "Direct Synthesis of Bifunctional Mesoporous Organosilicas Containing Chelating Groups in the Framework and Reactive Functional Groups in the Channel Pores," *J. Mater. Chem.* **2007**, *17*, 349-356.

CHAPTER 2 Literature Review on Periodic Mesoporous Organosilicas

2.1 Introduction

Periodic mesoporous organosilicas (PMOs) represent an exciting new class of organic-inorganic nanocomposites targeted for a broad range of applications such as catalysis [1-5], adsorption [6-10], and high-performance liquid chromatography [11]. The organic bridging groups in the PMOs framework can tune the chemical and physical properties of the mesostructured materials, such as the porosity, thermal stability, optical clarity, refractive index, hydrophobicity, and dielectric constant [12-15].

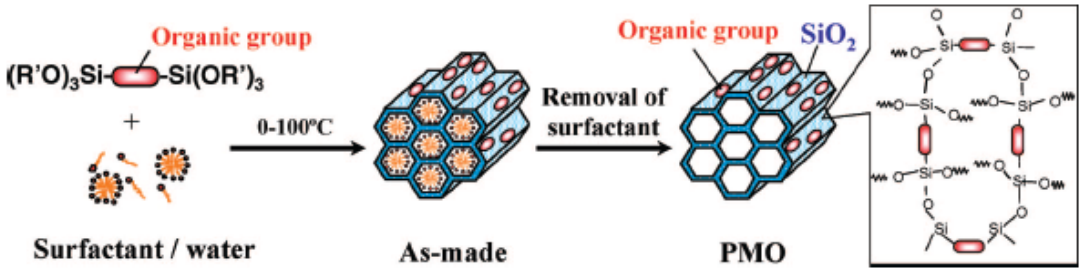

Figure 2.1. General synthetic pathway to PMOs that are from an organic-bridged silsesquioxane precursor, as ref [22].

The ordered mesoporous organosilicas have been prepared from 100 % silsesquioxane organic precursors by the surfactant-mediated synthesis strategy, with no cleavage of the C-Si bonds [16-19]. Therefore, PMOs can be produced with organic groups distributed totally homogeneously in the pore walls at a molecular level (Figure 2.1) [15, 20, 21].

In the present chapter, we review the history of the discovery and development of the PMOs emphasizing the most important advancements regarding composition, formation of large pores, and applications.

2.2 PMOs with Variable Organic Composition and its Derivatives

2.2.1 PMOs with Aliphatic Organic Groups

The hallmark of PMO was in 1999. In that year, for the first time, three different research groups successfully synthesized PMOs by assembling bridged organic precursors with supermolecules as templates. Some aliphatic organic groups successfully incorporated into PMOs are listed in Scheme 2.1.

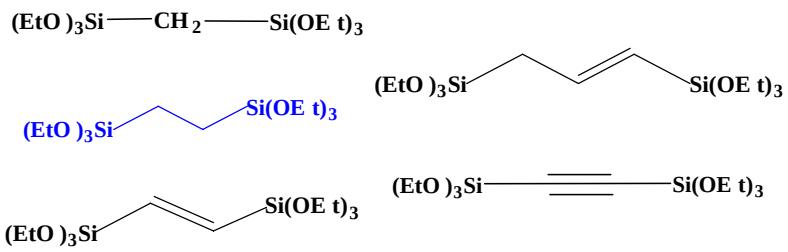

Scheme 2.1. Some silica precursors with aliphatic organic groups. (Note: OEt can be replaced by OMe)

The first of these groups was Inagaki and co-workers [16] who adopted cationic surfactant octadecyltrimethyl-ammonium chloride (OTAC) as a template, successfully synthesized ordered mesoporous organosilica hybrid phases, by assembling bridged dipodal alkoxysilane $(MeO)_3Si\text{-}CH_2CH_2\text{-}Si(OMe)_3$ (BTME) precursors under basic conditions. The two-dimensional (2D) and three-dimensional (3D) hexagonal mesostructures were produced by tuning the mixture ratios of the components in the reaction mixture. The corresponding pore size is 3.1 and 2.7 nm, surface area is 750 and 1170 $m^2 \cdot g^{-1}$, respectively. The methyl group is relatively stable, as confirmed by thermogravimetric analysis (TGA). It was shown that the Si-C bond can be cleaved above 400 °C. Furthermore, X-ray diffractometer (XRD) patterns confirmed that these materials had good hydrothermal stability after boiling at 100 °C for 8 hrs.

In 1999, Ozin and workers [17] prepared a series of PMOs with $(EtO)_3Si\text{-}CH{=}CH\text{-}Si(OEt)_3$ (BTE) as an organic precursor and cetyltrimethyl ammonium bromide (CTAB) as structure-directing agent (SDA) under basic conditions. The ethylene bonds are cleaved partly between 150 and 350 °C confirmed by TGA, which showed that the bromide reaction has occurred on double bond. Bromination reaction occurred on the C=C bonds with a degree of 10 %.

In the same year, the group of Stein [18] reported the synthesis of an ethene-bridged PMO material which was prepared with the same precursor and surfactant under basic conditions. The surface area of the wormlike material is approximately 1200 $m^2 \cdot g^{-1}$.

In a further study, Sayari and co-workers [23] investigated the influence of the chain length (carbon atoms varing from 10 to 18) of the surfactant on the synthesis of ethane-bridged PMOs. It was found that the pore diameter increased with increasing length of the surfactant, while the specific surface areas didn't show a clear trend.

An ethane-bridged PMO material with cubic symmetry (*Pm*3*n*) similar to SBA-1 was synthesized for the first time by using BTME as an organosilica precursor and hexadecyltrimethylammonium chloride (CTAC) as SDA in basic media [24, 25].

Under acidic conditions, the ethane-bridged PMOs could also be prepared. Zhao's group [26] obtained ethane-bridged PMOs by using triblock copolymer P123 ($EO_{20}PO_{70}EO_{20}$, EO = ethylene oxide, PO = propylene oxide) as a template under an acid condition. It was found that BTME is a better organosilica precursor than 1,2-bis(triethoxysilyl)ethane (BTSE). After that, they also investigated the influence of parameters on the final mesoporous structure, and finally got a series of SBA-15/PMO with interconnected micropores and mesopores.

The common organic precursors were mostly with short aliphatic chains, such as ethane and ethylene, because they are widely available, and with good physical geometrical stress [27-29]. However, the inherent hydrophobic character and steric structure may lead to a phase separation, poor organization of mesostructures, or disordered mesoporous materials. It is believed that alkyl chains should not be longer than six carbons. The ability to maintain the mesostructured frameworks is a concern with flexible organic bridges. Long chain bridged organic groups or large oligomeric building units easily form layered mesostructures rather than stable PMOs mainly due to the intramolecular cross-linkages. The hydrolysis of these organosilica precursors is difficult to control in solution. The layered materials with space 1.2 nm were successfully synthesized with organosilica precursor $(MeO)_3Si\text{-}(CH_2)_8\text{-}Si(OMe)_3$ by sol-gel method. It is necessary to employ templates with sufficient diameters to allow uniform encapsulation by the polymerizing bridge-bonded silsesquioxanes. It is obvious that the relationship between structure, function and application is very important, therefore, the selection and protection of functional organic groups should be considered in the synthesis process.

2.2.2 PMOs with Aromatic Organic Groups

By contrast with the PMOs described above containing only saturated aliphatic or ethene organic groups, much effort was put into the preparation of PMO materials with aromatic bridges, as more functionality can be introduced into the framework of PMOs. Some aromatic organic groups are listed in Scheme 2.2.

The first phenylene-bridged PMO material was reported by Ozin *et al.* [19] in 1999. The synthesis was performed with using 1,4-bis(triethoxysilyl)benzene (BTEB) and

2,5-bis(triethoxysilyl)thiophene (BTET) as precursors in the presence of CTAB as a SDA. It was noted that the well-ordered mesoporous material without Si-C bond cleavage could be achieved by using hexadecylpyridinium chloride (CPC) as SDA under a mild acidic condition, whereas all the organic groups were broken in the presence of ammonia.

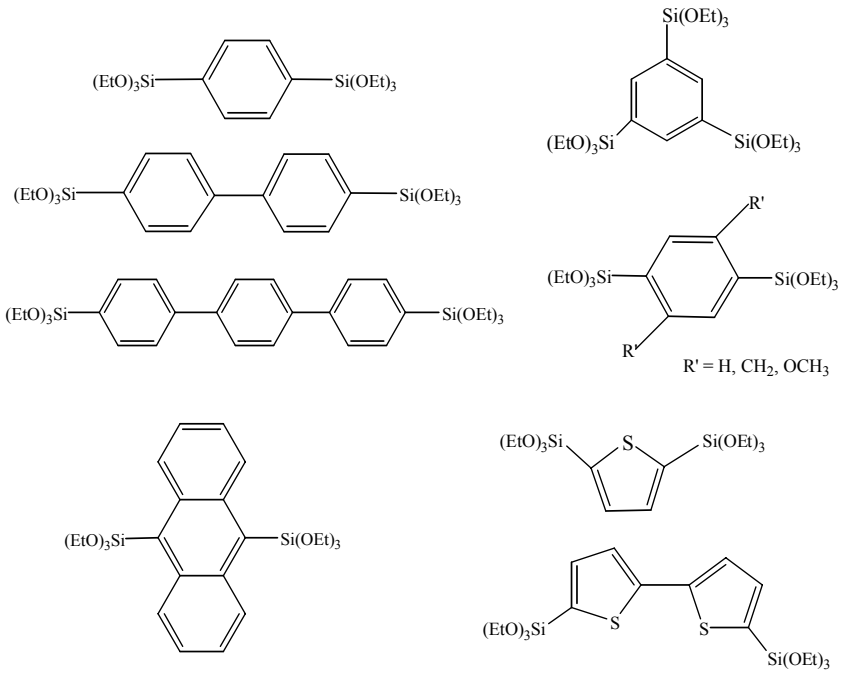

Scheme 2.2. Some orgainosilica precursors with aromatic organic groups. (Note: OEt can be replaced by OMe)

Ozin also [30] successfully synthesised 2D hexagonal PMO materials by using lab-made precursors (1,4-bis(triethoxysilyl)-2-methylbenzene, 1,4-bis(triethoxysilyl)-2,5-dimethylbenzene, and 1,4-bis (triethoxysilyl)-2,5-dimethoxybenzene) and CPC as a SDA under acidic conditions. The pore diameter was 2.3 nm and specific surface areas varied between 560 and 1100 $m^2 \cdot g^{-1}$. The aryl bridges could be stable below 360 °C detected by TGA.

In addition, some aromatic groups containing sulfide bridges were also used as precursors to prepare 4-phenyl ether and 4-phenyl sulfide bridged PMOs using Brij-76 ($C_{18}EO_{10}$) as a template [31]. The pore diameter and specific surface area were about 3 nm and 630 $m^2 \cdot g^{-1}$, respectively. The wall thickness of this wormlike material was about 3.0 nm.

Ozin's group synthesized thiophene-bridged PMOs by using the BTET precursor and CTAB as a template [19]. It was found that mild acidic condition was better for avoiding the cleavage of Si-C bonds, compared with that under basic conditions.

Furthermore, highly ordered bifunctional PMOs containing aromatic thiophene and benzene groups were successfully synthesized using BTET and BTEB as organosilica precursors and the triblock copolymer Pluronic P123 and the oligomeric surfactant Brij-76 as surfactants under acidic conditions [32]. The 2D hexagonal PMO material has a pore size of 5.4 nm.

2.2.2.1 PMOs with Crystal-Like Pore Walls

Ordered PMO materials with crystal-like pore walls were produced by several groups. The molecular periodicity in the pore walls could enhance the functionalities of PMOs in electronic, optical, and sensors. In this section, we discuss some ordered PMO mesostructures with molecular periodicity in the pore walls.

The first ordered benzene-bridged PMOs with crystal-like pore walls was synthesized by using BTEB in the presence of OTAC as SDA under basic conditions [33]. The Brunauer-Emmett-Teller (BET) specific surface area and pore size of the hexagonal benzene-bridged PMO were 818 $m^2 \cdot g^{-1}$ and 3.8 nm, respectively. Due to the π-π stacking of benzene bridging groups, the molecular periodicity in the pore walls along the channel directions was observed. The spacing of 7.6 Å along the channel direction detected by transmission electrons microscopy (TEM) confirmed the atomic-scale periodicity in the pore walls. Furthermore, TGA results showed that benzene groups were kept in the walls up to 500 °C in air or nitrogen, and the meso- and molecular-scale periodicity was completely preserved even after boiling the material in water for 8 hrs.

In a further study, 1,4-benzene-bridged PMO materials having crystal-like pore walls were prepared by using C14 to C18 trimethylammonium halide surfactants under basic conditions. The pore diameter increased with the increasing of the length of the hydrocarbon chain (C14 to C18) of the surfactant [34].

Later, Inagaki and his co-workers reported the post-synthesis treatment with basic solution to form molecular-scale periodicity within the pore walls of phenyl-bridged PMOs by using the triblock copolymer P123 as a template [35]. The mesopore structural arrangement and wall thickness appeared to decrease with the increase of basic concentration.

Interestingly, a nonlinear symmetrically bridged organosilica precursor, 1,3-bis(triethoxysilyl)benzene, was also used to prepare the crystal-like PMO material reported by Kapoor *et al.* [36]. The molecular spacing of phenyl group is 7.6 Å too.

Inagaki and co-workers demonstrated the synthesis of ordered PMO with molecular-scale periodicity prepared by using 4,4'-bis(triethoxysilyl)biphenyl (BTEBP) as the organosilica precursor in the presence of OTAC under basic conditions [37]. The BET specific surface area and pore size were 869 $m^2 \cdot g^{-1}$ and 3.5 nm, respectively. Hydrophobic biphenyl layers and hydrophilic silicate layers are arranged alternately at an interval of 11.6 Å along the channel direction. It should be pointed out that the ordered PMOs with crystal-like walls can also be obtained with other organic precursors, including BTSEB, bis(triethoxysilylethen-2-yl)benzene ($(C_2H_5O)_3Si\text{-}CH{=}CH\text{-}C_6H_4\text{-}CH{=}CH\text{-}Si(OC_2H_5)_3$) [28]. It was found that carbon-carbon double bonds and phenylene groups of BTSEB enable PMO materials with more chemical modifications. Fröba *et al.* synthesized the same vinylbenzene-bridged PMO with a pore size of 2.7 nm and a specific surface area of 800 $m^2 \cdot g^{-1}$ [38]. Therefore, the selection of organosilica precursors was a key issue identified by researchers.

In addition, Moyaka *et al.* synthesized ethylene-bridged PMO with crystal-like pore walls using BTE and CTAB as a template under basic conditions [39]. The BET specific surface area and pore size were 1300 $m^2 \cdot g^{-1}$ and 4 nm, respectively. The basal spacing between ethylene groups was 5.6 Å.

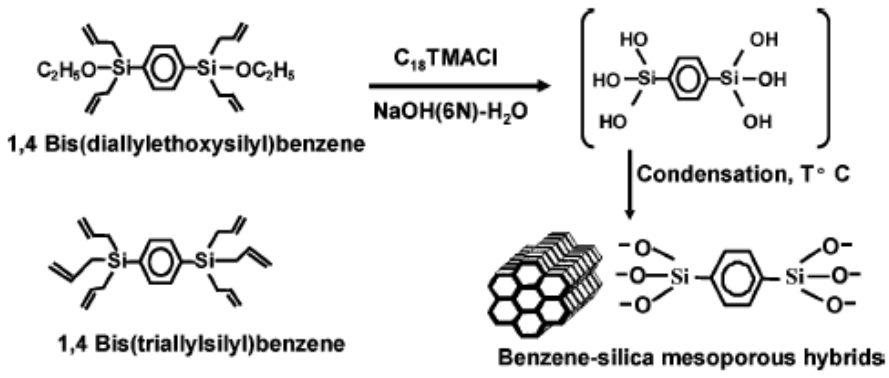

Figure 2.2. Alternate route for the synthesis of mesoporous phenylene-silicas from allylorganosilane precursors, as ref [40].

In another attempt, the ordered PMO materials with crystal-like pore walls were prepared by using the new bridged allylorganosilane precursors under basic conditions upon surfactant-assisted assembly (Figure 2.2) [40]. The BET specific surface area and pore size were 744 $m^2 \cdot g^{-1}$ and 2.4 nm, respectively. This work showed that the synthesis could be performed using alternative organosilane precursors, other than the existing ones that are difficult to obtain in high purity.

2.2.3 PMOs with Special Organic Groups

As mentioned above, the PMOs prepared with relatively small aromatic organic groups are constructed from bissilylated precursors, and the corresponding large-pore PMOs with ordered mesostructures can be prepared with non-ionic block polymers. By comparison, some special organosilica precursors are introduced into the PMO framework, thus a new kind of PMO material is formed.

It is worth mentioning that one hexagonal PMO structure was prepared with tris[3-(trimethoxysilyl)propyl]isocyanurate (ICS) and tetraethyl orthosilicate (TEOS) as precursors [41]. The pore size was less than 5 nm. This material has potential applications in adsorption of heavy metal ions.

Corriu's group synthesized functional mesoporous organosilicas containing chelating groups in the framework and reactive functional groups in the pores [42]. This material was obtained in one step by direct synthesis using co-condensation of TEOS and a organosilica precursor, 1,4,8,11-tetrakis[(triethoxysilyl)propyl]-1,4,8,11-tetraazacyclotetradecane, in the presence of the triblock copolymer P123 as a template. The content of the organic component in the framework was up to 33 wt %. A highly ordered mesostructure was not obtained, but monodisperse channel pores (pore size of 11 nm) with no long-range order formed.

In addition, the vanadyl Schiff bases with catalysis activity, such as Co(II) salen and VO(salen) [43, 44], were introduced into the PMOs framework, thus increases the PMO diversity and application in catalysis. Therefore, the constituent of organosilica precursor has a strong relationship with the potential application of PMO products, and should be considered in future work.

As the organic groups endow PMOs with the desired properties, it is necessary to find new organic precursors, which are different from silsesquioxanes of the type $(RO)_3Si\text{-}R'\text{-}Si(OR)_3$. That is to say, a high replacement of bridging O atoms by organic groups needs to be developed, so that the physical and chemical properties could be improved. Such nanocomposites consisting of SiO_2R_2, $SiOR_3$, or SiR_4 building units are called "high organic group content PMOs" [15].

Ozin's group took a lead in this aspect. A three-ring precursor was used and successfully self-assembled into a family of novel PMOs, which has a higher percentage of organic groups [27]. This kind of PMO has a uniform and highly ordered mesostructure and a high surface area of around 1700 $m^2 \cdot g^{-1}$. The PMO also

shows excellent thermal stability. No loss of organic groups occurs up to 500 °C in a nitrogen atmosphere, and the mesostructure does not change in terms of pore size and regularity. Interestingly, this PMO undergoes a similar distinctive thermal transformation as the methane-bridged PMOs, transforming CH_2 groups into CH_3 groups through the elimination of silanols between 300 and 500 °C.

To further improve the content of organic groups in the framework, Ozin and his co-workers [45] adopted a chemical reaction to make two separated $[Si(CH_2)]_3$ ring connected together, thus forming one kind of hybrid organosilicas with aliphatic and aromatic groups. The BET specific surface area and pore size are 967 $m^2 \cdot g^{-1}$ and 6.9 nm, respectively. The organic groups are stable at 400 °C in nitrogen atmosphere. These kinds of materials enrich the PMO structures and provide more opportunity for applications.

2.2.4 Carbon/Silica Nanocomposites Converted from PMOs

Pang *et al.* developed benzene-bridged PMO to other mesoporous materials [46]. They treated the PMO with crystal-like pore walls for 4 h at 900 ºC in nitrogen, and obtained ordered mesoporous carbon/silica nanocomposite materials with pore walls uniformly constructed from carbon and silica units, but without crystal-like pore walls The benzene units in the pore walls were pyrolysized into carbon after carbonization. The pore size was decreased from 2.5 to 2.0 nm by thermal treatment. By a further removal of the silica components from carbon/silica composites, disordered mesoporous carbon was obtained. This was a significant step in carbon synthesis since mesostructured carbon could be directly prepared through one-step compared with the two-step nanocasting method.

2.2.5 Nonsilica-based Nanocomposites Similar to PMOs

A new kind of inorganic-organic hybrid framework, called nonsilica-based mesoporous material was successfully synthesized using phosphonic acid by the surfactant templating similar to the synthesis of silica-based PMO materials [47-49]. Kimura reported a hexagonal mesoporous aluminum organophosphonate (AOP-2) by using a diphosphonic acid ($(HO)_2OPCH_2PO(OH)_2$) as a precursor and OTAC as a surfactant [47]. The mesostructure of AOP-2 is composed of alternative aluminophosphate-like domains and the bridged organic groups through Al-O-P bonds. Furthermore, Mutin *et al.* [50] also synthesised ordered mesoporous aluminum

organophosphonates by using aluminum chloride, methylene, ethylene, and propylene phosphonates as precursors, and the triblock copolymers P123, F68 ($EO_{80}PO_{27}EO_{80}$), and F127 ($EO_{106}PO_{70}EO_{106}$) as surfactants. The synthesis of non-siliceous nanocomposites not only enrich the applications of such materials in electronics, optics, but also provide opportunities for the preparation of nonsilica-based hybrid frameworks, as a variety of components could be introduced into the framework through metal-P bonds.

2.3 PMOs with Large Pores

2.3.1 Large-Pore PMOs with Ethane Bridging Groups

Much effort was put into the synthesis of enlarging the pore size of PMOs, as large-pore PMO materials have potential applications in catalysis, adsorption and separation. The pore sizes of the PMOs prepared with cationic alkyl ammonium surfactants (with chain lengths from C12 to C20) were from 2 to 5 nm. By contrast, large-pore PMO materials were obtained by using different triblock copolymers such as P123, F127, or B50-6600 ($EO_{39}BO_{47}EO_{39}$, BO = butyleneoxide) under acidic conditions by the $S^+X^-I^+$ pathway [26, 51-60].

The first 2D hexagonal large-pore PMOs was synthesized with BTME as a precursor and P123 as a template under an acidic condition in 2001 [55]. The BET specific surface area and pore size were 913 $m^2 \cdot g^{-1}$ and 6.5 nm, respectively.

The pore size expanding methods that are efficient for MPS materials have been utilized in an attempt to prepare large-pore PMOs. The use of 1,3,5-trimethylbenzene (TMB) in a triblock copolymer F127 templating synthesis resulted in a pore size of 8 nm, but the PMO mesostructural regularity could not be maintained [54]. In addition, the TMB amount had an effect on the mesostructure. A worm-like PMO composite was prepared without TMB, while the pore size could be enlarged from 6 to 20 nm by increasing the TMB amount in the reaction mixture of BTSE and P123. Moreover, a mesostructure transformation occurred from hexagonal arrays to spherical pores [61].

The effect of reaction parameters, such as the ratio of the organosilica precursor and P123 in the reaction mixture, acid concentration and addition of inorganic salts on the final mesostructure of ethane-bridged PMOs was also studied by researchers [26, 57, 59, 62]. The pore size and morphologies of the ethane-bridged PMO materials could be tuned by adjusting the acid concentrations without the aid of inorganic salts. It is also interesting to find that inorganic salts, such as sodium chloride (NaCl) could

improve the degree of order of large-pore PMO materials, as the inorganic salts enhanced the interaction between the positively charged head group of the surfactant and the inorganic silica species [57].

The triblock copolymer P123 usually leads to the 2D hexagonal phase in the synthesis of large-pore PMOs. By comparasion, large-pore PMOs with cubic structure are obtained under acidic conditions by using F127 or B50-6600 as a template. Thus, Cho *et al.* [63] prepared a large-pore ethane-bridged PMO by co-condensation of BTSE (<10 % by weight) and TEOS in the presence of the triblock copolymer F127. The cubic mesostructure is similar to that of SBA-16. Another large-pore ethane-bridged PMO with cubic symmetry (*Im*3*m*) were obtained with BTME (100 % by weight) as an organosilica precursor and F127 as a template under acidic conditions with the addition of K_2SO_4 [51]. The BET specific surface area and pore size were 989 $m^2 \cdot g^{-1}$ and 9.8 nm, respectively. Followed these, a highly ordered ethane-bridged PMO material was reported to exhibit an *Fm*3*m*-symmetric cage-like pore system [54]. It was synthesized by using BTME (100 % by weight) and F127 under acidic conditions and with the addition of potassium chloride (KCl). The BET specific surface area and pore size were 796 $m^2 \cdot g^{-1}$ and 5.6 nm, respectively.

More recently, combined with CFM pathway and low temperature (~ 10 – 15 ºC) synthesis method, a highly ordered ethane-bridged PMO material with a cage-like pore system (*Fm*3*m*) was obtained with the use of BTME as an organosilica precursor, triblock copolymer F127 as the template and TMB as the swelling agent under acidic conditions [64]. The pore size was up to 14.7 nm, an ultralarge one till now.

Using the more hydrophobic triblock copolymer B50-6600 as a template, a cubic ethane-bridged PMO composite was synthesized under acidic conditions with cagelike pores (pore size up to 10 nm) [65].

The PMO materials mentioned above were synthesized by a cooperative formation mechanism. By constrast, by the TLCT pathway, a large-pore ethane-bridged PMO composite was prepared by using a liquid-crystalline phase as templates [56]. This PMO material exhibited ordered 2D hexagonal mesostructure. The BET specific surface area and pore size were 957 $m^2 \cdot g^{-1}$ and 7.7 nm, respectively.

2.3.2 Large-Pore PMOs with Functional Groups

In comparison with large-pore ethane-bridged PMO materials synthesized with BTME and BTSE precursors, the PMO composites with large pores and complex organic groups offer more opportunities for chemical modification.

The first 2D hexagonal benzene-bridged PMO with large pores was synthesized under an acidic condition [66]. However, unlike the corresponding benzene-bridged silicas synthesized under a basic condition in the presence of alkylammonium surfactants, this material has no crystal-like pore walls. The BET specific surface area and pore size are 1029 $m^2 \cdot g^{-1}$ and 7.4 nm, respectively. The framework was stable up to 550 °C.

The ordered ethene-bridged PMO material with pore size up to 8.0 nm was obtained by the addition of butanol to the polymeric reaction solution [67]. About 30 % of the ethene bridging groups took the bromination reaction. Moreover, thiophene organic groups were introduced into the PMO framework [68]. The thiophene-bridged PMO had 2D hexagonal mesostructure which was analogous to that of SBA-15. The BET specific surface area and pore size were 550 $m^2 \cdot g^{-1}$ and 5 ~ 6 nm, respectively. The solid could be stable up to 400 ºC in air within less than 4 % cleavage of the Si-C bonds.

At present, enlarging the pore size of ordered PMO materials is still a significant challenge, as reports on large-pore PMOs with complex organic groups are rare. Much effort was therefore devoted in this project to the synthesis of large-pore PMO materials with the aid of triblock copolymers.

2.4 Applications of PMOs

2.4.1 Chromatography

For chromatographic applications such as high-performance liquid chromatography (HPLC), spherical particles with an average size of about 5 ~ 10 μm and a very narrow size distribution are preferred. The benzene-bridged PMO particles with tunable diameters between 3 and 15 μm have been synthesized, and this material could separate three different mixtures containing up to four components with different polarities [11]. Moreover, the spherical PMO particles with ethane bridging groups in the framework has a diameter between 1.4 and 2.5 μm, which can be used for HPLC applications [69]. By using this composite, eight components were separated within both columns.

2.4.2 Adsorbents

The flexibility of the organic bridging groups and large surface area of PMO composites provide good opportunities for the application of PMO materials applying to the sorption area. The 2D tetrasulfide-bridged PMO materials were synthesized with organic precursor $(EtO)_3Si(CH_2)_3S\text{-}S\text{-}S\text{-}S\ (CH_2)_3Si(OEt)_3$ and TEOS by the co-condensation method [8]. This material could remove several different kinds of metal cations from aqueous solution. However, it especially showed a high affinity for Hg^{2+} cations with a loading of 2710 $mg \cdot g^{-1}$. Meanwhile, another hexagonal PMO structure with pore size less than 5 nm was prepared with ICS and TEOS as precursors [41]. This material also exhibited high affinity to Hg (II) ions with 1.8 g of Hg^{2+}/g of adsorbent.

2.4.3 Low-k Materials

The PMO thin-films are important as they can be used in the applications of sensors, and microelectronics. Using the evaporation induced self assembly (EISA) method, ethane-bridged PMO films were prepared with different amount of TEOS during the synthesis process [70]. It was found that the dielectric values increased with decreasing the amount of organic moieties in the framework. Furthermore, by employing the spin-coating method, PMO films with different organic bridging groups were obtained and their low dielectric constant properties were also studied [71].

2.4.4 Catalysis

It was noted that much effort was put into the catalysis studies of PMO materials in the past years.

PMOs with sulfonic acid groups, PMO-SO_3H was the most studied one. Yuan *et al.* [72] synthesized ethane-bridged PMO-SO_3H exhibiting an acid capacity up to 0.93 $mmol \cdot g^{-1}$. Its activity could be retained for more than 25 h, which was higher than that of MCM-41-SO_3H.

In a further study, PMO-SO_3H with ethane- or benzene-bridging groups in the framework was prepared by co-condensation method under acidic conditions [1]. This material showed high catalytic ability for the condensation of phenol and acetone to form bisphenol A, which is an important precursor in resin and polymer chemistry. It

was interesting that the ethane-bridged PMO-SO_3H material showed higher catalytic activity than the corresponding benzene-bridged PMO one. Similarly, in another study, Yang *et al.* provided some explaination for the higher activity of ethane organic groups, where its pore surface structures could enhance the selectivity and activity during esterification [73].

Furthermore, heteroatoms were introduced into the PMO framework to improve the catalytic properties of the materials. The ethane-bridged titanium-incorporated PMO material with gold nanoparticles could enhance vapor-phase epoxidation of propene using H_2 and O_2 [74]. And the ethane-bridged aluminum-incorporated PMO material showed superiority in acid catalysis [75]. Meanwhile, the PMO with palladium nanowires inside exhibited better catalysis ability for detecting the reaction rate of CO oxidation in the presence of excess O_2 [76]. Based on the above mentioned, it is proposed that PMO materials could be a basis for creation of efficient catalysts in future.

2.4.5 Photochemistry

Photochemical PMOs were also studied by some researchers. Garcia *et al.* synthesized a PMO containing 4,4′-bipyridinium units, which could be used as electron-acceptor termini in photochemical and thermal activation [77]. The azobenzene-bridged PMO was synthesized by using 4,4′-[[(triisopropoxysilyl) propyl]oxy]azobenzene as the precursor, which showed photoresponsive properties [78]. Moreover, the polydiacetylene-bridged PMO material was obtained by using diacetylene-bridged silsesquioxane as organic precursor and CTAB as a template, which was reported by Peng and co-workers [79]. This composite exhibited 2D hexagonal mesostructure with *p6mm* symmetry. The reversible chromatic rapid responses to external stimuli were demonstrated by subjecting this material to thermal cycles between 20 and 103 °C.

References

[1] Q. H. Yang, J. Liu, J. Yang, M. P. Kapoor, S. Inagaki, C. Li, “Synthesis, Characterization, and Catalytic Activity of Sulfonic Acid-Functionalized Periodic Mesoporous Organosilicas,” *J. Catal.* **2004**, *228*, 265-272.

[2] S. Hamoudi, S. Royer, S. Kaliaguine, "Propyl- and Arene-Sulfonic Acid Functionalized Periodic Mesoporous Organosilicas," *Micropor. Mesopor. Mater.* **2004**, *71*, 17-25.

[3] Q. H. Yang, M. P. Kapoor, S. Inagaki, N. Shirokura, J. N. Kondo, K. Domen, "Catalytic Application of Sulfonic Acid Functionalized Mesoporous Benzene-Silica with Crystal-Like Pore Wall Structure in Esterification," *J. Mol. Catal. A* **2005**, *230*, 85-89.

[4] K. Nakajima, I. Tomita, M. Hara, S. Hayashi, K. Domen, J. N. Kondo, "A Stable and Highly Active Hybrid Mesoporous Solid Acid Catalyst," *Adv. Mater.* **2005**, *17*, 1839-1842.

[5] Y. Wan, D. Q. Zhang, Y. P. Zhai, C. M. Feng, J. Chen, H. X. Li, "Periodic Mesoporous Organosilicas: A Type of Hybrid Support for Water-Mediated Reactions," *Chem. Asian J.* **2007**, *2*, 875-881.

[6] M. C. Burleigh, S. Dai, E. W. Hagaman, J. S. Lin, "Imprinted Polysilsesquioxanes for the Enhanced Recognition of Metal Ions," *Chem. Mater.* **2001**, *13*, 2537-2546.

[7] S. Dai, M. C. Burleigh, Y. H. Ju, H. J. Gao, J. S. Lin, S.J. Pennycook, C. E. Barnes, Z. L. Xue, "Hierarchically Imprinted Sorbents for the Separation of Metal Ions," *J. Am. Chem. Soc.* **2000**, *122*, 992-993.

[8] L. X. Zhang, W. H. Zhang, J. L. Shi, Z. L. Hua, Y. S. Li, J. N. Yan, "A New Thioether Functionalized Organic-Inorganic Mesoporous Composite as a Highly Selective and Capacious Hg^{2+} Adsorbent," *Chem. Commun.* **2003**, 210-211.

[9] J. Liu, J. Yang, Q. H. Yang, G. Wang, Y. Li, "Hydrothermally Stable Thioether-Bridged Mesoporous Materials with Void Defects in the Pore Walls," *Adv. Funct. Mater.* **2005**, *15*, 1297-1302.

[10] K. Z. Hossain, L. Mercier, "Intraframework Metal Ion Adsorption in Ligand-Functionalized Mesoporous Silica," *Adv. Mater.* **2002**, *14*, 1053-1056.

[11] V. Rebbin, R. Schmidt, M. Fröba, **"**Spherical Particles of Phenylene-Bridged Periodic Mesoporous Organosilica for High-Performance Liquid Chromatography," *Angew. Chem. Int. Ed.* **2006**, *45*, 5210-5214.

[12] M. C. Burleigh, M. A. Markowitz, M. S. Spector, B. P. Gaber, "Direct Synthesis of Periodic Mesoporous Organosilicas: Functional Incorporation by Co-condensation with Organosilanes," *J. Phys. Chem. B.* **2001**, *105*, 9935-9942.

[13] Q. H. Yang, M. P. Kapoor, S. Inagaki, "Sulfuric Acid-Functionalized Mesoporous Benzene-Silica with a Molecular-Scale Periodicity in the Walls," *J. Am. Chem. Soc.* **2002**, *124*, 9694-9695.

[14] Q. H. Yang, J. Yang, J. Liu, Y. Li, C. Li, "Synthesis and Characterization of Phosphonic Acid Functionalized Organosilicas with Bimodal Nanostructure," *Chem. Mater.* **2005**, *17*, 3019-3024.

[15] B. Hatton, K. Landskron, W. Whitnall, D. Perovic, G. A. Ozin, "Past, Present, and Future of Periodic Mesoporous Organosilicas: The PMOs," *Acc. Chem. Res.* **2005**, *38*, 305-312.

[16] S. Inagaki, S. Guan, Y. Fukushima, T. Ohsuna, O. Terasaki, "Novel Mesoporous Materials with a Uniform Distribution of Organic Groups and Inorganic Oxide in Their Frameworks," *J. Am. Chem. Soc.* **1999**, *121*, 9611-9614.

[17] T. Asefa, M. J. MacLachlan, N. Coombos, G.A. Ozin, "Periodic Mesoporous Organosilicas with Organic Groups inside the Channel Walls," *Nature* **1999**, *402*, 867-871.

[18] B. J. Melde, B. T. Holland, C. F. Blanford, A. Stein, "Mesoporous Sieves with Unified Hybrid Inorganic/Organic Frameworks," *Chem. Mater.* **1999**, *11*, 3302-3308.

[19] C. Y. Ishii, T. Asefa, N. Coombs, M. J. MacLachlan, G. A. Ozin, "Periodic Mesoporous Organosilicas, PMOs: Fusion of Organic and Inorganic Chemistry Inside the Channel Walls of Hexagonal Mesoporous Silica," *Chem. Commun.* **1999**, 2539-2540.

[20] F. Hoffmann, M. Cornelius, J. Morell, M. Fröba, "Periodic Mesoporous Organosilicas (PMOs): Past, Present, and Future," *J. Nanosci. Nanotechnol,* **2006**, *6*, 265-288.

[21] F. Hoffmann, M. Cornelius, J. Morell, M. Fröba, M. **"**Silica-Based Mesoporous Organic-Inorganic Hybrid Materials," *Angew. Chem. Int. Ed.* **2006**, *45*, 3216-3251.

[22] S. Fujita, S. Inagaki, "Self-Organization of Organosilica Solids with Molecular-Scale and Mesoscale Periodicities," *Chem. Mater.* **2008**, *20*, 891-908.

[23] S. Hamoudi, Y. Yang, I. L. Moudrskovski, S. Lang, A. Sayari, "Synthesis of Porous Organosilicates in the Presence of Alkytrimethylammonium Chlorides: Effect of the Alkyl Chain Length," *J. Phys. Chem. B* **2001**, *105*, 9118-9123.

[24] S. Guan, S. Inagaki, T. Ohsuna, O. Terasaki, "Cubic Hybrid Organic-Inorganic Mesoporous Crystal with a Decaoctahedral Shape," *J. Am. Chem. Soc.* **2000**, *122*, 5660-5661.

[25] A. Sayari, S. Hamoudi, Y. Yang, I. L. Moudrakovski, J. R. Ripmeester, "New Insights into the Synthesis, Morphology, and Growth of Periodic Mesoporous Organosilicas," *Chem. Mater.* **2000**, *12*, 3857-3863.

[26] X. Y. Bao, X. S. Zhao, X. Li, P. A. Chia, J. Li, "A Novel Route toward the Synthesis of High-Quality Large-Pore Periodic Mesoporous Organosilicas," *J. Phys. Chem. B* **2004**, *108*, 4684-4689.

[27] K. Landskron, B. D. Hatton, D. D. Perovic, G. A. Ozin, "Periodic Mesoporous Organosilicas Containing Interconnected $[Si(CH_2)]_3$ Rings," *Science* **2003**, *302*, 266-269.

[28] A. Sayari, W. H. Wang, "Molecularly Ordered Nanoporous Organosilicates Prepared with and without Surfactants," *J. Am. Chem. Soc.* **2005**, *127*, 12194-12195.

[29] W. J. Hunks, G. A. Ozin, "Periodic Mesoporous Organosilicas with Phenylene Bridging Groups, 1,4-$(CH_2)_nC_6H_4$ (n = 0-2)," *Chem. Mater.* **2004**, *16*, 5465-5472.

[30] G. Temtsin, T. Asefa, S. Bittner, G. A. Ozin, "Aromatic PMOs: Tolyl, Xylyl and Dimethoxyphenyl Groups Integrated within the Channel Walls of Hexagonal Mesoporous Silicas," *J. Mater. Chem.* **2001**, *11*, 3202-3206.

[31] W. J. Hunks, G. A. Ozin, "Periodic Mesoporous Phenylene silicas with Ether or Sulfide Hinge Groups-A New Class of PMOs with Ligand Channels," *Chem. Commun.* **2004**, 2426-2427.

[32] J. Morell, M. Gungerich, G. Wolter, J. Jiao, M. Hunger, M. J. Klar, M. Fröba, "Synthesis and Characterization of Highly Ordered Bifunctional Aromatic Periodic Mesoporous Organosilicas with Different Pore Sizes," *J. Mater. Chem.* **2006**, *16*, 2809-2818.

[33] S. Inagaki, S. Guan, T. Ohsuna, O. Terasaki, "An Ordered Mesoporous Organosilica Hybrid Material with A Crystal-Like Wall Structure," *Nature* **2002**, *416*, 304-307.

[34] N. Bion, P. Ferreira, A. Valente, I. S. Goncalves, J. Rocha, "Ordered Benzene-Silica Hybrids with Molecular-Scale Periodicity in the Walls and Different Mesopore Sizes," *J. Mater. Chem.* **2003**, *13*, 1910-1913.

[35] Y. Goto, K. Okamoto, S. Inagaki, "The Formation of Periodicity within the Pore Walls of Mesoporous Organosilica by Post-Synthesis Treatment," *Bull. Chem. Soc. Jpn.* **2005**, *78*, 932-936.

[36] M. P. Kapoor, Q. H. Yang, S. Inagaki, "Organization of Phenylene-Bridged Hybrid Mesoporous Silisesquioxane with a Crystal-Like Pore Wall from a Precursor with Nonlinear Symmetry," *Chem. Mater.* **2004**, *16*, 1209-1213.

[37] M. P. Kapoor, Q. H. Yang, S. Inagaki, "Self-Assembly of Biphenylene-Bridged Hybrid Mesoporous Solid with Molecular-Scale Periodicity in the Pore Walls," *J. Am. Chem. Soc.* **2002**, *124*, 15176-15177.

[38] M. Cornelius, F. Hoffman, M. Fröba, "Periodic Mesoporous Organosilicas with a Bifunctional Conjugated Organic Unit and Crystal-like Pore Walls," *Chem. Mater.* **2005**, *17*, 6674-6678.

[39] Y. Xia, W. Wang, R. Moyaka, "Bifunctional Hybrid Mesoporous Organoaluminosilicates with Molecularly Ordered Ethylene Groups," *J. Am. Chem. Soc.* **2005**, *127*, 790-798.

[40] M. P. Kapoor, S. Inagaki, S. Ikeda, K. Kakiuchi, M. Suda, T. Shimada, "An Alternate Route for the Synthesis of Hybrid Mesoporous Organosilica with Crystal-Like Pore Walls from Allylorganosilane Precursors," *J. Am. Chem. Soc.* **2005**, *127*, 8174-8178.

[41] O. Olkhovyk, M. Jaroniec, "Periodic Mesoporous Organosilica with Large Heterocyclic Bridging Groups," *J. Am. Chem. Soc.* **2005**, *127*, 60-61.

[42] J. Alauzun, A. Mehdi, C. Reye, R. J. P. Corriu, "Direct Synthesis of Bifunctional Mesoporous Organosilicas Containing Chelating Groups in the Framework and Reactive Functional Groups in the Channel Pores," *J. Mater. Chem.* **2007**, *17*, 349-356.

[43] R. J. P. Corriu, E. L. Beltran, A. mehdi, C. Reye, S. Brandes, R. Guilard, "Hybrid Materials Containing Metal(II) Schiff Base Complex Covalently Linked to the Silica Matrix by Two Si-C Bonds: Reaction with Dioxygen," *Chem. Mater.* **2003**, *15*, 3152-3160.

[44] C. Baleizão, B. Gigante, D. Das, M. Álvaro, "Periodic Mesoporous Organosilica Incorporating a Catalytically Active Vanadyl Schiff Base Complex in the Framework," *J. Catal.* **2004**, *223*, 106-113.

[45] K. Landskron, G. A. Ozin, "Periodic Mesoporous Organosilicas: Self-Assembly from Bridged Cyclic Silsesquioxane Precursors," *Angew. Chem. Int. Ed.* **2005**, *44*, 2107-2109.

[46] J. Pang, V. T. John, D. A. Loy, Z. Yang, Y. Lu, "Hierarchical Mesoporous Carbon/Silica Nanocomposites from Phenyl-Bridged Organosilane," *Adv. Mater.* **2005**, *17*, 704-707.

[47] T. Kimura, "Synthesis of Novel Mesoporous Aluminum Organophosphonate by Using Organically Bridged Diphosphonic Acid," *Chem. Mater.* **2003**, *15*, 3742-3744.

[48] T. Kimura, "Oligomeric Surfactant and Triblock Copolymer Syntheses of Aluminum Organophosphonates with Ordered Mesoporous Structures," *Chem. Mater.* **2005**, *17*, 5521-5528.

[49] T. Kimura, K. Kato, "Synthesis of Ordered Mesoporous Aluminium Alkylenediphosphonates with Integrated Inorganic-Organic Hybrid Frameworks," *J. Mater. Chem.* **2007**, *17*, 559-566.

[50] P. H. Mutin, G. Guerrero, A. Vioux, "Hybrid Materials from Organophosphorus Coupling Molecules," *J. Mater. Chem.* **2005**, *15*, 3761-3768.

[51] W. P. Guo, I. Kim, C. S. Ha, "Highly Ordered Three-Dimensional Large-Pore Periodic Mesoporous Organosilica with *Im*3*m* Symmetry," *Chem. Commun*. **2003**, 2692-2693.

[52] Z. D. Zhang, B. Z. Tian, X. X. Yan, S. D. Shen, X. Y. Liu, D. H. Chen, G. S. Zhu, D. Y. Zhao, S. L. Qiu, "An Easy Route for the Synthesis of Ordered Three-Dimensional Large-Pore Mesoporous Organosilicas with *Im-3m* Symmetry," *Chem. Lett.* **2004**, *33*, 1132-1133.

[53] Z. D. Zhang, X. X. Yan, B. Z. Tian, S. D. Shen, D. H. Chen, G. S. Zhu, S. L. Qiu, D. Y. Zhao, "Synthesis of Large-Pore Periodic Mesoporous Organosilica (PMO) with Biocontinuous Cubic Structure of *Ia-3d* Symmetry," *Chem. Lett.* **2005**, *34*, 133-134.

[54] L. Zhao, G. S. Zhu, D. L. Zhang, Y. Di, Y. Chen, O. Terasaki, S. L. Qiu, "Synthesis and Structural Identification of a Highly Ordered Mesoporous Organosilica with Large Cage-like Pores," *J. Phys. Chem. B* **2005**, *109*, 764-768.

[55] O. Muth, C. Schellbach, M. Fröba, "Triblock Copolymer Assisted Synthesis of Periodic Mesoporous Organosilicas (PMOs) with Large Pores," *Chem. Commun.* **2001**, 2032-2033.

[56] H. G. Zhu, D. J. Jones, J. Zajac, J. Roziere, R. Dutartre, "Periodic Large Mesoporous Organosilicas from Lyotropic Liquid Crystal Polymer Templates," *Chem. Commun.* **2001**, 2568-2569.

[57] W. P. Guo, J. Y. Park, M. O. Oh, H. W. Jeong, W. J. Cho, I. Kim, C. S. Ha, "Triblock Copolymer Synthesis of Highly Ordered Large-Pore Periodic Mesoporous Organosilicas with the Aid of Inorganic Salts," *Chem. Mater.* **2003**, *15*, 2295-2298.

[58] S. Z. Qiao, C. Z. Yu, W. Xing, Q. H. Hu, H. Djojoputro, G. Q. Lu, "Synthesis and Bio-adsorptive Properties of Large-Pore Periodic Mesoporous Organosilica Rods," *Chem. Mater.* **2005**, *17*, 6172-6176.

[59] X. Y. Bao, X. S. Zhao, S. Z. Qiao, S. K. Bhatia, "Comparative Analysis of Structural and Morphological Properties of Large-Pore Periodic Mesoporous Organosilicas and Pure Silicas," *J. Phys. Chem. B* **2004**, *108*, 16441-16450.

[60] S. Z. Qiao, C. Z. Yu, Q. H. Hu, Y. G. Jin, X. F. Zhou, X. S. Zhao, G. Q. Lu, "Control of Ordered Structure and Morphology of Large-Pore Periodic Mesoporous Organosilicas by Inorganic Salt," *Micropor. Mesopor. Mater.* **2006**, *91*, 59-69.

[61] M. C. Burleigh, M. A. Markowitz, E. M. Wong, J. S. Lin, B. P. Gaber, "Synthesis of Periodic Mesoporous Organosilicas with Block Copolymer Templates," *Chem. Mater.* **2001**, *13*, 4411-4412.

[62] X. Bao, X. S. Zhao, X. Li, J. Li, "Pore Structure Characterization of Large-Pore Periodic Mesoporous Organosilicas Synthesized with Varying SiO_2/Template Ratios," *Appl. Surf. Sci.* **2004**, *237*, 380-386.

[63] E. B. Cho, K.-W. Kwon, H. Char, "Mesoporous Organosilicas Prepared with PEO-Containing Triblock Copolymers with Different Hydrophobic Moieties," *Chem. Mater.* **2001**, *13*, 3837-3839.

[64] X. F. Zhou, S. Z. Qiao, N. Hao, X. Wang, C. Z. Yu, K. L. Wang, D. Y. Zhao, G. Q. Lu, "Synthesis of Ordered Cubic Periodic Mesoporous Organosilicas with Ultra-Large Pores," *Chem. Mater.* **2007**, *19*, 1870-1876.

[65] J. R. Matos, M. Kruk, L. P. Mercuri, M. Jaroniec, T. Asefa, N. Coombs, G. A. Ozin, T. Kamiyama, O. Terasaki, "Periodic Mesoporous Organosilica with Large Cagelike Pores," *Chem. Mater.* **2002**, *14*, 1903-1905.

[66] Y. Goto, S. Inagaki, "Synthesis of Large-Pore Phenylene-Bridged Mesoporous Organosilica using Triblock Copolymer Surfactant," *Chem. Commun.* **2002**, 2410-2411.

[67] W. Wang, S. Xie, W. Zhou, A. Sayari, "Synthesis of Periodic Mesoporous Ethylenesilica under Acidic Conditions," *Chem. Mater.* **2004**, *16*, 1756-1762.

[68] J. Morell, G. Wolter, M. Fröba, "Synthesis and Characterization of Highly Ordered Thiophene-Bridged Periodic Mesoporous Organosilicas with Large Pores," *Chem. Mater.* **2005**, *17*, 804-808.

[69] D. J. Kim, J. S. Chung, W. S. Ahn, G. W. Kam, W. J. Cheong, "Morphology Control of Organic-Inorganic Hybrid Mesoporous Silica by Microwave Heating," *Chem. Lett.* **2004**, *33*, 422-423.

[70] Y. Lu, H. Fan, N. Doke, D. A. Loy, R. A. Assink, D. A. LaVan, C. J. Brinker, "Evaporation-Induced Self-Assembly of Hybrid Bridged Silsesquioxane Film and Particulate Mesophases with Integral Organic Functionality," *J. Am. Chem. Soc.* **2000**, *122*, 5258-5261.

[71] B. D. Hatton, K. Landskron, W. Whitnall, D. D. Perovic, G. A. Ozin, "Spin-Coated Periodic Mesoporous Organosilica Thin Films-Towards a New Generation of Low-Dielectric-Constant Materials," *Adv. Funct. Mater.* **2005**, *15*, 823-829.

[72] X. D. Yuan, H. I. Lee, J. W. Kim, J. E. Yie, J. M. Kim, "Periodic Mesoporous Organosilicas Functionalized with Sulfonic Acid Group. Synthesis and Alkylation of Phenol," *Chem. Lett.* **2003**, *32*, 650-651.

[73] Q. H. Yang, M. P. Kapoor, N. Shirokura, M. Ohashi, S. Inagaki, J. N. Kondo, K. Domen, "Ethane-Bridged Hybrid Mesoporous Functionalized Organosilicas with Terminal Sulfonic Groups and Their Catalytic Applications," *J. Mater. Chem.* **2005**, *15*, 666-673.

[74] M. P. Kapoor, A. K. Sinha, S. Seelan, S. Inagaki, S. Tsubota, H. Yoshida, M. Haruta, "Hydrophobicity Induced Vapor-Phase Oxidation of Propene over Gold Supported on Titanium Incorporated Hybrid Mesoporous Silsesquioxane," *Chem. Commun.* **2002**, 2902-2903.

[75] B. J. Hughes, J. B. Guilbaud, M. Allix, Y. Z. Khimyak, "Synthesis of Periodic Mesoporous Organosilicas with Incorporated Aluminium," *J. Mater. Chem.* **2005**, *15*, 4728-4733.

[76] A. Fukuoka, H. Araki, Y. Sakamoto, S. Inagaki, Y. Fukushima, M. Ichikawa, "Palladium Nanowires and Nanoparticles in Mesoporous Silica Templates," *Inorg. Chim. Acta* **2003**, *350*, 371-378.

[77] M. Álvaro, B. Ferrer, V. Fornés, H. García, "A Periodic Mesoporous Organosilica Containing Electron Acceptor Viologen Units," *Chem. Commun.* **2001**, 2546-2547.

[78] E. Besson, A. Mehdi, D. A. Lerner, C. Reyé, R. J. P. Corriu, "Photoresponsive Ordered Hybrid Materials Containing a Bridged Azobenzene Group," *J. Mater. Chem.* **2005**, *15*, 803-809.

[79] H. S. Peng, J. Tang, L. Yang, J. B. Pang, H. S. Ashbaugh, C. J. Brinker, Z. Z. Yang, Y. F. Lu, "Responsive Periodic Mesoporous Polydiacetylene/Silica Nanocomposites," *J. Am. Chem. Soc.* **2006**, *128*, 5304-5305.

CHAPTER 3 Experimental Methods and Characterisation

3.1 Chemicals

All chemicals were used as received without any further purification. Millipore water was used in all studies.

Chemicals Used in Experiments and Corresponding Abbreviations:

Benzene-----Analysis grade, anhydrous, 99.8 %, Aldrich Company

BSA-----Bovine serum albumin, 98%, molecular weight in solution is 66400, Aldrich Company

BTEB-----$(C_2H_5O)_3Si\text{-}C_6H_4\text{-}Si(OC_2H_5)_3$, 1,4-bis(triethoxysily)benzene, 90 %, Gelest Company

BTSE-----$(C_2H_5O)_3Si\text{-}CH_2\text{-}CH_2\text{-}Si(OC_2H_5)_3$, 1,2-bis(triethoxysilyl)ethane, 96 %, Aldrich Company

BTSPDS-----$(C_2H_5O)_3Si\text{-}(CH_2)_3\text{-}S\text{-}S\text{-}(CH_2)_3\text{-}Si(OC_2H_5)_3$, bis(triethoxysilylpropyl)-disulfide, 90 %, Gelest Company

C_2H_5OH----- Ethanol, Aldrich Company

CTAB-----$C_{16}H_{33}N(CH_3)_3Br$, hexadecyltrimethylammonium bromide, Aldrich Company

DMF-----N,N-dimethylformamide, Aldrich Company

EO_n-----$(CH_2CH_2O)_n$, poly(ethylene oxide)

HCl-----Hydrochloride acid, Aldrich Company

$Hg(NO_3)_2$-----Mercury(II) nitrate, Aldrich Company

HF-----Hydrofluoric acid, 48 wt % in H_2O, Aldrich Company

KCl-----Potassium chloride, Aldrich Company

NaOH-----Sodium hydroxide, Aldrich Company

PEO-PPO-PEO-----Poly(ethylene oxide)-*b*-poly(propylene oxide)-*b*-poly(ethylene oxide)

Phenol, formalin solution (37 wt %)-----Aldrich Company

Pluronic F127-----$EO_{106}PO_{70}EO_{106}$, Mn = 13400, Aldrich Company

Pluronic P123-----$EO_{20}PO_{70}EO_{20}$, Mw = 5,800, Aldrich Company

PO_n-----$(CH(CH_3)CH_2O)_n$, poly(propylene oxide)

TEOS-----$Si(OC_2H_5)_4$, tetraethyl orthosilicate, 99%, Aldrich Company

TMB-----1,3,5-trimethylenebenzene, Aldrich Company

$Zn(NO_3)_2 \cdot 6H_2O$----- Zinc nitrate hexahydrate, Aldrich Company

3.2 Experimental Methods

3.2.1 Evaporation-Induced Self-Assembly (EISA) Method

It is the nonaqueous synthesis that makes the preparation of ordered mesoporous materials easier and more convenient. The EISA process is the mostly popular pathway among the nonaqueous synthesis. EISA does not have strict requirements for SDAs, which avoids the cooperative self-assembling process between the precursor and surfactant template. It is found that the ordered mesostructures are difficult to obtain using the triblock copolymers F108 ($EO_{132}PO_{50}EO_{132}$) and F98 ($EO_{123}PO_{47}EO_{123}$) as templates under aqueous conditions, while such templates could lead to the successful synthesis of the ordered composites through the EISA process. Furthermore, three-dimensional (3D) cubic silica mesophase (*Im*3*m*) is easy to prepare in the EISA pathway [1-3].

Mostly solvents with weak polarity are used, while nonpolar and oily solvents are seldom adopted. In the EISA process, the surfactant self-assembly would be difficult as the surfactants lose the hydrophilic/hydrophobic properties in weak polarity solvents. However, the assembly can be induced as the solvent evaporation proceeded [4, 5].

The final mesoporous materials prepared by EISA approach usually have low surface areas and dense inorganic framework, which results in the lack of microporosity [6-11]. The nonaqueous solvents with weak polarity may screen the charge coupling or other interactions between the inorganic species and the hydrophilic corona. This fact may also lead to dense inorganic frameworks [2].

3.2.2 Co-Condensation Method

The co-condensation method is the process in which tetraalkoxysilanes (TEOS or TMOS) and organosilica ($(R'O)_3Si\text{-}R\text{-}Si(OR')_3$ or $(R'O)_3Si\text{-}R$) precursors condense simultaneously in the presence of SDAs, by the surfactant self-assembly approach, the mesoporous materials, such as mesostructured silica, PMOs, or functional mesoporous silicas, could be synthesized.

The advantages of the co-condensation method are as follows: (1) The organic groups are usually distributed homogeneously in the framework; (2) The problem of pore blocking is avoided. However, this method also has some disadvantages: (1) The degree of order of the composites generally decreases with increasing the amount of organosilica precursor in the reaction mixture, so more disordered materials are finally obtained; (2) As the silica and organosilica precursors have different hydrolysis and condensation rates, the proportion of "soft" organic bridging groups introduced into the framework is still a challenge in the synthesis process; (3) A relatively low specific surface areas, small pore diameter of the final products could be obtained with more organic groups incorporated into the framework; (4) The removal of the surfactant should be considered, as calcination at high temperature could lead to the cleavage of the organic bridging groups [12].

3.2.3 Postsynthesis Treatment

3.2.3.1 Secondary Synthesis

The secondary synthesis is generally employed to increase the pore wall thickness, improve the mesostructured ordering or thermal stability. The hydrothermal stability of MCM-41 materials is enhanced by treating the MCM-41 with $AlCl_3$ vapor or $AlCl_3$ solution. The increased pore wall thickness after treatment could lead to better hydrothermal stability [13]. Moreover, the treatment with ammonia gas improves the thermal stability of the mesoporous silicate thin films [14]. It is found that the secondary synthesis is more effective for as-made materials than the final products.

3.2.3.2. Recrystallization

Recrystallization is the process in which as-made samples without washing are put into deionized water at 100 ~ 150 ºC, and kept for several days, which is effective to improve the regularity or thermal stability of mesoporous materials [15, 16]. For the recrystallization process, it is preferred to use samples without washing. And dissolution and crystallization of silicate species and reorganization of mesostructures may take place. The solvents without polarity as the heating media are the key for the phase transformation of mesostructure [6]. It should be mentioned that recrystallization process is different from the hydrothermal treatment.

3.3 Characterisation

In order to understand the properties and the characteristics of the samples prepared, different characterisation techniques were employed and will be discussed here in detail.

3.3.1 Mesostructure and Framework Analysis

3.3.1.1 Small-angle X-ray Scattering (SAXS) and X-ray Diffraction (XRD) Analysis

The SAXS measurements were made on a NanoStar small-angle X-ray scattering system (Bruker, Germany) using Cu Kα radiation at 40 kV and 35 mA. The *d*-spacing values were calculated by the formula $d = 2\pi/q$. The low- and wide-angle XRD was performed on a German Bruker D4 X-ray diffractometer with Ni-filtered Cu Kα radiation (40 kV, 40 mA).

3.3.1.2 Scanning Electrons Microscopy (SEM) and Transmission Electrons Microscopy (TEM)

SEM images were recorded on a JEOL 6400 scanning electron microscope operated at 10 kV. The samples were coated with about 3 nm gold.

TEM images were obtained with a JEOL 2011 electron microscope operated at 200 kV. Before TEM measurements, the powder samples were dispersed in ethanol, ground in a mortar and then dipped and dried on Cu grids.

3.3.1.3 Nitrogen Adsorption/Desorption Measurements (Surface area and pore properties)

Nitrogen adsorption/desorption isotherms of samples were measured by a Micromeritics ASAP 2010 system at 77 K. The samples were degassed at 120 °C overnight on a vacuum line before measurements. The Brunauer-Emmett-Teller (BET) method was utilized to calculate the specific surface areas (S_{BET}) using adsorption data in a relative pressure range from 0.04 to 0.2. The total pore volume was calculated by the N_2 amount adsorbed at the highest P/P_0. The pore size distributions the surfactant-free composites were derived from the adsorption branches of the isotherms based on the Barrett-Joyner-Halenda (BJH) method.

3.3.1.4 ^{29}Si and ^{13}C Solid-State NMR Spectra

The cross-polarization magic angle spinning (CP-MAS) ^{29}Si NMR solid-state spectra with proton decoupling and ^{13}C CP-MAS NMR spectra were acquired on a Bruker DSX 300 NMR spectrometer. The ^{29}Si NMR spectra were collected at room temperature with a frequency of 59.6 MHz, a recycling delay of 600 s, a radiation frequency intensity of 62.5 kHz, and a reference sample of Q_8M_8 ($[(CH_3)_3SiO]_8Si_8O_{12}$). ^{13}C NMR spectra were collected at room temperature with a frequency of 75.5 MHz (2 s recycle, 3 ms contact time) using adamantane as a reference.

3.3.1.5 Fourier Transform Infrared (FT-IR) Spectra

FT-IR spectra were collected on a FT-IR 360 spectrometer with a resolution of 2 cm^{-1} in the wavelength range of 400 ~ 4000 cm^{-1} using KBr pallet.

3.3.1.6 Thermogravimetric Analysis (TGA)

Weight changes of the products were monitored using a Mettler Toledo TGA-SDTA851 analyzer (Switzerland) from 25 to 900 °C under nitrogen or 25 to 800 °C in air with a heating rate of 5 °C/min, respectively.

3.3.1.7 Inductively Coupled Plasma (ICP) Spectrometry

The residue mercury (II) in the solution was measured by inductively coupled plasma (ICP) spectrometry (Model-IRIS Intrepid) from English Thermo Elemental Company.

3.3.1.8 Element Analysis

The S and Zn contents were measured using a Vario EL III elemental analyzer (Germany).

3. 3.1.9 Ultra-Visible (UV) Spectra

UV-vis (Ultraviolet-visible spectrophotometry) spectra were collected on a SHIMADZU-UV-2450 UV-vis spectrophotometer.

Characterisation Abbreviations:

BET-----Brunauer-Emmett-Teller

BJH-----Barrett-Joyner-Halenda

CP-MAS NMR cross-polarization magic angle spinning nuclear magnetic resonance

EPR-----Electronic spin resonance

FT-IR-----Fourier transform infrared

HPLC-----High-performance liquid chromatography

HRTEM-----High-resolution transition electron microscopy

ICP----- Inductively coupled plasma

SAXS-----Small-angle X-ray scattering

S_{BET}-----Specific BET surface area

SEM-----Scanning electron microscopy

TEM-----Transition electron microscopy

TGA-----Thermogravimetric analysis

UV-vis-----Ultraviolet-visible spectrophotometry

XRD-----X-ray diffraction

3.3.2 Adsorption Equilibrium Measurements

3.3.2.1 Toluene Adsorption Equilibrium Measurement

Toluene adsorption equilibrium measurements at 25 °C were carried out using a digital microbalance (Hiden Isochema Instrument, Model IGA-002) connected to a high-vacuum system. In the first step, 10 – 20 mg of the powder sample was loaded on a small pan. The sample was heated to 180 °C for at least 6 h under a high-vacuum of 5 − 10 mbar to remove all adsorbed impurities. Then the sample was cooled to the required temperature. Isothermal measurements were carried out by introducing a dose amount of toluene vapor directly to the sample chamber, and recording the weight change after reaching a stable equilibrium pressure. Further consecutive measurements were taken by increasing the vapor pressure by steps.

3.3.2.2 Benzene Adsorption Equilibrium Measurement

The vapor benzene was used as a probe for the adsorption experiments. Adsorption equilibrium measurements were carried out using a digital microbalance (IGA Instrument, Model 001) connected to a high-vacuum system. In the first step, 10 – 20 mg of the powder sample was loaded on a small pan. The sample was heated to 180 °C for at least 6 h under a high-vacuum of 5 − 10 mbar to remove all adsorbed impurities. Then the sample was cooled to the required temperature. Isotherm measurements were carried out by introducing a dose amount of benzene vapor directly to the sample chamber, and recording the weight change after reaching a stable equilibrium pressure. Further consecutive measurements were taken by increasing the vapor pressure by steps. The vapor-saturated pressure of benzene at 25 °C was about 125 mbar.

3.3.2.3. BSA Adsorption Equilibrium Measurement

BSA adsorption was measured by the classical batch equilibration method with acetate buffer (pH 4.7) and sodium phosphate buffer (pH 7.8), respectively. Typically, BSA was dissolved in acetate buffer (pH 4.7) to get a stock solution (2.0 $mg \cdot mL^{-1}$). The adsorption rate measurements were performed to determine the adsorbed amount of BSA as a function of contact time by mixing 20 mL of (2.0 $mg \cdot mL^{-1}$) BSA solution with 10 mg of PMO-F composites and stirring at 25 °C. The sample was then centrifuged and withdrawn periodically for immediate analysis and then returned to the mixture. The equilibrium concentration of BSA was analyzed by a UV-vis spectrophotometer at 280 nm. The adsorbed amount of BSA was calculated from the BSA concentrations before and after adsorption at different times.

3.3.2.4 Mercury (II) Adsorption Measurement

Mercury (II) adsorption capacities for the disulfide-bridged mesoporous organosilicas were measured using a batch adsorption process. Typically, 100 mg of the PMO adsorbent was stirred at room temperature for 12 h in 50 mL of $Hg(NO_3)_2$ aqueous solution (6630 ppm of Hg^{2+}). To prevent the precipitation of the metal ions during the adsorption experiment, the pH of $Hg(NO_3)_2$ solution was adjusted to 2.0 by HCl. The mixture was then filtered and the residue mercury (II) in the solution was measured by inductively coupled plasma (ICP) spectrometry (Model-IRIS Intrepid) from English Thermo Elemental Company. Each measurement was repeated three times.

Other Abbreviations in the Thesis:

AMS-----Anionic mesoporous silica

AOP-----Aluminum organophosphonate

APS-----3-aminopropyltrimethoxysilane

BTE-----1,2-bis(triethoxysilyl)ethylene, $(EtO)_3Si\text{-}CH{=}CH\text{-}Si(OEt)_3$

BTEBP-----4,4'-bis(triethoxysilyl)biphenyl

BTET-----2,5-bis(triethoxysilyl)thiophene

BTME-----1,2-bis(trimethoxysilyl)ethane

B50-6600-----$EO_{39}BO_{47}EO_{39}$, BO = butylene oxide

Brij76----- $C_{18}H_{37}(OCH_2CH_2)_{10}OH$, $C_{18}EO_{10}$

CFM-----Cooperative Formation Mechanism

CPC-----Hexadecylpyridinium chloride

CSDAs-----Co-structure directing agents

CTAC-----Hexadecyltrimethylammonium chloride

C_{16}TEABr-----$C_nH_{2n+1}N(CH_2CH_3)_3Br$ (n = 16)

EISA-----Evaporation induced self assembly

FDU-----Fudan University

FSM-----Folded sheet mechanism

F108-----$EO_{132}PO_{50}EO_{132}$

F98-----$EO_{123}PO_{47}EO_{123}$

F68-----$EO_{80}PO_{27}EO_{80}$

HMS-----Hexagonal Mesoporous Silica

I-----Inorganic precursor

IBN-----Institute of Bioengineering and Nanotechnology

ICS-----Tris[3-(trimethoxysilyl)propyl]isocyanurate

IUPAC-----International Union of Pure and Applied Chemistry

KIT-----Korea Advanced Institute of Science and Technology

KSW-----Kagami Memorial Lab. for Materials science and technology, Waseda University (Japan)

LCT-----Liquid crystal templating

MCM-----Mobil's Composition of Matter

MSU-----Michigan State University

OTAC-----Octadecyltrimethylammonium chloride

PMO-----Periodic mesoporous organosilica

S-----Surfactant headgroup

SBA-----Santa Barbara Amorphous

SDAs-----Structure-directing agents

SDS-----Sodium dodecyl sulfonate

SRA-----Silicate Rod Assembly

TLCT-----True liquid-crystal templating

TMAPS-----N-trimethoxylsilypropyl-*N*, *N*, *N*-trimehylammonium chloride

TMOS-----Tetramethoxysilane (tetramethylorthosilica)

TUD-----Delft University of Technology

X-----Counteranion

References

[1] Y. F. Lu, R. Ganguli, C. A. Drewien, M. T. Anderson, C. J. Brinker, W. L. Gong, Y. X. Guo, H. Soyez, B. Dunn, M. H. Huang, J. I. Zink, "Continuous Formation of Supported Cubic and Hexagonal Mesoporous Films by Sol-Gel Dip-Coating," *Nature* **1997**, *389*, 364-368.

[2] Y. Wan, D. Y. Zhao, "On the Controllable Soft-Templating Approach to Mesoporous Silicates," *Chem. Rev.* **2007**, *107*, 2821-2860.

[3] D. Y. Zhao, P. D. Yang, N. Melosh, J. Feng, B. F. Chmelka, G. D. Stucky, "Continuous Mesoporous Silica Films with Highly Ordered Large Pore Structures," *Adv. Mater.* **1998**, *10*, 1380-1385.

[4] C. Z. Yu, B. Z. Tain, J. Fan, B. Tu, D. Y. Zhao, "Synthesis of Hierarchically Arrayed Silica Nanorods via Reverse Amphiphilic Block Copolymer Mesophases," *Chem. J. Chin. Univ.-Chin.* **2003**, *24*, 5-8.

[5] C. Z. Yu, B. Z. Tian, J. Fan, G. D. Stucky, D. Y. Zhao, "Synthesis of Siliceous Hollow Spheres with Ultra Large Mesopore Wall Structures by Reverse Emulsion Templating," *Chem. Lett.* **2002**, 62-63.

[6] B. Z. Tian, X. Y. Liu, L. A. Solovyov, Z. Liu, H. F. Yang, Z. D. Zhang, S. H. Xie, F. Q. Zhang, B. Tu, C. Z. Yu, O. Terasaki, D. Y. Zhao, "Facile Synthesis and Characterization of Novel Mesoporous and Mesorelief Oxides with Gyroidal Structures," *J. Am. Chem. Soc.* **2004**, *126*, 865-875.

[7] N. A. Melosh, P. Lipic, F. S. Bates, F. Wudl, G. D. Stucky, G. H. Fredrickson, B. F. Chmelka, "Molecular and Mesoscopic Structures of Transparent Block Copolymer-Silica Monoliths," *Macromolecules* **1999**, *32*, 4332-4342.

[8] N. A. Melosh, P. Davidson, B. F. Chmelka, "Monolithic Mesophase Silica with Large Ordering Domains," *J. Am. Chem. Soc.* **2000**, *122*, 823-829.

[9] N. A. Melosh, P. Davidson, P. Feng, D. J. Pine, B. F. Chmelka, "Macroscopic Shear Alignment of Bulk Transparent Mesostructured Silica," *J. Am. Chem. Soc.* **2001**, *123*, 1240-1241.

[10] K. Yu, B. Smarsly, C. J. Brinker, "Self-Assembly and Characterization of Mesostructured Silica Films with a 3D Arrangement of Isolated Spherical Mesopores," *Adv. Funct. Mater.* **2003**, *13*, 47-52.

[11] B. Smarsly, G. Xomeritakis, K. Yu, N. G. Liu, H. Y. Fan, R. A. Assink, C. A. Drewien, W. Ruland, C. J. Brinker, "Microstructural Characterization of Polystyrene-block-poly(ethylene oxide)-Templated Silica Films with Cubic-Ordered Spherical Mesopores," *Langmuir* **2003**, *19*, 7295-7301.

[12] F. Hoffmann, M. Cornelius, J. Morell, M. Fröba, "Silica-Based Mesoporous Organic-Inorganic Hybrid Materials," *Angew. Chem. Int. Ed.* **2006**, *45*, 3216-3251.

[13] M. C. Xu, A. Arnold, A. Buchholz, W. Wang, M. Hunger, "Low-Temperature Modification of Mesoporous MCM-41 Material with Sublimated Aluminum Chloride in Vacuum," *J. Phys. Chem. B* **2002**, *106*, 12140-12143.

[14] R. Vogel, C. Dobe, A. Whittaker, G. Edwards, J. D. Riches, M. Harvey, M. Trau, P. Meredith, "Postsynthesis Stabilization of Free-standing Mesoporous Silica Films," *Langmuir* **2004**, *20*, 2908-2914.

[15] Q. S. Huo, D. I. Margolese, G. D. Stucky, "Surfactant Control of Phases in the Synthesis of Mesoporous Silica-Based Materials," *Chem. Mater.* **1996**, *8*, 1147-1160.

[16] D. Khushalani, A. Kuperman, G. A. Ozin, K. Tanaka, J. Garces, M. M. Olken, N. Coombs, "Metamorphic Materials: Restructuring Siliceous Mesoporous Materials," *Adv. Mater.* **1995**, *7*, 842-846.

CHAPTER 4 Synthesis of Large Pore Phenyl-Bridged Mesoporous Organosilica with Thick Walls by EISA for Efficient Benzene Adsorption

4.1 Introduction

In the past few years, periodic mesoporous organosilicas (PMOs) have received considerable attention in materials science owing to their homogeneous distribution of organic groups in the framework as well as unique surface properties imparted from different functional groups [1]. They have various potential applications in catalysis [2-6], adsorption [7-11], and high-performance liquid chromatography [12]. PMOs were first reported independently by several research groups in 1999 [13-15]. Following the hydrothermal synthesis method, a variety of PMOs with different organic bridges, mesostructures [16-20], pore sizes [21-24], and morphologies [25-31] have been successfully prepared. However, the limited pore size of PMO materials restricts their applications in some areas where large-pores are in demand as substrates, such as the adsorption and immobilization of large biomolecules. It is known that nonionic and triblock copolymers in aqueous solution have an advantage of preparing mesoporous silica materials with large-pores and thick walls [32, 33]. Recently, using a low-temperature approach, Zhou *et al.* [34] reported the synthesis of ordered ethylene-bridged PMOs with large-pore sizes up to 14.7 nm by using triblock copolymer Pluronic F127 as a structure-directing agent and 1,3,5-trimethylbenzene (TMB) as a pore expander. However, functional groups of bridging ethylene in the large-pore mesoporous PMO materials are not suitable for further modification. Phenyl-bridged PMOs are good candidates for functionality, as the groups can be modified through chemical reactions, as well as form molecular periodicity in the framework walls by the π-π interaction between benzene rings. To date, most ordered phenyl-bridged PMOs have been successfully synthesized under basic conditions, using cationic alkyltrimethylammonium as templates [35-37]. The pore size is limited to 4.0 nm because of the relatively short chain lengths of the templates. In contrast, few studies have been reported on the synthesis of large-pore phenyl-bridged PMOs under acidic conditions. To the best of our knowledge, the largest pore sizes of phenyl-bridged PMOs are up to 7.4 and 8.4 nm when prepared with $EO_{20}(PO_{70})EO_{20}$ (P123) and $EO_{16}(L_{29}G_7)EO_{16}$ (LGE538), respectively [38, 39]. On the other hand, Inagaki and his co-workers treated phenyl-bridged materials with basic solution to form periodicity within the pore walls of PMOs [32]. The mesopore structural

arrangement and wall thickness appeared to decrease with the increase of basic concentration. Therefore, the design and synthesis of large-pore phenyl-bridged PMO materials with thick walls are valuable for further modification and adsorption.

Nonaqueous synthesis is an easy and convenient method for preparing ordered mesoporous materials especially for films, membranes, monoliths, and spheres [40-42]. This method has become more and more powerful. Most of the syntheses conducted in organic solvent adopt the well-known evaporation-induced selfassembly (EISA) approach [43]. The EISA method avoids the cooperative assembling process which requires strong interaction between the precursor and the surfactant template, and facilitates the liquid–crystal-templating assembly of long-chain organosilanes to form ordered PMOs [44, 45]. The phenyl-bridged PMOs prepared by EISA using alkyltrimethylammonium surfactants displayed small pores (< 4 nm) and thin pore walls [46], however, using triblock polymer as a template to obtain the large-pore and thick wall materials has not been reported.

In this chapter, we report the synthesis of large-pore phenyl-bridged mesoporous materials with thick walls under acidic conditions through the EISA approach by using triblock polymer Pluronic F127 as a template. The obtained materials have the largest pore size (up to 9.9 nm) and pore walls (up to 6.9 nm) reported for ordered phenyl-bridged PMOs. It is found that the pore size can be gradually expanded with the decrease of acidity and increase of F127 content. The further mixed-solvothermal treatment can increase the pore wall thickness to 7.7 nm and improve the periodicity in the walls. Most importantly, mesostructures with large-pores and thick walls can be obtained directly after calcination at 350 °C in a nitrogen atmosphere. Compared to the hydrothermal synthesis method under acidic conditions, our results show that the EISA method is more facile in the formation of large-pores and thick walls of PMO materials. The adsorption capacity of the composites was tested using volatile benzene as a probe molecule at 25 °C.

4.2 Experimental

4.2.1 Synthesis of phenyl-bridged PMOs

Ordered PMO materials with phenylene groups were prepared through an EISA strategy by using Pluronic F127 as a template and BTEB as a silica source in ethanol solution at 40 °C. Different amounts of F127 and concentrations of hydrochloride acid were adopted in the batch experiments. A typical synthesis was carried out as follows:

0.40 g of Pluronic F127 was completely dissolved in 0.37 g of 0.2 M HCl and 2.0 g of ethanol, and then stirred for 1 h at 40 °C to produce a clear solution. The amount of 0.30 g of BTEB was added to the above solution under vigorous stirring for 2 h at the same temperature. The solution was then transferred to Petri dishes to evaporate ethanol over 24 h at room temperature (22 °C). The as-made products, flaxen and transparent membranes, were scraped from the petri dishes and ground into fine powder. The mixed-solvothermal treatment of the as-made powder samples (300 mg) was carried out in a mixture solvent (50 mL) of DMF and water (V:V = 1:1) at 100 °C for 3 days. After cooling to room temperature, the solid powder was filtered, washed with water, and dried. Calcination was carried out in a tubular furnace at 350 °C for 3 h under N_2 flow to remove the copolymer templates [25, 47, 48]. The resulting samples were denoted as Ph-PMO-x-y and *T-Ph-PMO-x-y* without and with mixed-solvothermal treatment respectively, x refers to the Pluronic F127 content (g) in the initial mixture, and y represents the concentration of hydrochloride acid (mol/L).

4.3 Results and discussion

4.3.1 Mesostructure

Small-angle XRD patterns (Figure 4.1A) of the template-free phenylbridged mesoporous material Ph-PMO-0.4-0.2 prepared by the EISA approach with high F127 content and high HCl concentration exhibit one intense and two poorly resolved diffraction peaks with d-value ratios of $1:\sqrt{3}:2$. These diffractions can be indexed as the 100, 110, and 200 reflections, respectively, for the two-dimensional (2D) hexagonal mesostructure with space group of *p6mm*. The corresponding unit cell parameter a_0 is calculated to be as large as 16.2 nm. The results clearly suggest that using the EISA approach can simply prepare ordered PMO mesostructures with large cells from long-chain phenyl-bridged silanes. Similarly, all Ph-PMO samples prepared with different F127 contents and HCl concentration show similar XRD patterns, demonstrating that ordered hexagonal phenyl-bridged PMO composites are obtained by the EISA approach. With decreasing F127 content, the 100 diffraction peak shifts to a higher angle, suggesting a decrease of the mesostructural cell parameter (Table 4.1) [49]. In addition, wide-angle XRD patterns of all Ph-PMO samples prepared from the EISA approach by using Pluronic F127 show no obvious

diffraction peak at 2 θ angles of 7 ~ 70 ◦ (Figure 4.1B). One broad diffraction with a shoulder is observed, indicating no periodicity of the mesopore walls.

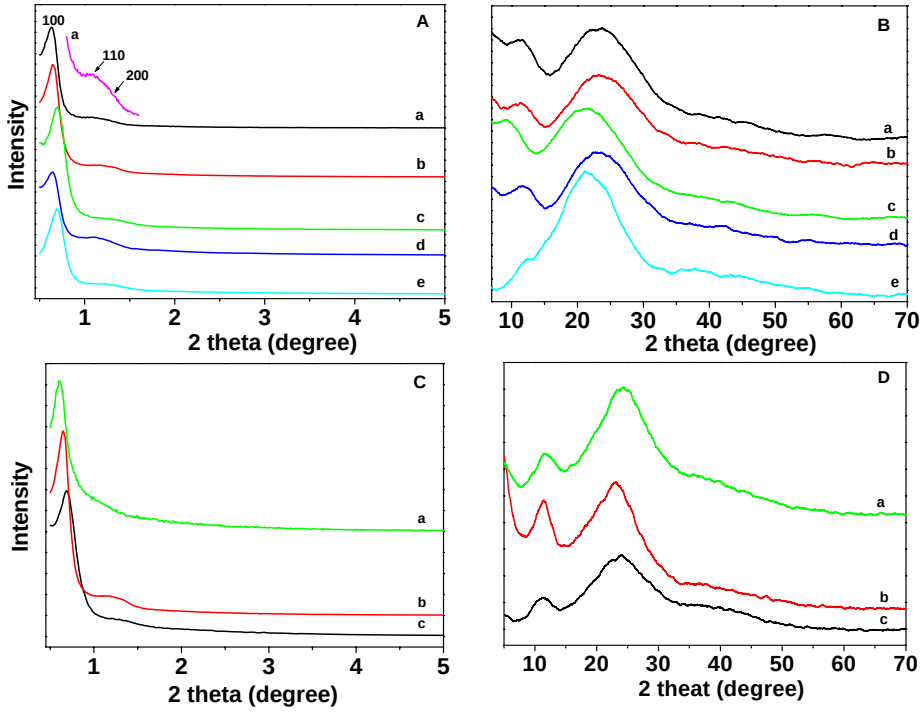

Figure 4.1. (A) Low- and (B) high-angle XRD patterns of the template-free phenyl-bridged PMOs synthesized by EISA approach with different F127 content and HCl concentrations: Ph-PMO-0.4-0.2 (a), Ph-PMO-0.3-0.2 (b), Ph-PMO-0.2-0.2 (c), Ph-PMO-0.3-0.1 (d) and Ph-PMO-0.2-0.1 (e), (C) Low- and (D) high-angle XRD patterns of the template-free phenyl-bridged PMOs after the mixed-solvothermal treatment at 100 °C for 3 days in the mixture of DMF and water (V: V = 1: 1): *T-Ph-PMO-0.4-0.2* (a), *T-Ph-PMO-0.3-0.2* (b) and *T-Ph-PMO-0.2-0.2* (c).

TEM images of the template-free mesoporous Ph-PMO-0.4-0.2 material show large domains of ordered hexagonal and stripe-like arranged arrays (Figure 4.2a and b), clearly indicating an ordered 2D hexagonal mesostructure with 1D pore channels. The unit cell parameter (a_0) is estimated from TEM images to be approximately 17.0 nm, which is in good agreement with the value calculated from the XRD data. The above observations clearly demonstrate that the assembly between the silicate precursors and F127 does not easily form the cubic mesostructure, as the synthesis is performed in the nonaqueous solution by the EISA approach [51]. In our case, 100 % silane (BTEB) is used as a silica source, which contains a hydrophobic organic group and makes the assembly much different from that in the TEOS case. Therefore, it is reasonable that a 2D hexagonal mesostructure is formed by using BTEB as a silica source and F127 as a template via an EISA method.

Table 4.1

Structural textural properties of the phenyl-bridged mesoporous organosilicas (Ph-PMO) synthesized by EISA approach with different F127 content and HCl concentration. And comparison with *T-Ph-PMO-x-0.2* composites after mixed-solvothermal treatment at 100 °C for 3 days in mixture of DMF and water (V: V = 1:1) (x = 0.4, 0.3 and 0.2).

Samples	S_{BET} ($m^2 \cdot g^{-1}$)	V_t ($cm^3 \cdot g^{-1}$)	V_{micro} ($cm^3 \cdot g^{-1}$)	d_{100} Spacing (nm)	a_0 (nm)	Pore size (D) (nm)	Wall Thickness[a] (nm)
Ph-PMO-0.4-0.2	1150	1.39	0.09	14.0	16.2	9.9	6.3
Ph-PMO-0.3-0.2	643	1.03	-	13.6	15.7	8.8	6.9
Ph-PMO-0.2-0.2	796	0.79	0.07	12.6	14.5	8.2	6.3
Ph-PMO-0.4-0.1	868	1.50	0.05	-	-	8.8/ 16.1	-
Ph-PMO-0.3-0.1	708	0.96	0.02	13.8	15.9	9.3	6.6
Ph-PMO-0.2-0.1	663	0.73	0.07	12.8	14.8	9.0	5.8
T-Ph-PMO-0.4-0.2	875	1.16	-	14.5	16.7	9.0	7.7
T-Ph-PMO-0.3-0.2	704	0.65	0.08	13.6	15.7	8.1	7.6
T-Ph-PMO-0.2-0.2	500	0.50	0.04	12.8	14.8	7.8	7.0

[a] Wall thickness = a_0 – D

d_{100}: the interplanar spacing, was calculated by the formula of $2d\sin\theta = \lambda$ (λ = 0.15418 nm).

a_0: the unit cell parameter, was determined from the interplanar spacing of the (100) plane using the formula of $a_0 = 2\ d_{100}/\sqrt{3}$.

V_{micro}: the micropore volume, was calculated by *t*-plot method using experimental points at relative pressure of P/P_0 = 0.10 - 0.20.

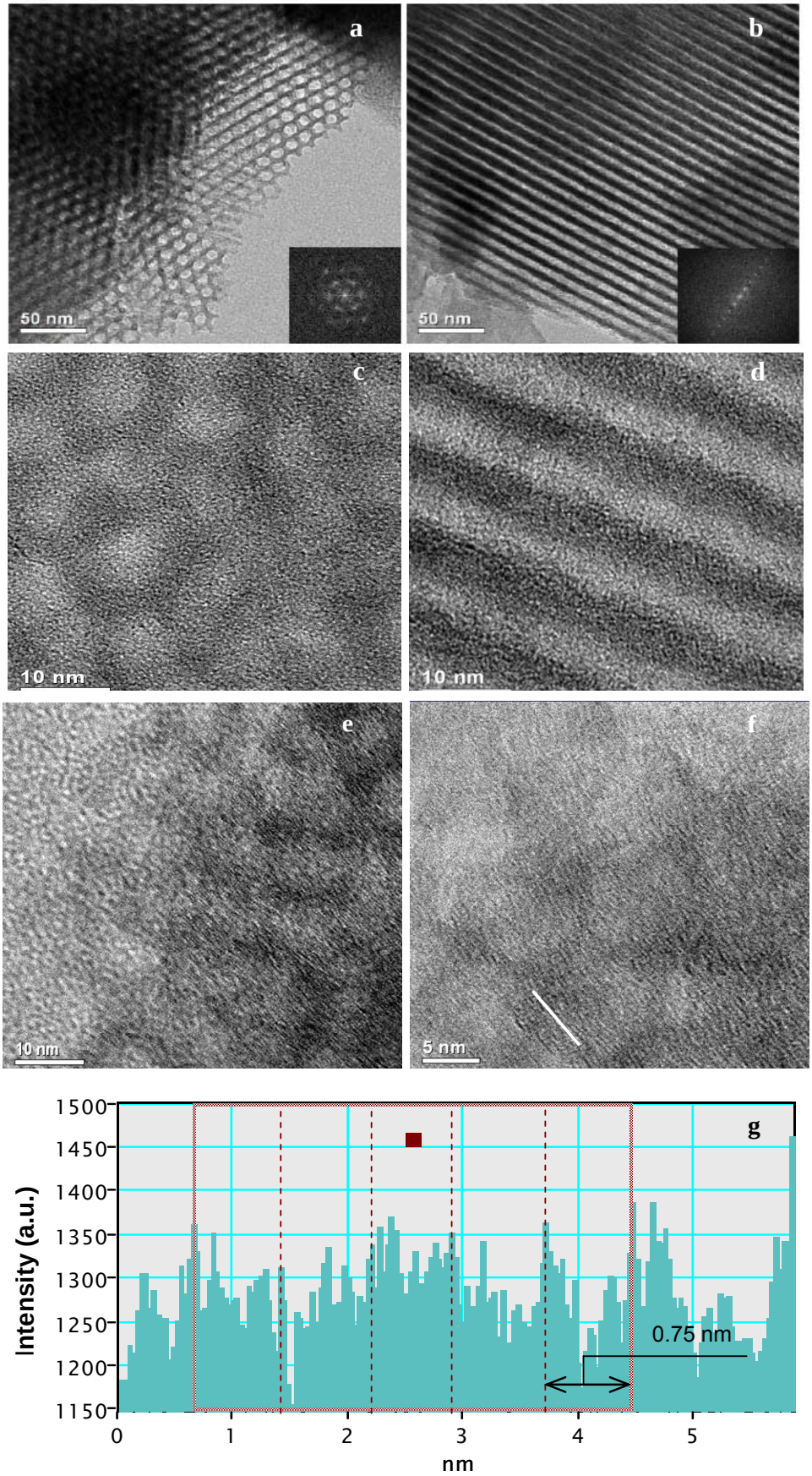

Figure 4.2. TEM and HRTEM images (a-d) of the template-free Ph-PMO-0.4-0.2 composites synthesized by the EISA approach, and HRTEM images (e, f) for the

template-free *T-Ph-PMO-0.3-0.2* composite synthesized by the EISA approach after the mixed-solvothermal treatment at 100 °C for 3 days in mixture solvent of DMF and water (V: V = 1: 1) and intensity across parallel fringes (g) along the white line.

However, HRTEM images (Figure 4.2c and d) do not provide any evidence of molecular scale periodicity, suggesting that it is difficult to form the periodicity in the pore walls with triblock copolymer as a template, though the calcination process can retain the overall mesostructure. The absence of molecular periodicity in the pore walls could be related to the penetration of the PEO moieties of Pluronic F127 into the walls, which may break the π-π interaction between phenyl-bridging groups.

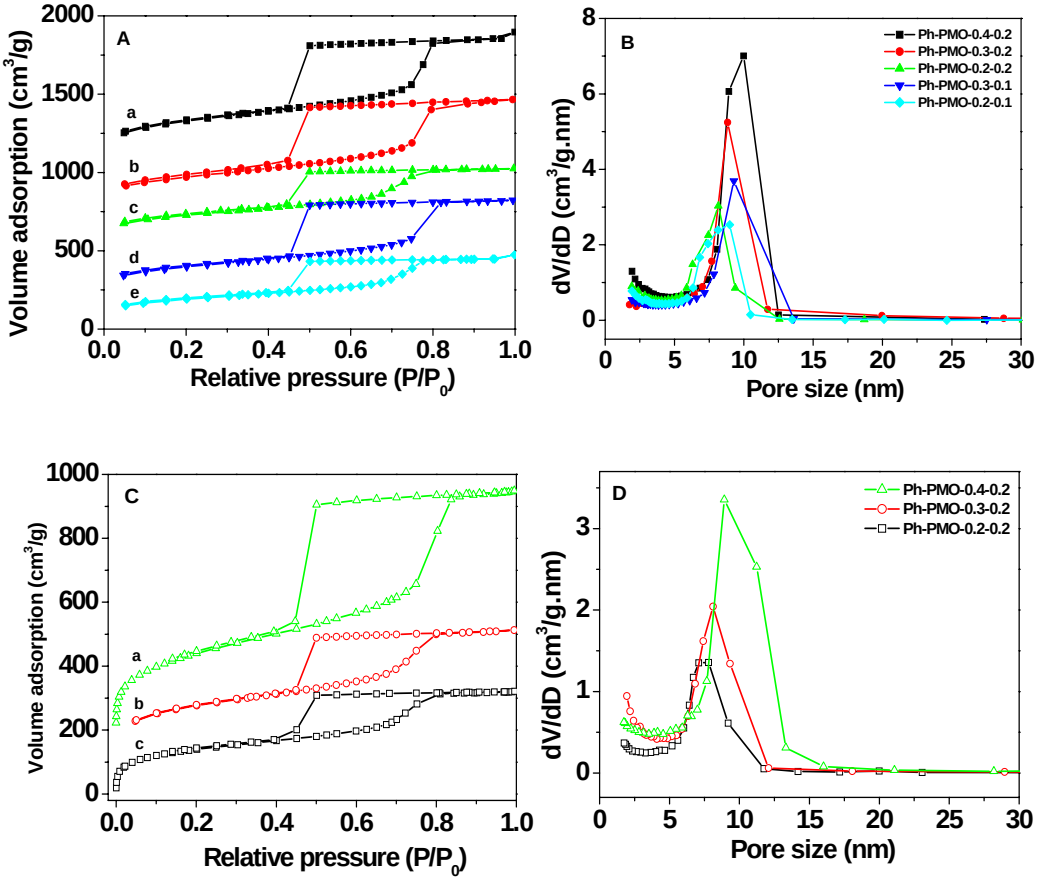

Figure 4.3. N_2 adsorption/desorption isotherms (A) and pore size distributions (B) for the phenyl-bridged mesoporous Ph-PMOs composites synthesized with different F127 content (0.2 ~ 0.4 g) and HCl concentration (0.1 and 0.2 M): Ph-PMO-0.4-0.2 (a), Ph-PMO-0.3-0.2 (b), Ph-PMO-0.2-0.2 (c), Ph-PMO-0.3-0.1 (d) and Ph-PMO-0.2-0.1 (e). The isotherms are offset vertically by 800 (a), 700 (b), 600 (c), and 200 $cm^3 \cdot g^{-1}$ (d), respectively; (C) and (D) for the phenyl-bridged mesoporous *T-Ph-PMOs* composites after mixed-solvothermal treatment at 100 °C for 3 days in the mixture of DMF and water (V: V = 1: 1): *T-Ph-PMO-0.4-0.2* (a), *T-Ph-PMO-0.3-0.2* (b) and *T-Ph-PMO-0.2-0.2* (c). The isotherms are offset vertically by 200 (a), and 50 $cm^3 \cdot g^{-1}$ (b), respectively.

Nitrogen sorption isotherms (Figure 4.3A) of the template-free mesoporous Ph-PMO-0.4-0.2 composites exhibit representative type IV curves with a sharp capillary condensation step at a relative pressure range of 0.7 ~ 0.8, indicative of a large uniform mesopore. A large H2-type-like hysteresis loop at a relative pressure of 0.4 ~ 0.5 is observed, implying a cage-like mesostructure with imperfect cylinder channels and a window size smaller than 5.0 nm. It may be caused by the different shrinkage between organosilica and F127 template [50, 51], which is in agreement with the poorly resolved XRD patterns (Figure 4.1A). The phenyl-bridged mesoporous Ph-PMO-0.4-0.2 material has a BET surface area of 1150 $m^2 \cdot g^{-1}$, a pore volume of 1.39 $cm^3 \cdot g^{-1}$. The pore diameter is calculated according to the BJH model to be 9.9 nm (Figure 4.3B), which is the largest ever reported for ordered phenyl-bridged PMO materials. Based on N_2 sorption and XRD results, the pore wall thickness is calculated to be as large as 6.3 nm, which is larger than that reported previously [32, 39, 46].

Similarly, all template-free mesoporous samples Ph-PMO exhibit typical type IV isotherms with imperfect pores larger than 6 nm. With decreasing the F127 content or increasing HCl concentration, the nitrogen condensation shifts to low relative pressure (P/P_0), indicating a decrease of mesopore size. These results are consistent with the decrease of unit cell parameters calculated from the XRD data, which could suggest that increasing the F127 contents or lowering the HCl concentration is of benefit in producing ordered 2D hexagonal PMOs with large-pores in our case. It should be noted that the HCl concentration has a greater effect than F127 content on the formation of the thick pore wall. When the acid concentration increases, the pore wall thickness shows an increased tendency from 5.8 to 6.9 nm, while the wall thickness does not appear to be correlated with the increase of F127 content. The thick pore wall is therefore possibly related to the thickness of silicate layers (SiO_2), because high acid concentration yields fast condensation of silica oligomers and thick layers.

4.3.2 Mesopore frameworks

^{29}Si MAS NMR spectrum (Figure 4.4a) of the template-free Ph-PMO-0.4-0.2 sample show two signals at -68.0, and -75.0 ppm, which can be assigned to T^2 [C-Si(OH)$(OSi)_2$] and T^3 [C-Si$(OSi)_3$] sites, respectively. It suggests an incorporation of the phenyl-bridged groups into the pore walls. Two other resonances around -90.9 and -100.0 ppm ascribed to Q^2 $(OH)_2Si(OSi)_2$, and Q^3 (OH)Si$(OSi)_3$ sites of silicates are also observed [52, 53]. The T^3/T^2 ratio is about 0.77, which is lower than that for Ph-

PMOs prepared from alkyltrimethylammonium under basic conditions [35], and comparable to that from Pluronic P123 and the hydrothermal approach under acid conditions [38], further suggesting a full incorporation of phenyl-bridged groups. The ratio of Q/(T + Q) is about 0.25, suggesting that a partial cleavage of the Si-C bonds occurs during the calcination. The ^{13}C CP-MAS NMR NMR spectrum (Figure 4.4b) of the template-free sample Ph-PMO-0.4-0.2 further reveal that the silica framework is bonded covalently through the phenyl-bridging groups. The occurrence of a strong signal at about 133.2 ppm along with sidebands (denoted with asterisks) is attributed to the carbons in the phenyl group connected to Si atoms. Additionally, no signal is observed for Pluronic F127, suggesting that the template is completely removed after the calcination.

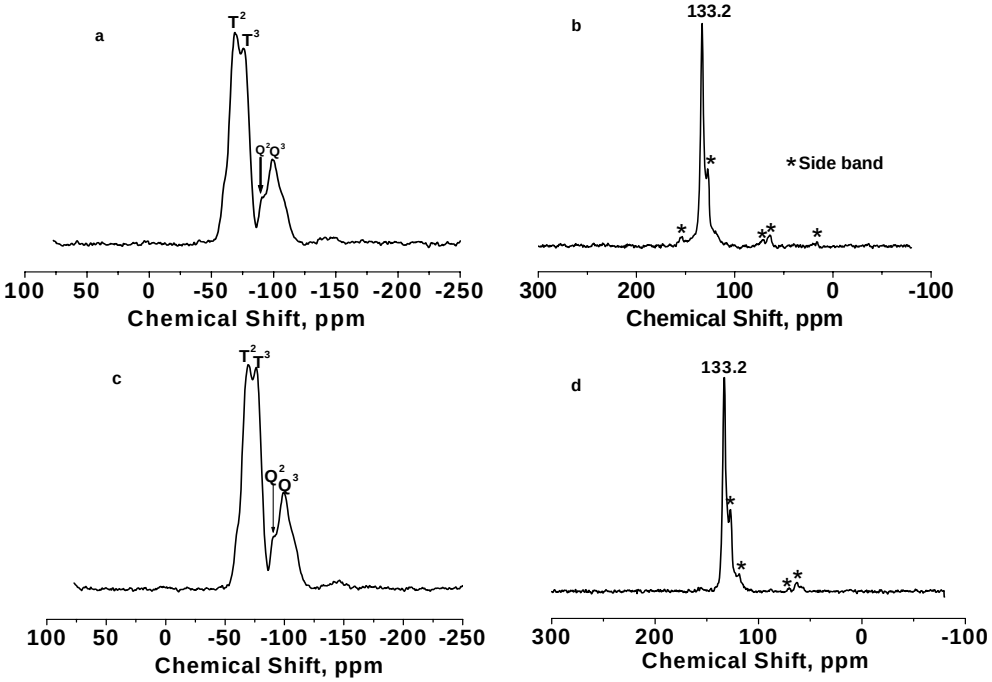

Figure 4.4. ^{29}Si-NMR and ^{13}C-NMR MAS NMR spectra (a, b) for the template-free mesoporous Ph-PMO-0.4-0.2 composite synthesized by the EISA approach and (c, d) for the template-free *T-Ph-PMO-0.4-0.2* composite after the mixed-solvothermal treatment at 100 °C for 3 days in DMF and water (V: V = 1: 1).

FTIR spectra (Figure 4.5) of the template-free Ph-PMO samples prepared with different F127 contents and HCl concentrations show two intense bands at 525 and 1648 cm^{-1}, which are attributed to the Si-C and asymmetric phenylene (C=C) stretching modes, respectively. The peaks at 1159 and 2891 cm^{-1} are attributed to the bridging phenyl C-H vibration and stretching, respectively. These findings indicate the Si-C stability and the integrity of phenyl groups within the silica matrix in the

synthetic and calcinations process. Furthermore, the sharp band at 1075 cm^{-1} from Si-O stretching confirms the formation of siloxane bonds. The band at 3435 cm^{-1} is from the Si-OH groups [54]. These results further reveal that the frameworks are inorganic-organic hybrid composites of the phenyl-bridging groups and silicates.

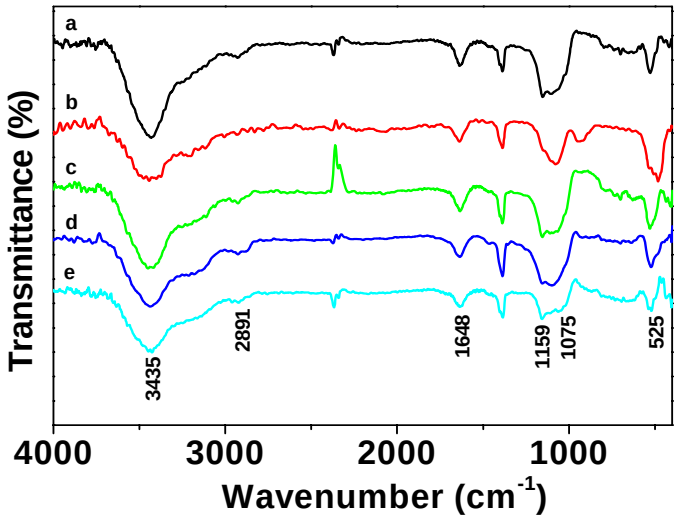

Figure 4.5. FT-IR spectra of the template-free phenyl-bridged PMOs synthesized by the EISA approach with different Pluronic F127 content and HCl concentration: Ph-PMO-0.2-0.1 (a), Ph-PMO-0.3-0.1 (b), Ph-PMO-0.2-0.2 (c), Ph-PMO-0.3-0.2 (d) and Ph-PMO-0.4-0.2 (e).

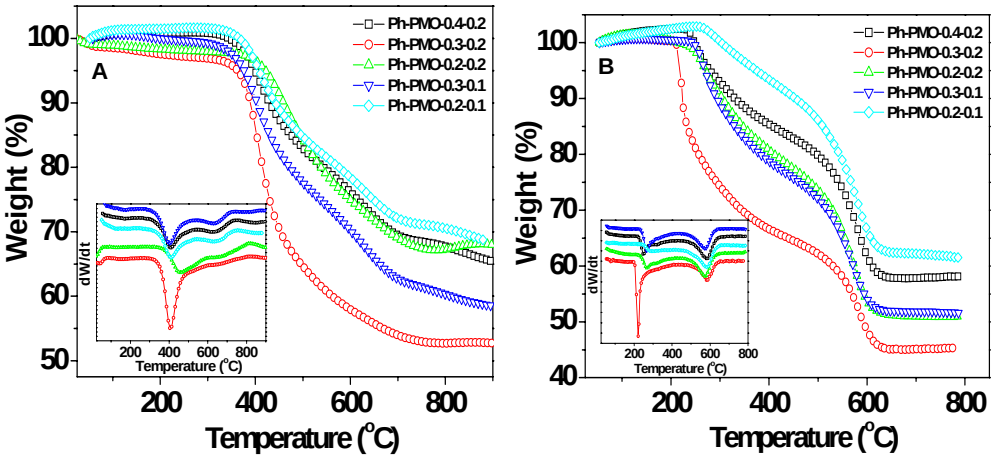

Figure 4.6. TGA and corresponding differential thermogravimetric (DTG) curves (A) in nitrogen of the template-free Ph-PMOs composites synthesized by the EISA approach with different F127 content and HCl concentration. (B) in air of the template-free Ph-PMOs composites synthesized by the EISA approach with different F127 content and HCl concentration.

Thermogravimetric analyses (TGA) of the template-free Ph-PMO materials show three major weight losses at 25 ~ 900 °C in a nitrogen atmosphere (Figure 4.6A). A

weight loss of less than 3 % below 150 °C is observed, probably due to physical absorbed water. The absence of a major weight loss between 250 ~ 400 °C suggests the successful removal of triblock copolymer F127 by calcination. The sharp weight loss from 400 to 800 °C results from the decomposition of the phenyl-bridging groups, suggesting a stable organic–inorganic composite framework. During this period, it is noted that the weight loss follows the order: Ph-PMO-0.3-0.2 > Ph-PMO-0.3-0.1 > Ph-PMO-0.2-0.2 ≈ Ph-PMO-0.4-0.2 > Ph-PMO-0.2-0.1, which suggests that the higher the acid concentration, the more phenyl groups are incorporated into the framework. It is related to a fast condensation and cross-linking of silicates.

Comparatively, TGA in air of template-free Ph–PMO materials (Figure 4.6B) displays a weight loss between 250 ~ 400 °C, which could be assigned to the decomposition of a small amount of bridged phenyl groups or a small portion of residual template. The weight loss from 400 to 800 °C mainly results from the decomposition of phenyl moieties or oxidation of carbon in air. The weight loss (22 ~ 30 %) of samples from 400 to 800 °C is less than the theoretical values of carbon content (37.5 %), assuming that much of the phenyl groups is incorporated into the framework during the synthesis process.

4.3.3 Mixed-solvothermal treatment

It is well-known that hydrothermal treatment is usually adopted for the as-synthesized powder samples or after the solution reaction, which is one of the most efficient methods for improving the regularity of products where the mesostructures undergo reorganization, growth, and crystallization [44]. The hydrolysis, cross-linking, and recrystallization of silicate species can further proceed during the hydrothermal process [45]. Based on our results, the mesoporous Ph-PMO materials have no periodicity in the pore walls by using Pluronic triblock polymer as a template, which may be related to the penetration of the PEO moieties and breakage of the π-π interaction between phenyl-bridging groups. Taking advantage of hydrothermal treatment and recrystallization, the arrangement of the phenyl groups and the periodicity in the pore walls could be improved, because of the reorganization. We treated the Ph-PMO samples under a mixed-solvothermal condition in water and DMF solvents at 100 °C for 3 days. The water may interact with silicate species and DMF molecules interact with phenyl groups, which would retract Pluronic F127

molecules from the pore walls and reorganize the π-π stacking of the phenyl groups, probably improving the periodicity.

In our case, the as-made Ph-PMO-x-0.2 materials prepared from the EISA approach mixed solvothermally were treated in a solution of water and DMF (V:V = 1:1) at 100 °C for 3 days. Low-angle XRD patterns of the template-free *T-Ph-PMO-x-0.2* materials after the treatment are still resolved, suggesting that the ordered hexagonal *p6mm* mesostructures are well retained (Figure 4.1C). Moreover, the intensity and d_{100} spacing increase a little after the mixed-solvothermal treatment, implying a slight improvement of mesotructure and enlargement of unit cell parameter. The high-angle XRD patterns of the template-free products display two broad diffraction peaks at 2 θ = 11.5 and 23.2 ◦ (Figure 4.1D), which corresponds to the *d*-spacing of about 0.76 and 0.38 nm. After the DMF-water mixed-solvothermal treatment, diffraction intensity for both diffraction peaks obviously increase, clearly suggesting an improvement of the molecular periodicity of the mesopore walls. However, the diffractions are too broad and their intensity is too weak to assign a periodicity at the molecular level. HRTEM images of the template-free *T-Ph-PMO-0.3-0.2* material after the mixed-solvothermal treatment (Figure 4.2e and f) show some weak lattice fringes stacked along the channel axes. The intensity across parallel fringes along the white line in Figure 4.2f reveals the lattice fringes with about 0.75 nm spacing between two adjacent peaks (Figure 4.2g), which is close to the length of phenyl-bridging group. This further implies that the mixed-solvothermal treatment can improve the regularity of the lamellar structure in the pore walls.

N_2 sorption measurements (Figure 4.3C, D) show that all template-free mesoporous *T-Ph-PMO-x-0.2* composites after the mixed-solvothermal treatment at 100 °C for 3 days also exhibit typical type-IV isotherms with large H_2-type-like hysteresis loops, indicating imperfect cylinder mesopores similar to that before the treatment. The nitrogen condensation shifts to a lower relative pressure, suggesting a decrease of mesopore sizes from 9.0 to 7.8 nm (Table 4.1). The wall thicknesses are calculated to increase up to 7.7 nm (Table 4.1). The pore volume also decreases from 1.39 to 0.50 $cm^3 \cdot g^{-1}$, whereas the surface area decreases slightly. These results further confirm that a reorganization occurs during the mixed-solvothermal treatment. ^{29}Si MAS NMR spectrum (Figure 4.4c) of the template-free *T-Ph-PMO-0.4-0.2* composite after the mixed-solvothermal treatment also show two signals at -69.4 and -76.1 ppm for T^2

and T^3 sites, respectively. Two other resonances around -91.0 and -99.0 ppm from Q^2 and Q^3 sites of silicates are also observed. The T^3/T^2 ratio increases to about 0.92, which is slightly higher than that without solvothemal treatment. The ratio of Q/(T + Q) is about 0.27, close to that before the treatment, suggesting that the Si-C bond cleavage does not occur during the treatment. The ^{13}C CP-MAS NMR spectrum (Figure 4.4d) of the template-free *T-Ph-PMO-0.4-0.2* sample after the mixed-solvothermal treatment further reveals that the framework is bonded covalently through the phenyl-bridging groups.

On the basis of the above observations, we postulate that unlike the cationic surfactant, Pluronic triblock copolymers interact with silicate species *via* hydrogen bonding to assemble the ordered mesostructure. The long PEO moieties possibly penetrate into the silica pore walls, thereby breaking the π-π interaction between phenyl groups. This induces a collapse of the molecular periodicity in the pore walls. During the mixed-solvothermal treatment, the water can retract Pluronic F127 molecules from the pore walls and enlarge the wall thickness. Simultaneously, DMF, a strong polar solvent, can dissolve in water completely and may help to reorganize the π-π stacking of the phenyl groups to some extent, improving the molecular periodicity on the walls. Therefore, water-DMF mixed-solvothermal treatment proposed here may provide a proper micro-environment to improve the structural arrangement of organic-inorganic composites.

4.3.4 Adsorption of volatile benzene

All the benzene isotherms of the large-pore Ph-PMO composites prepared with different F127 contents and HCl concentrations show similar curves, which are nearly type IV isotherms (Figure 4.7). A steep increase at low relative pressure (< 0.04), corresponding to micropore filling, is observed. After the micropores are partially saturated, it exhibits a sharp uptake at a relative pressure of 0.24 ~ 0.36 due to capillary condensation of benzene in the mesopores. The mesopores can gradually take up gas molecules with the increase of pressure, thus showing the gradual adsorption increase in the isotherms. This may be because the silicate layers of the PMO frameworks are hydrophilic, while the phenyl groups inside the pore walls are hydrophobic. When the pressure is high, the interaction of benzene molecules with the phenyl-bridging groups is dominant, which contributes to an increase of the adsorption. The mesoporous phenyl-bridged Ph-PMO-0.4-0.2 material exhibits a high

adsorption capability of volatile benzene up to 2.06 mmol·g^{-1} at high pressure (P/P_0 ~ 0.90), due to its large surface area. With the increase of surface area, the adsorption capacity increases. Comparatively, the Ph-PMO-0.3-0.2 composite shows the lowest benzene adsorption of 0.86 mmol·g^{-1}, suggesting that the capability is also related to wall thickness as well as the low surface area. As the pore wall thickness increases, the packing of phenyl-bridging groups in the walls tends to be denser and disordered, which does not favor interaction with benzene rings by the π-π stacking, resulting in a decrease of the amount of adsorption.

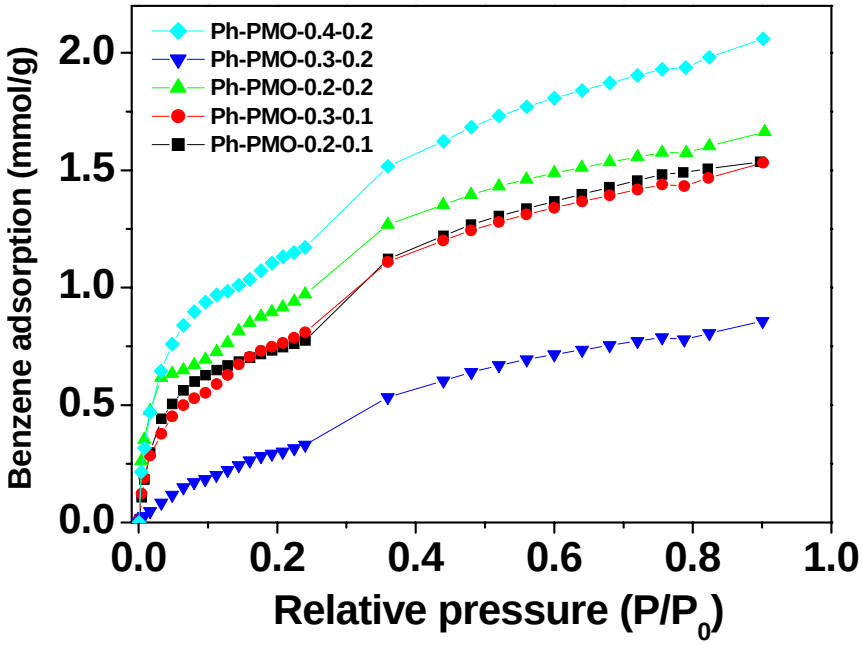

Figure 4.7. Adsorption isotherms of volatile benzene on the obtained Ph-PMO materials at 25 °C.

4.4 Conclusions

Phenyl-bridged PMOs with ordered hexagonal mesostructures and imperfect cylinder pores have been synthesized *via* simple EISA approach by using Pluronic F127 as a template. By adjusting the F127 content and HCl concentration, the pore size and wall thickness can be simply tuned. The obtained organic-functional materials show a high BET surface area (~ 1150 m^2·g^{-1}), and a large uniform pore size (up to 9.9 nm). The increased wall thickness from 5.8 to 6.9 nm is in proportion to the thickness of silicate layers in the framework during the synthesis process. The mixed-solvothermal treatment is first demonstrated to improve the periodicity in the pore walls somewhat, as well as increase the wall thickness up to 7.7 nm. The presence of phenyl functional groups in the framework endows these materials with the

adsorption capacity of benzene up to 2.06 $mmol \cdot g^{-1}$, which suggests that they are a potential candidates for adsorption of organic compounds.

References

[1] F. Hoffmann, M. Cornelius, J. Morell, M. Fröba, "Silica-Based Mesoporous Organic-Inorganic Hybrid Materials," *Angew. Chem. Int. Ed.* **2006**, *45*, 3216-3251.

[2] Q. H. Yang, J. Liu, J. Yang, M. P. Kapoor, S. Inagaki, C. Li, "Synthesis, Characterization, and Catalytic Activity of Sulfonic Acid-Functionalized Periodic Mesoporous Organosilicas," *J. Catal.* **2004**, *228*, 265-272.

[3] S. Hamoudi, S. Royer, S. Kaliaguine, "Propyl- and Arene-Sulfonic Acid Functionalized Periodic Mesoporous Organosilicas," *Micropor. Mesopor. Mater.* **2004**, *71*, 17-25.

[4] Q. H. Yang, M. P. Kapoor, S. Inagaki, N. Shirokura, J. N. Kondo, K. Domen, "Catalytic Application of Sulfonic Acid Functionalized Mesoporous Benzene-Silica with Crystal-Like Pore Wall Structure in Esterification," *J. Mol. Catal. A* **2005**, *230*, 85-89.

[5] K. Nakajima, I. Tomita, M. Hara, S. Hayashi, K. Domen, J. N. Kondo, "A Stable and Highly Active Hybrid Mesoporous Solid Acid Catalyst," *Adv. Mater.* **2005**, *17*, 1839-1842.

[6] Y. Wan, D. Q. Zhang, Y. P. Zhai, C. M. Feng, J. Chen, H. X. Li, "Periodic Mesoporous Organosilicas: A Type of Hybrid Support for Water-Mediated Reactions," *Chem. Asian J.* **2007**, *2*, 875-881.

[7] M. C. Burleigh, S. Dai, E. W. Hagaman, J. S. Lin, "Imprinted Polysilsesquioxanes for the Enhanced Recognition of Metal Ions," *Chem. Mater.* **2001**, *13*, 2537-2546.

[8] S. Dai, M. C. Burleigh, Y. H. Ju, H. J. Gao, J. S. Lin, S. J. Pennycook, C. E. Barnes, Z. L. Xue, "Hierarchically Imprinted Sorbents for the Separation of Metal Ions," *J. Am. Chem. Soc.* **2000**, *122*, 992-993.

[9] L. X. Zhang, W. H. Zhang, J. L. Shi, Z. L. Hua, Y. S. Li, J. N. Yan, "A New Thioether Functionalized Organic-Inorganic Mesoporous Composite as A Highly Selective and Capacious Hg^{2+} Adsorbent," *Chem. Commun.* **2003**, 210-211.

[10] J. Liu, J. Yang, Q. H. Yang, G. Wang, Y. Li, "Hydrothermally Stable Thioether-Bridged Mesoporous Materials with Void Defects in the Pore Walls," *Adv. Funct. Mater.* **2005**, *15*, 1297-1302.

[11] K. Z. Hossain, L. Mercier, "Intraframework Metal Ion Adsorption in Ligand-Functionalized Mesoporous Silica," *Adv. Mater.* **2002**, *14*, 1053-1056.

[12] V. Rebbin, R. Schmidt, M. Fröba, "Spherical Particles of Phenylene-Bridged Periodic Mesoporous Organosilica for High-Performance Liquid Chromatography," *Angew. Chem. Int. Ed.* **2006**, *45*, 5210-5214.

[13] S. Inagaki, S. Guan, Y. Fukushima, T. Ohsuna, O. Teresaki, "Novel Mesoporous Materials with a Uniform Distribution of Organic Groups and Inorganic Oxide in Their Frameworks," *J. Am. Chem. Soc.* **1999**, *121*, 9611-9614.

[14] T. Asefa, M. J. MacLachlan, N. Coombos, G.A. Ozin, "Periodic Mesoporous Organosilicas with Organic Groups inside the Channel Walls," *Nature* **1999**, *402*, 867-871.

[15] B. J. Melde, B. T. Holland, C. F. Blandford, A. Stein, "Mesoporous Sieves with Unified Hybrid Inorganic/Organic Frameworks," *Chem. Mater.* **1999**, *11*, 3302-3308.

[16] A. Sayari, S. Hamoudi, Y. Yang, I. L. Moudrakovski, J. R. Ripmeester, "New Insights into the Synthesis, Morphology, and Growth of Periodic Mesoporous Organosilicas," *Chem. Mater.* **2000**, *12*, 3857-3863.

[17] W. P. Guo, I. Kim, C. S. Ha, "Highly Ordered Three-Dimensional Large-Pore Periodic Mesoporous Organosilica with *Im3m* Symmetry," *Chem. Commun.* **2003**, 2692-2693.

[18] Z. D. Zhang, B. Z. Tian, X. X. Yan, S. D. Shen, X. Y. Liu, D. H. Chen, G. S. Zhu, D. Y. Zhao, S. L. Qiu, "An Easy Route for the Synthesis of Ordered Three-Dimensional Large-Pore Mesoporous Organosilicas with *Im-3m* Symmetry," *Chem. Lett.* **2004**, *33*, 1132-1133.

[19] Z. D. Zhang, X. X. Yan, B. Z. Tian, S. D. Shen, D. H. Chen, G. S. Zhu, S. L. Qiu, D. Y. Zhao, "Synthesis of Large-Pore Periodic Mesoporous Organosilica (PMO) with Biocontinuous Cubic Structure of *Ia-3d* Symmetry," *Chem. Lett.* **2005**, *34*, 133-134.

[20] L. Zhao, G. S. Zhu, D. L. Zhang, Y. Di, Y. Chen, O. Terasaki, S. L. Qiu, "Synthesis and Structural Identification of a Highly Ordered Mesoporous Organosilica with Large Cagelike Pores," *J. Phys. Chem. B* **2005**, *109*, 764-768.

[21] O. Muth, C. Schellbach, M. Fröba, "Triblock Copolymer Assisted Synthesis of Periodic Mesoporous Organosilicas (PMOs) with Large Pores," *Chem. Commun.* **2001**, 2032-2033.

[22] H. G. Zhu, D. J. Jones, J. Zajac, J. Roziere, R. Dutartre, "Periodic Large Mesoporous Organosilicas from Lyotropic Liquid Crystal Polymer Templates," *Chem. Commun.* **2001**, 2568-2569.

[23] W. P. Guo, J. Y. Park, M. O. Oh, H. W. Jeong, W. J. Cho, I. Kim, C. S. Ha, "Triblock Copolymer Synthesis of Highly Ordered Large-Pore Periodic Mesoporous Organosilicas with the Aid of Inorganic Salts," *Chem. Mater.* **2003**, *15*, 2295-2298.

[24] X. Y. Bao, X. S. Zhao, X. Li, P. A. Chia, J. Li, "A Novel Route toward the Synthesis of High-Quality Large-Pore Periodic Mesoporous Organosilicas," *J. Phys. Chem. B* **2004**, *108*, 4684-4689.

[25] Y. F. Lu, H.Y. Fan, N. Doke, D.A. Loy, R.A. Assink, D.A. LaVan, C.J. Brinker, "Evaporation-Induced Self-Assembly of Hybrid Bridged Silsesquioxane Film and Particulate Mesophases with Integral Organic Functionality," *J. Am. Chem. Soc.* **2000**, *122*, 5258-5261.

[26] S. Guan, S. Inagaki, T. Ohsuna, O. Terasaki, "Cubic Hybrid Organic-Inorganic Mesoporous Crystal with a Decaoctahedral Shape," *J. Am. Chem. Soc.* **2000**, *122*, 5660-5661.

[27] M. P. Kapoor, S. Inagaki, "Synthesis of Cubic Hybrid Organic-Inorganic Mesostructures with Dodecahedral Morphology from a Binary Surfactant Mixture," *Chem. Mater.* **2002**, *14*, 3509-3514.

[28] D. J. Kim, J. S. Chung, W. S. Ahn, G. W. Kam, W. J. Cheong, "Morphology Control of Organic-Inorganic Hybrid Mesoporous Silica by Microwave Heating," *Chem. Lett.* **2004**, *33*, 422-423.

[29] V. Rebbin, M. Jakubowski, S. Potz, M. Fröba, "Synthesis and Characterisation of Spherical Periodic Mesoporous Organosilicas (sph-PMOs) with Variable Pore Diameters," *Micropor. Mesopor. Mater.* **2004**, *72*, 99-104.

[30] M. P. Kapoor, S. Inagaki, "Synthesis of Phenylene Bridged Mesoporous Silsesquioxanes with Spherical Morphology in Ammonia Solution," *Chem. Lett.* **2004**, *33*, 88-89.

[31] S. Z. Qiao, C. Z. Yu, W. Xing, Q. H. Hu, H. Djojoputro, G. Q. Lu, "Synthesis and Bio-adsorptive Properties of Large-Pore Periodic Mesoporous Organosilica Rods," *Chem. Mater.* **2005**, *17*, 6172-6176.

[32] Y. Goto, K. Okamoto, S. Inagaki, "The Formation of Periodicity within the Pore Walls of Mesoporous Organosilica by Post-Synthesis Treatment," *Bull. Chem. Soc. Jpn.* **2005**, *78*, 932-936.

[33] D. Y. Zhao, J. L. Feng, Q. S. Huo, N. Melosh, G. H. Fredrickson, B. F. Chmelka, G. D. Stucky, "Triblock Copolymer Syntheses of Mesoporous Silica with Periodic 50 to 300 Angstrom Pores," *Science* **1998**, *279*, 548-552.

[34] X. F. Zhou, S. Z. Qiao, N. Hao, X. L. Wang, C. Z. Yu, K. L. Wang, D. Y. Zhao, G. Q. Lu, "Synthesis of Ordered Cubic Periodic Mesoporous Organosilicas with Ultra-Large Pores," *Chem. Mater.* **2007**, *19*, 1870-1876.

[35] S. Inagaki, S. Guan, T. Ohsuna, O. Terasaki, "An Ordered Mesoporous Organosilica Hybrid Material with A Crystal-Like Wall Structure," *Nature* **2002**, *416*, 304-307.

[36] M. P. Kapoor, Q. H. Yang, S. Inagaki, "Self-Assembly of Biphenylene-Bridged Hybrid Mesoporous Solid with Molecular-Scale Periodicity in the Pore Walls," *J. Am. Chem. Soc.* **2002**, *124*, 15176-15177.

[37] M. P. Kapoor, S. Inagaki, S. Ikeda, K. Kakiuchi, M. Suda, T. Shimada, "An Alternate Route for the Synthesis of Hybrid Mesoporous Organosilica with Crystal-Like Pore Walls from Allylorganosilane Precursors," *J. Am. Chem. Soc.* **2005**, *127*, 8174-8178.

[38] Y. Goto, S. Inagaki, "Synthesis of Large-Pore Phenylene-Bridged Mesoporous Organosilica using Triblock Copolymer Surfactant," *Chem. Commun.* **2002**, 2410-2411.

[39] E. B. Cho, D. Kim, M. Jaroniec, "Role of Aluminum Salts in the Synthesis of Polymer-Templated Periodic Mesoporous Organosilicas," *Chem. Mater.* **2008**, *20*, 2468-2475.

[40] B. Z. Tian, X. Y. Liu, L. A. Solovyov, Z. Liu, H. F. Yang, Z. D. Zhang, S. H. Xie, F. Q. Zhang, B. Tu, C. Z. Yu, O. Terasaki, D. Y. Zhao, "Facile Synthesis and Characterization of Novel Mesoporous and Mesorelief Oxides with Gyroidal Structures," *J. Am. Chem. Soc.* **2004**, *126*, 865-875.

[41] D. Y. Zhao, P. D. Yang, N. Melosh, J. L. Feng, B. F. Chmelka, G. D. Stucky, "Continuous Mesoporous Silica Films with Highly Ordered Large Pore Structures," *Adv. Mater.* **1998**, *10*, 1380-1385.

[42] B. Z. Tian, X. Y. Liu, Z. D. Zhang, B. Tu, D. Y. Zhao, "Syntheses of High-Quality Mesoporous Materials Directed by Blends of Nonionic Amphiphiles under Nonaqueous Conditions," *J. Solid State Chem.* **2002**, *167*, 324-329.

[43] Y. F. Lu, R. Ganguli, C. A. Drewien, M. T. Anderson, C. J. Brinker, W. L. Gong, Y. X. Guo, H. Soyez, B. Dunn, M. H. Huang, J. I. Zink, "Continuous Formation of

Supported Cubic and Hexagonal Mesoporous Films by Sol-Gel Dip-Coating," *Nature* **1997**, *389*, 364-368.

[44] Y. Wan, D. Y. Zhao, "On the Controllable Soft-Templating Approach to Mesoporous Silicates," *Chem. Rev.* **2007**, *107*, 2821-2860.

[45] Y. Wan, Y. F. Shi, D. Y. Zhao, "Designed Synthesis of Mesoporous Solids via Nonionic-Surfactant-Templating Approach," *Chem. Commun.* **2007**, 897-926.

[46] S. S. Park, D. H. Park, C. S. Ha, "Free-Standing Periodic Mesoporous Organosilica Film with a Crystal-like Wall Structure," Chem. *Mater.* **2007**, *19*, 2709-2711.

[47] E. B. Cho, K. W. Kwon, K. Char, "Mesoporous Organosilicas Prepared with PEO-Containing Triblock Copolymers with Different Hydrophobic Moieties," Chem. *Mater.* **2001**, *13*, 3837-3839.

[48] J. R. Matos, M. Kruk, L. P. Mercuri, M. Jaroniec, T. Asefa, N. Coombs, G. A. Ozin, T. Kamiyama, O. Terasaki, "Periodic Mesoporous Organosilica with Large Cagelike Pores," Chem. *Mater.* **2002**, *14*, 1903-1905.

[49] C. Z. Yu, B. Z. Tian, J. Fan, G. D. Stucky, "Salt Effect in the Synthesis of Mesoporous Silica Templated by Non-Ionic Block Copolymers," *Chem. Commun.* **2001**, 2726-2727.

[50] D. H. Chen, Z. Li, Y. Wan, X. J. Tu, Y. F. Shi, Z. X. Chen, W. Shen, C. Z. Yu, B. Tu, D. Y. Zhao, "Anionic Surfactant Induced Mesophase Transformation to Synthesize Highly Ordered Large-Pore Mesoporous Silica Structures," *J. Mater. Chem.* **2006**, *16*, 1511-1519.

[51] R. L. Liu, Y. F. Shi, Y. Wan, Y. Meng, F. Q. Zhang, D. Gu, Z. X. Chen, B. Tu, D. Y. Zhao, "Triconstituent Co-assembly to Ordered Mesostructured Polymer-Silica and Carbon-Silica Nanocomposites and Large-Pore Mesoporous Carbons with High Surface Areas," *J. Am. Chem. Soc.* **2006**, *128*, 11652-11662.

[52] J. S. Beck, J. C. Vartuli, W. J. Roth, M. E. Leonowicz, C. T. Kresge, K. D. Schmitt, C. T. W. Chu, D. H. Olson, E. W. Sheppard, "A New Family of Mesoporous Molecular Sieves Prepared with Liquid Crystal Templates," *J. Am. Chem. Soc.* **1992**, *114*, 10834-10843.

[53] W. H. Zhang, X. N. Zhang, Z. L. Hua, P. Harish, F. Schroeder, S. Hermes, T. Cadenbach, J. L. Shi, R. A. Fischer, "Synthesis, Bifunctionalization, and Application of Isocyanurate-Based Periodic Mesoporous Organosilicas," *Chem. Mater.* **2007**, *19*, 2663-2670.

[54] M. Cornelius, F. Hoffmann, M. Fröba, “Periodic Mesoporous Organosilicas with a Bifunctional Conjugated Organic Unit and Crystal-like Pore Walls,” *Chem. Mater.* **2005**, *17*, 6674-6678.

CHAPTER 5 A Metal-Ion-Assisted Assembly Approach to Synthesize Disulfide-Bridged PMOs with High Sulfide Contents and Efficient Adsorption

5.1 Introduction

One of the significant breakthroughs in the area of nanostructured organic-inorganic hybrid materials was the discovery of periodic mesoporous organosilicas (PMOs), which contain organic groups instead of oxygen in siloxane bridges of the silica framework [1-3]. This discovery opened almost unlimited possibilities to design novel PMOs with uniformly distributed organic and organometallic groups within silica framework and to tailor their chemical reactivity in catalysis [4-8], and adsorption performance [9-14] as well as their electronic, and optical properties [15-18]. It has been known that ordered PMOs can be synthesized by using silesquioxane precursors with organic bridging groups as a silica precursor and amphiphilic surfactants as a template *via* the self-assembly method, similar to that for mesoporous silicates [1-3]. However, compared with the mesoporous silicas or/and functional mesoporous silicas with terminally bonded organic groups, many advantages of PMOs are evident, such as (a) up to 100 % of Si atoms can be connected to organic functional groups; (b) the organic groups are homogeneously distributed in the frameworks to form organic – inorganic composites; (c) the organic groups inside the silicate frameworks impart characteristics or various surface polarity, thus endowing PMOs a wide range of opportunities for designing materials with unique properties. So far, "rigid" organic chain bridging groups originating from methane, ethane, ethylene, as well as small organic aromatic ones such as thiophene, xylene, benzene and biphenylene have successfully been incorporated into the ordered PMO frameworks by amphiphilic-surfactant-assembly synthesis approaches [17, 19-30]. However, PMOs with long chain silesquioxane functional moieties are not easily synthesized, because the large molecular size or complexity of bridging organic groups could not benefit the self-assembly of mesostructures with surfactant to be immobilized in a 3D continuous framework [9, 31, 32]. The utilization of 100 % "soft" bridging organic silanes as a silica precursor usually leads to disordered or worm-like mesostructures.

Much effort has been made by previous researchers but without success. A possible but undesirable method is to incorporate a certain amount of fully hydrolysible silanes

such as TMOS, TEOS in the co-condensation process to help construction of the ordered mesostructural framework [12]. However, the incorporated amount of "soft" bridging organic silane precursors is quite low (normally < 5 %). Therefore, it remains a challenge to enhance the content of the functional organic moieties with ordered mesostructures and open frameworks.

Thiother groups show strong affinity for metal ions and ideal functional sites on mesoporous materials as an efficient adsorbent to remove heavy metal ions in wastewaters. Furthermore, thioether can be oxidized to sulfonic acid groups functioning as an acid catalyst. Much attention has been paid to the synthesis of ordered mesoporous materials with high loading of thioether groups. Shi and co-workers have synthesized thioether functionalized mesoporous silicas by the one-pot co-condensation method of TEOS and tetrasulfidesilane (BTESPTS). However, when the thiother content was higher than 10 %, the obtained functional mesoporous silica became a wormlike disordered structure [12]. Recently, Jaroniec and co-workers have reported a synthesis of ordered large-pore PMO materials with disulfide bridging groups via a co-condensation method by using the mixture of BTSPDS and TEOS as silica precursors and triblock copolymers as a template [33]. However, the disulfide content was as low as 3.0 % (molar ratio) in the framework. With the increasing disulfide content, disordered mesostructured PMOs are obtained. In order to improve the mesostructural regularity, they demonstrated a microwaveassisted approach and obtained ordered hexagonal disulfidebridged PMOs. Unfortunately, the disulfide content was as low as 2.5 % [34]. Yang and co-workers conducted the synthesis in a buffer solution by using Pluronic P123 as a template, however, the ordered disulfide-bridged PMOs could not be obtained when the disulfide content is higher than ~ 5.0 % [35].

In this chapter, a novel and simple metal-ion-assisted approach to synthesize well-ordered hexagonal disulfide-bridged PMOs by using BTSPDS as a precursor and Pluronic P123 as a template is reported. The BTSPDS content in the 3D open frameworks is as high as 20 %, while the ordered mesostructure is maintained. Our results clearly show that the metal ions play an important role in the formation of regular mesostructure and incorporation of the long chain disulfide groups into the framework. Furthermore, the adsorption properties for the removal of heavy metal mercury ions from wastewaters were also investigated.

5.2 Experimental

5.2.1 Synthesis of disulfide-bridged PMOs

The ordered mesoporous organosilicas materials with the disulfide groups were hydrothermally prepared by using Pluronic P123 as a template and a blend of BTSPDS and TEOS as a silica source in the 2 M HCl aqueous solution at 35 °C. Different BTSPDS/TEOS molar ratios of 5: 95, 10: 90, 15: 85 and 20: 80 were adopted in the batch experiments. A typical synthesis was carried out as follows: 0.50 g of Pluronic P123 was completely dissolved in 15.0 g of 2.0 M HCl and 3.8 g of H_2O at 35 °C. To this solution, 0.905 g of TEOS was added under vigorous stirring. Then 0.056 g (0.19 mmol) of $Zn(NO_3)_2 \cdot 6H_2O$ was added into the above mixture. After stirring for about 10 min, 0.369 g of BTSPDS with the molar ratio of BTSPDS/TEOS = 15: 85 was added to the above solution. The reaction mixture was stirred at the same temperature for 24 h, and then transferred into Teflon-lined autoclaves and heated at 100 °C without stirring for another 24 h. After filtering, the sample was washed by water, and dried in air at 40 °C. The solid products were collected and then solvent-extracted with 80 mL of (99.0 %) ethanol and 2.0 mL of (37 wt %) HCl at 60 °C for 24 h in air to remove the copolymer templates. The final mesoporous organosilica materials were obtained after filtration, water washing and air drying at 40 °C. The resultant samples were denoted as DSPMO-x and DS-PMO-NM-x and PMS, where DS-PMO denotes the disulfide-bridged PMO products and PMS represents the periodic mesoporous silica; x refers to the BTSPDS molar contents in the initial silane mixture, and NM represents the synthesis without metal-ion addition.

5.3 Results and discussion

5.3.1 Mesostructure

Small-angle XRD patterns (Figure 5.1a) of the surfactant-free sulphur-containing mesoporous material DS-PMO-15 prepared by the metal-ion (Zn^{2+}) assisted triblock-copolymer assembly approach with BTSPDS molar content of 15 % exhibits three resolved diffraction peaks with *d*-value ratios of 1: $\sqrt{3}$: 2,which can be indexed as the 100, 110 and 200 reflections, respectively, for the 2D ordered hexagonal mesostructure with space group *p6mm*. The corresponding unit cell parameter a_0 is calculated to be 10.8 nm. Similarly, all the DS-PMO samples with different BTSPDS contents of 5 ~ 20 % prepared by the metal-ionassisted assembly approach show

resolved three-peak XRD patterns, clearly demonstrating that highly ordered hexagonal disulfide-bridged PMO composites are obtained. With the increase of BTSPDS/TEOS ratio, the 100 diffraction peak shifts to a higher angle and the mesostructure regularity gradually degenerates to some extent. The result is related to the incorporation of the long hydrophobic disulfide-bridged groups. Compared with that of the tetrasulfide-bridged PMOs prepared under a basic condition [13] and disulfide-bridged one obtained under a buffer solution [35], our 2D hexagonal mesostructure is well retained by the metal-ion assisted with a larger incorporated amount of disulfide groups. By contrast, in the absence of metal ions (Zn^{2+}), XRD patterns (Figure 5.1b) of the DS-PMO-NM-x materials prepared by using mixed BTSPDS and TEOS as a silica source and Pluronic P123 as a template under similar conditions show one broad diffraction peak at a low ratio of BTSPDS/TEOS, suggesting that disordered PMO mesostructures are formed. As the ratio increases, the diffraction peak becomes broader, and disappears when the ratio is higher than 20 %, suggesting a complete collapse of the mesostructure. These results clearly indicate that the incorporation of metal ions into disulfide functional silane precursors can improve the mesostructural regularity during the assembly.

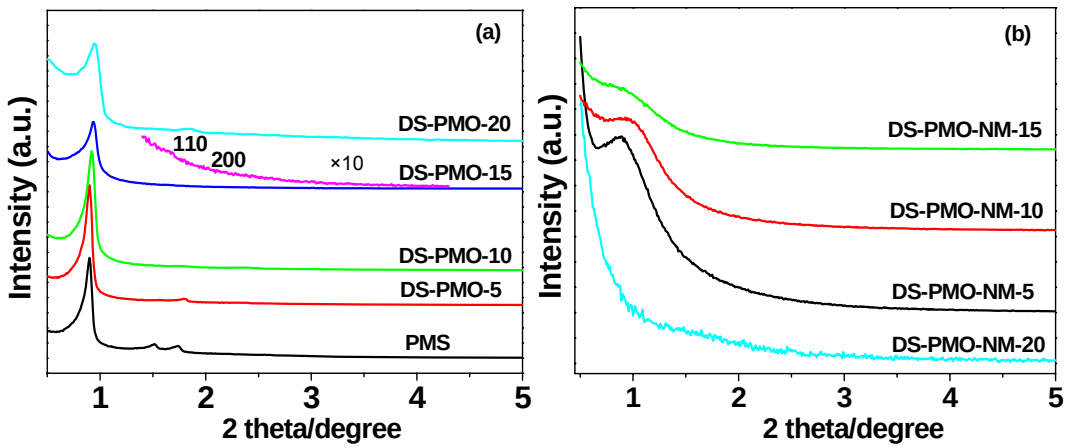

Figure 5.1. XRD patterns of (a) surfactant-free periodic mesoporous silica (PMS), organosilicas (DS-PMO-x) synthesized by the metal-ion (Zn^{2+}) assisted assembly approach with different content of disulfide-bridged group; x = 0, 5; 10; 15; 20 and (b) surfactant-free periodic organosilicas (DS-PMO-x) prepared without adding metal-ion DS-PMO-NW-x (x = 5, 10, 15, and 20).

TEM images reveal more detailed structural information, as shown in Figure 5.2. The surfactant-free mesoporous DS-PMO-15 material prepared with 15 % disulfide-bridged groups show large domains of ordered hexagonal and stripe-like

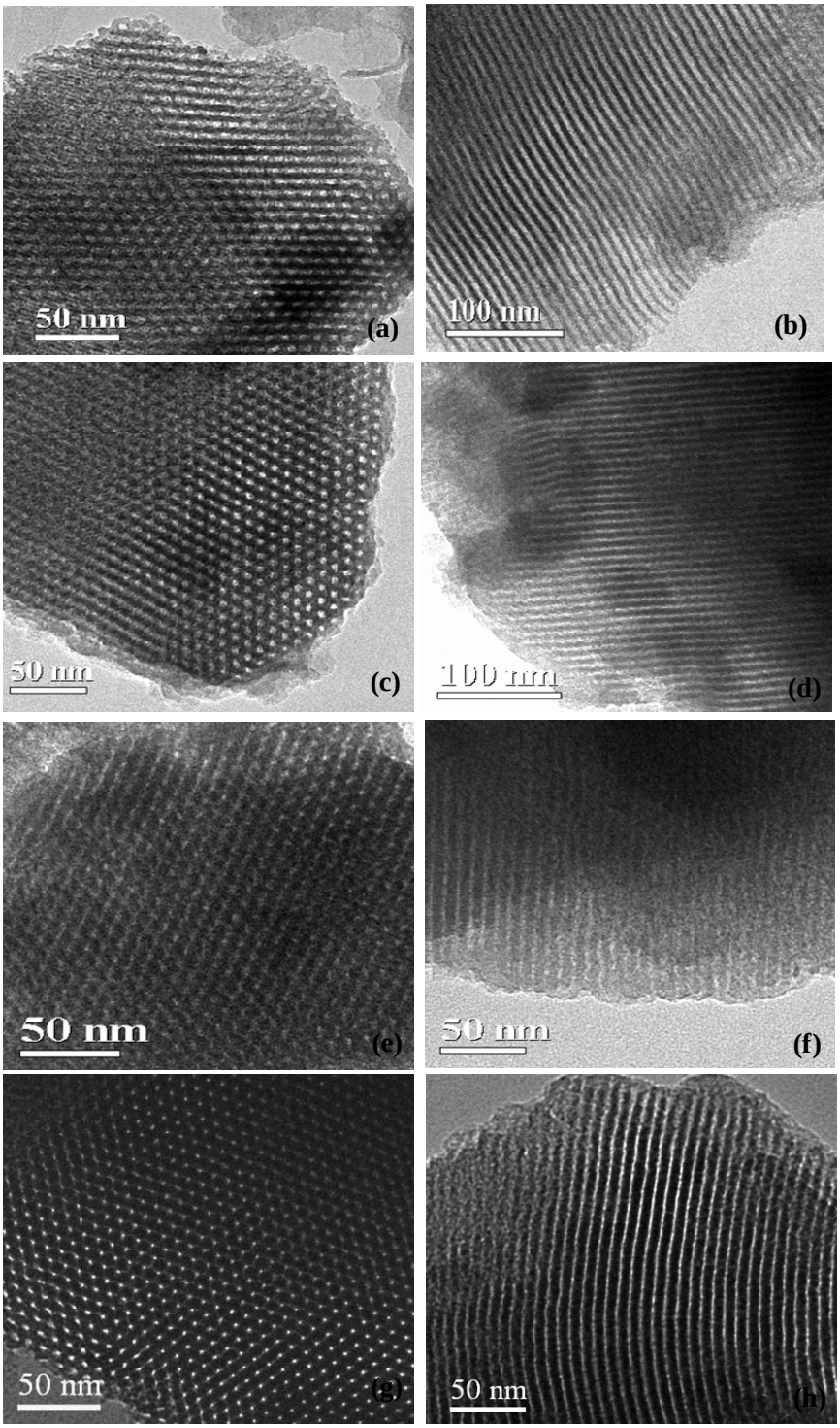

Figure 5.2. TEM images of surfactant-free mesoporous organosilicas synthesized by metal-ion (Zn^{2+}) assisted assembly approach with different content of disulfide-bridged group; (a, b) DS-PMO-5; (c, d) DS-PMO-10; (e, f) DS-PMO-15 and (g, h) DS-PMO-20.

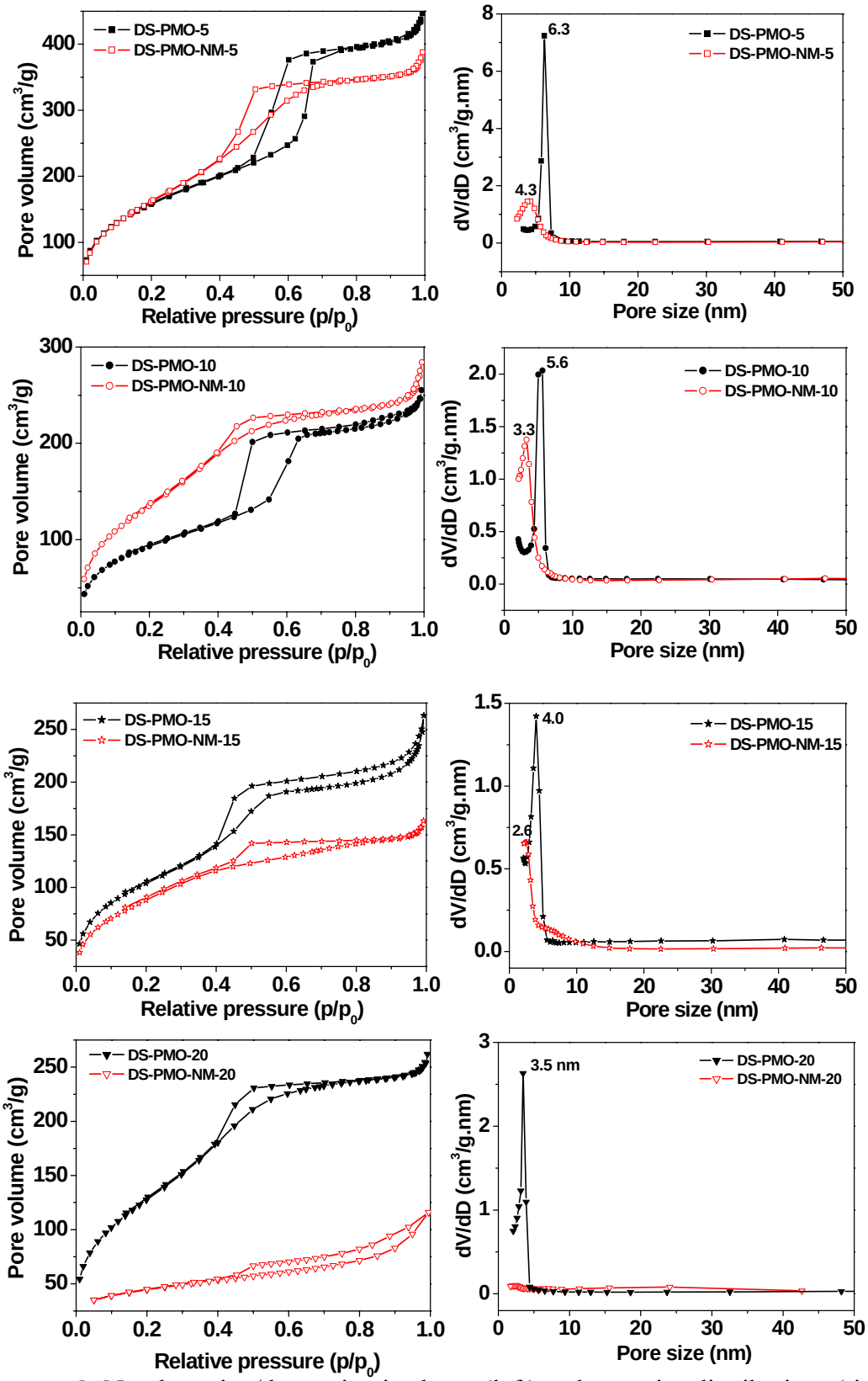

Figure 5.3. N_2 adsorption/desorption isotherm (left) and pore size distributions (right) for disulfide-bridged mesoporous DS-PMO-x synthesized with adding of Zn^{2+} ions and DS-PMO-NW-x without adding of metal Zn^{2+} ions (x = 5, 10, 15 and 20).

arranged arrays. It clearly indicates a well-ordered hexagonal mesostructure with 1D pore channels. The unit cell parameter (a_0) estimated from the TEM images is approximately 11.0 nm, which is in good agreement with the value calculated from the XRD data. Similarly, well-ordered hexagonal and stripe-like arrangements are also observed for the DS-PMO samples prepared with the BTSPDS contents from 5 to 20 %, confirming that the disulfide-bridged PMO mesostructure templated by P123 possesses ordered hexagonal *p6mm* symmetry. In contrast, the DS-PMO-NM materials prepared without metal-ion addition display a worm-like mesostructure (not shown here), further suggesting that the metal ions can assist the self-assembly process involved by the "soft" disulfide silane precursor.

The nitrogen sorption isotherms (Figure 5.3) of the surfactant-free mesoporous material DS-PMO-15 exhibit representative type-IV curves with a sharp capillary condensation step in the relative pressure range of 0.45 ~ 0.55, indicative of uniform mesopores. An H4-type-like hysteresis loop is observed, implying some structural defects in the frameworks [13]. The sample DS-PMO-15 has a BET surface area of 382 $m^2 \cdot g^{-1}$, a pore volume of 0.40 $cm^3 \cdot g^{-1}$, and a narrow pore distribution at about 4.0 nm. Similarly, all the surfactant-free mesoporous samples DS-PMO-x (x = 5 - 20) exhibit typical type-IV isotherms. With the increase of the disulfide contents, the nitrogen condensation shifts to low relative pressure (P/P_0), indicating the decrease of mesopore size. These results are consistent with the decrease of unit cell parameters calculated from the XRD data. This could be attributed to the geometrical constrictions of the triblock copolymer template to accommodate a high content of disulfide bridging groups in the pore walls [36]. The surface area and pore volume also decreases with the disulfide contents, due to the mesostructural degeneration. It should be noted that the mesoporous materials (DS-PMO-5 and DS-PMO-10) with low BTSPDS contents (5 - 10 %) show an H1-type hysteresis loop in the isotherms (Figure 5.3), suggesting uniform cylindrical mesopores. These results further confirm that the mesoporous materials obtained with a low amount of disulfidged groups have a high degree of structural regularity and narrow pore size distribution. Comparatively, mesoporous materials (DS-PMO-NM) prepared without adding metal-ion display irregular nitrogen sorption isotherms, suggesting a disordered and wormlike mesostructure. The pore sizes are a little smaller than that with the addition of metal ions (Table 5.1), which is related to the salt effect of surfactant. Based on the N_2 sorption and XRD results, the pore wall thickness of DS-PMO-15 material is

calculated to be as large as 6.8 nm, which is larger than that reported previously. The value is even larger than its mesopore diameter (4.0 nm). With the increase of the disulfide content, the pore wall thickness increases from 5.0 to 7.1 nm. The thick pore wall is possibly attributed to the large incorporation of long disulfide groups in the frameworks.

5.3.2 Mesopore frameworks

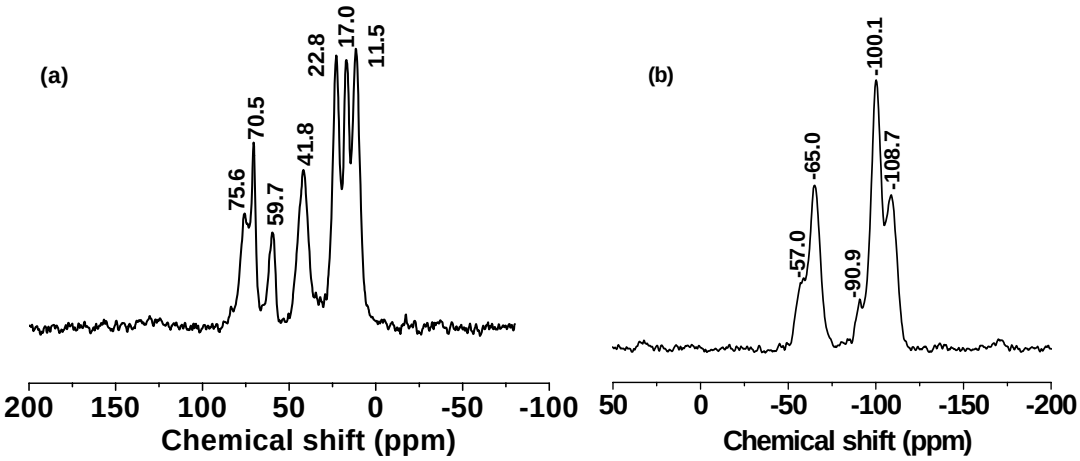

Figure 5.4. MAS NMR spectra of surfactant-free mesoporous DS-PMO-15 composite synthesized by metal-ion assisted assembly approach with 15% of disulfide-bridged group: (a) ^{13}C-NMR and (b) ^{29} Si-NMR spectra.

The ^{13}C CP-MAS NMR spectrum (Figure 5.4a) of the surfactant-free sample DS-PMO-15 shows seven obvious peaks. The signals at about 11.5, 22.8 and 41.8 ppm are assigned to the ^{1}C, ^{2}C and ^{3}C of Si-$^{1}CH_2{}^{2}CH_2{}^{3}CH_2$ -S-S-$^{3}CH_2{}^{2}CH_2{}^{1}CH_2$-Si, respectively [35, 37], suggesting that the framework is hybrid and bonded covalently with the disulfide bridging groups. The peak centered at 17.0 ppm is attributed to the side-chain carbons of methyl groups of Pluronic P123. Additionally, it could also be assigned to the carbons of ethoxy groups formed during surfactant extraction [38]. The signals at about 70.5 and 75.6 ppm are due to the main-chain carbons of ethylene oxide (EO) and propylene oxide segments of Pluronic P123 respectively, suggesting a partial residue of the surfactant template [39]. ^{29}Si MAS NMR spectrum (Figure 5.4b) of the surfactant-free sample DS-PMO-15 prepared with the BTSPDS contents of 15 % show two signals at at -57.0, and -65.0 ppm, which can be assigned to T^2 [C-Si(OH)$(OSi)_2$] and T^3 [C-Si$(OSi)_3$] sites, respectively. It suggests incorporation of the

disulfide-bridged groups into the pore walls. Three other resonances around -90.9, -100.1 and -108.7 ppm which can be assigned as Q^2 $(OH)_2Si(OSi)_2$, Q^3 $(OH)Si(OSi)_3$ and Q^4 $Si(OSi)_4$ sites of silicates are also observed [38]. The ratio of T/(T + Q) is calculated as high as ~ 0.33. According to the silicon molar percentage of 2BTSPDS/[2BTSPDS + TEOS], the BTSPDS concentration in the initial gel mixture is ~ 16.5 %, which is consistent with the initial high BTSPDS content of 15 %. These results also confirm that no significant Si-C bond cleavage occurs during the synthesis or solvent extraction. The elemental analysis results reveal that the surfactant-free disulfide-bridged DS-PMO products contain about 1.25 ~ 3.37 $mmol \cdot g^{-1}$ of sulfur (Table 5.2), which increases with the BTSPDS/TEOS ratio.

Table 5.1. Structural textural properties of the mesoporous organosilicas synthesized by with and without adding metal Zn^{2+} ions and functioned with different content of disulfide-bridged group, DS-PMO-x and DS-PMO-NW-x (x = 5, 10, 15 and 20).

Sample	Surface area ($m^2 \cdot g^{-1}$)	Pore volume ($cm^3 \cdot g^{-1}$)	Pore size (nm)	d_{100} (nm)	a_0 (nm)	Wall thickness (nm)
PMS	550	1.02	8.8	9.8	11.3	2.5
DS-PMO-5	580	0.69	6.3	9.8	11.3	5.0
DS-PMO-10	341	0.39	5.6	9.6	11.1	5.5
DS-PMO-15	382	0.40	4.0	9.4	10.8	6.8
DS-PMO-20	472	0.40	3.5	9.2	10.6	7.1
DS-PMO-NW-5	596	0.60	4.3	9.9	11.4	7.1
DS-PMO-NW-10	498	0.44	3.3	9.2	10.6	7.3
DS-PMO-NW-15	324	0.25	2.6	9.0	10.4	7.8
DS-PMO-NW-20	95	0.14	-	-	-	-

FT-IR spectra (Figure 5.5) of the surfactant-free DS-PMO samples with different BTSPDS/TEOS ratios show intense bands at 698 and 2931 cm^{-1}, which are attributed to the C-S and asymmetric methylene ($-CH_2CH_2-$) stretching modes. These findings indicate that the C-S and C-C bonds are stable in the synthetic process. However, the band at 2931 cm^{-1} could arise from asymmetric methylene ($-CH_2CH_2-$) stretching modes from Pluronic P123, implying that the partial template may not be removed by the use of ethanol/HCl extraction. Furthermore, the vibrations at 952, and 798 cm^{-1}, and the sharp bands at 952 and 1089 cm^{-1} from Si-O stretching confirm the formation of siloxane bonds. The signal at 1635 cm^{-1} suggests a little bit amount of water (H_2O)

physically adsorbed in the final products. These results further reveal that the frameworks are inorganic-organic hybrid composites composed of the disulfide-bridged groups and silicates.

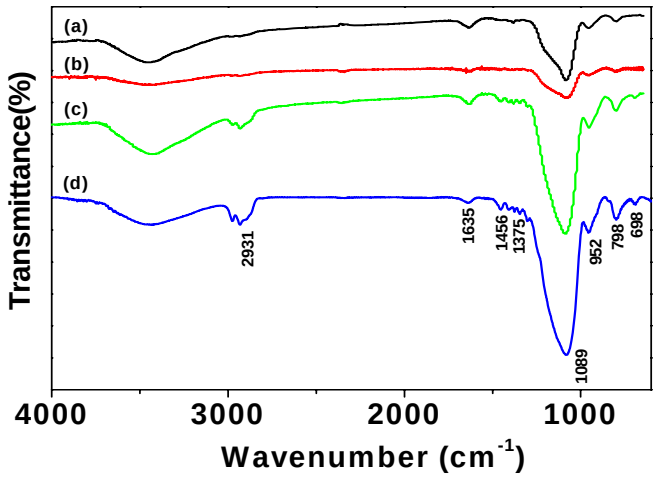

Figure 5.5. FT-IR spectra of surfactant-free mesoporous organosilicas synthesized by metal-ion (Zn^{2+}) assisted assembly approach with different content of disulfide-bridged group: DS-PMO-5 (a) DS-PMO-10 (b) DS-PMO-15 (c) and DS-PMO-20 (d).

5.3.3 Stability

Thermogravimetric analyses (Figure 5.6) of the surfactant-free DSPMO materials show three major weight losses at 25 - 700 °C in air atmosphere. A weight loss of less than 8 % below 150 °C is observed, probably due to desorption of physisorbed water [40]. Also, the lack of the characteristic peak for template P123 removal at ~ 170 °C in the DTG curves demonstrates that most of the template was removed by the ethanol/HCl extraction [9]. Moreover, a gradual weight loss in the range of 250 - 450 °C is proportional to the content of the disulfide groups incorporated in the framework. The result implies that the disulfide-bridged groups can be stable up to 300 °C in air.

The hydrothermal stability of the DS-PMO materials prepared from the metal-ion-assisted assembly approach was investigated in boiling water for 5 days. The XRD patterns of the template-free DS-PMO materials after the treatment are still resolved, suggesting that the ordered hexagonal *p6mm* mesostructures are well retained (Figure 5.7). The intensity and d_{100} spacing reduce a little, suggesting a slight degeneration of the mesostructure. These results clearly demonstrate that the disulfide-bridged PMO materials have an excellent hydrothermal stability. With the increase of

BTSPDS/TEOS ratio, the XRD intensity is reduced and d_{100} spacing decreased, suggesting that the hydrothermal stability probably increases and has a relationship with the thickness of the pore walls. The hydrophobic groups in the framework probably repel the action of water molecules, resulting in an improvement of the hydrothermal stability.

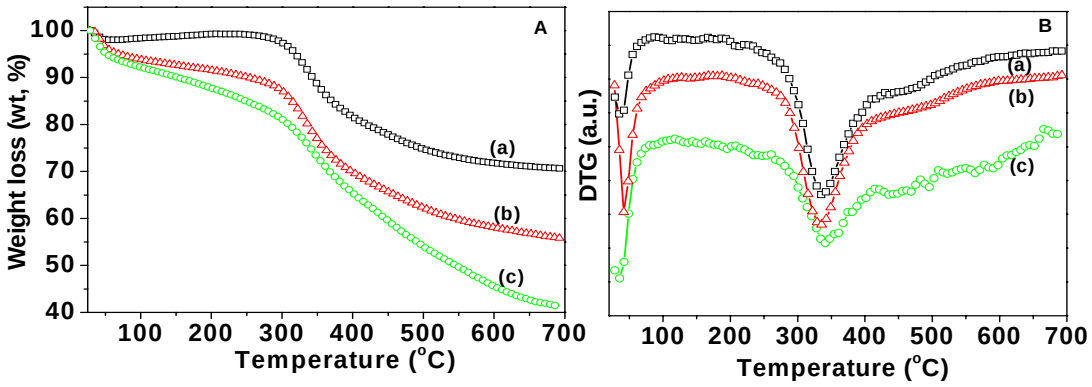

Figure 5.6. (A) TGA and (B) corresponding differential thermogravimetric (DTG) curves of surfactant-free mesoporous organosilicas synthesized by metal-ion (Zn^{2+})-assisted assembly approach with different content of disulfide-bridged groups: DS-PMO-5 (a) DS-PMO-10 (b) and DS-PMO-15 (c).

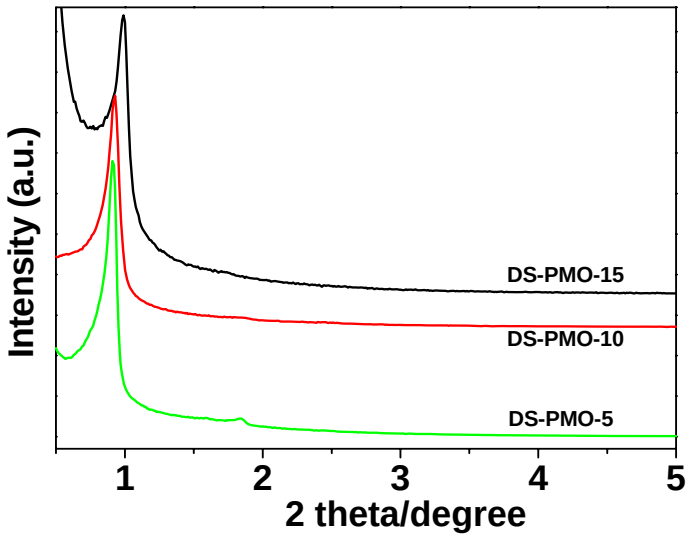

Figure 5.7. Powder XRD patterns of surfactant-free mesoporous organosilicas DS-PMO materials after boiling water treatment for 5 days.

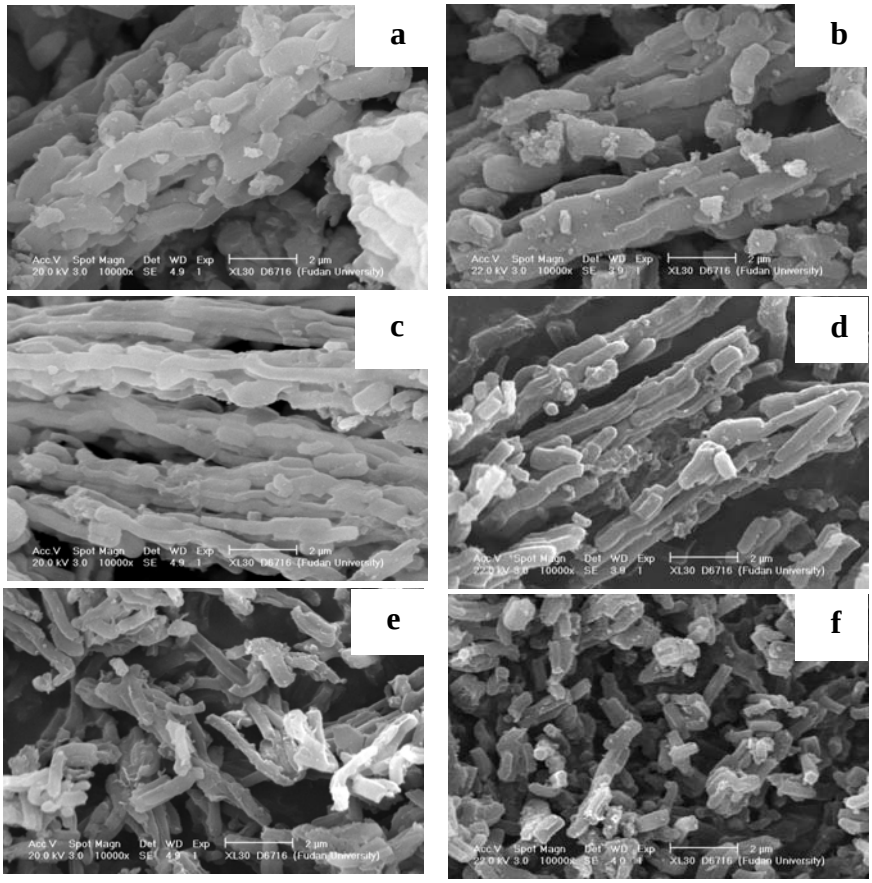

Figure 5.8. SEM images of disulfide-bridged mesoporous organosilicas synthesized with different BTSPDS/TEOS ratio DS-PMO-5, DS-PMO-10 and DS-PMO-15 materials before (a, c, e) and after (b, d, f) boiling water treatment for 5 days, respectively.

The SEM images show similar rope-like morphology before and after the boiling water treatment (Figure 5.8), further implying a good hydrothermal stability. Similar to that for mesoporous silica SBA-15, all the mesoporous DS-PMO materials prepared from the metal-ion-assisted assembly approach with different BTSPDS/TEOS ratios show wheat-shaped macrostructures aggregated into rope-like particles. The size of the ropes appears to slightly decrease from 0.7 to 0.4 μm in a diameter with the increase of the disulfide group content. It is interesting to note that the wheat-shaped fibers almost disappear when the BTSPDS molar content increases to 15 %. Instead, uniform rods with a diameter of ~ 0.4 μm are formed. This phenomenon may be related to the change of the interfacial tension driven from hydrophobic disulfide organic groups.

5.3.4 Formation of mesostructures

Our results show that the addition of the metal-ion greatly influences the formation of the disulfide-bridged DW-PMO mesostructure. With the increased addition of zinc ions, the XRD patterns (Figure 5.9) become more resolved and the d_{100} spacing increases slightly, suggesting an improvement of mesostructural regularity. Therefore, it is clear that metal ion addition can assist the self-assembly of mesostructures. Our results show that not all metal ions (such as Mg^{2+}) can improve the assembly, some heavy metal ions such as Zn^{2+} and Cd^{2+} do assist the incorporation of the disulfide-bridged groups, probably implying that the salt effect may not improve the assembly. Elemental analysis reveals that no zinc is contained in the final as-made DS-PMO materials.

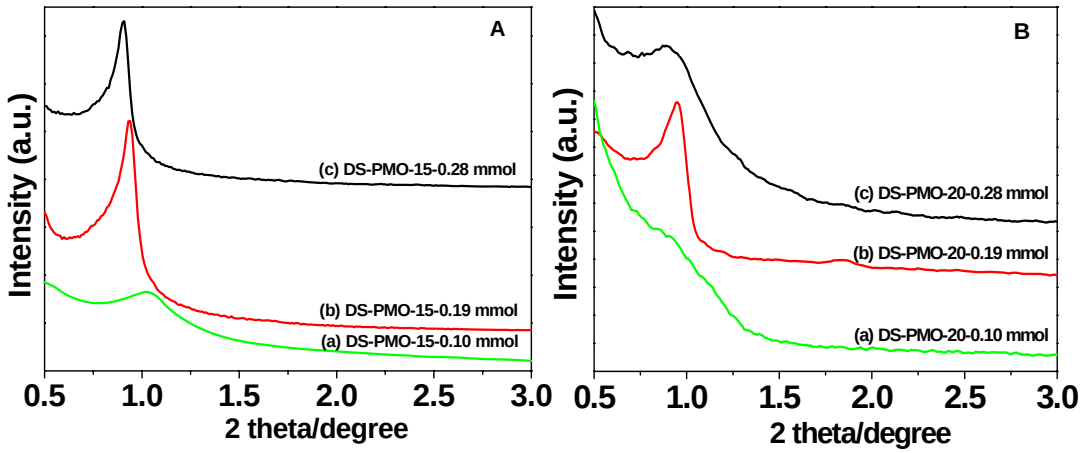

Figure 5.9. XRD patterns of surfactant-free mesoporous organosilicas DS-PMO-15 (A) and DS-PMO-20 (B) synthesized with different contents of Zn^{2+}: (a) 0.10 mmol, (b) 0.19 mmol, and (c) 0.28 mmol.

On the basis of the above observations, we speculate that the formation of ordered mesostructure with "soft" disulfide organic groups undergoes a metal-ion-assisted process. First, the metal ion (Zn^{2+}) can interact with disulfide groups of the organic-bridged silane by coordination bonds, reducing the mobility and hydrophobicity of the silicate precursors. Therefore, it results in more incorporation of disulfide groups. On the other hand, during the self-assembly process, the Zn^{2+} ions in the complexes with the disulfide groups could also coordinate with ethylene oxide of Pluronic P123

template, which benefits the co-assembly of silicate and organic silicate oligomers with surfactants, improving the mesostructural regularity [41, 42]. Finally, the zinc ions could be etched off in strongly acidic solution because of the weak coordination interaction. As a result, no zinc ion is contained in the final PMO products.

5.3.5 Adsorption of mercury (II)

Table 5.2. Adsorption capacity of Hg^{2+} for different mesoporous materials synthesized by metal-ion (Zn^{2+}) assisted assembly approach and comparison of reported thiol-functionalized mesoporous materials.

Sample	S content ($mmol \cdot g^{-1}$)	Hg^{2+} adsorption capability ($mg \cdot g^{-1}$)	Hg/S
PMS	0	0	0
DS-PMO-5	1.25	230	0.92
DS-PMO-10	2.03	428	1.05
DS-PMO-15	2.72	577	1.06
DS-PMO-20	3.37	716	1.06
FMMS [45]	3.20	502	0.78
MP(2)-MSU-2 [46]	2.30	461	1.00
MP-MCM-41 [47]	0.57	118	1.03

The mesoporous DS-PMO materials exhibit a high adsorption capability of heavy metal Hg^{2+} ions up to 716 $mg \cdot g^{-1}$ (Table 5.2), due to large incorporation of disulfide-bridged groups. Remarkably, the mesoporous silica PMS without the organic group shows no obvious adsorption of Hg^{2+} ions, similar to the result of unmodified SBA-15 [43], suggesting that the capability is mainly related to the disulfide groups. With the increase of the sulfide content, the adsorption capacity increases, which is in proportion to the sulfur content (Table 5.2). Approximately one incorporated disulfide group in each DS-PMO adsorbent is accessible for the mercury ions binding with the Hg/S molar ratio ≈ 1, which is slightly larger than the values reported previously for the functionalized mercaptopropylsilyl mesoporous silica (Table 5.2) [44-46]. It implies that the DS-PMO materials are a potential adsorbent for heavy metal-ion removal from waste waters.

5.4 Conclusions

Disulfide-bridged PMOs with the ordered hexagonal mesostructure have been synthesized by the metal-ion-assisted assembly approach with co-condensation of BTSPDS and TEOS. By adding Zn^{2+} ions, which can coordinate either with the dsulfide-bridged groups or ethylene oxide moieties of P123 template, the interaction between silicate species and P123 template can be enhanced, therefore high disulfide groups incorporation (~ 20 %) into the framework can be achieved and the mesostructural ordering and pore size can be improved, compared to that in the absence of metal-ion during the self-assembly process. The increased wall thickness from 5.0 to 7.1 nm is in proportion to the content of disulfide groups incorporated in the framework. The obtained organic-functional materials show a high BET surface area (~ 580 $m^2 \cdot g^{-1}$), a large uniform pore size (up to 6.3 nm) and an excellent hydrothermal stability in boiling water for 5 days, which could be attributed to thick pore walls and hydrophobicity of disulfide groups. The presence of disulfide functional groups in the framework endows these materials with the adsorption capacity of up to716 mg Hg^{2+}/g, which indicates that it is a potential candidate for heavy metal adsorption. The metal-ion-assistant approach demonstrated here be applied for preparation of PMOs containing other new "soft" organic groups.

References

[1] T. Asefa, M. J. MacLachlan, N. Coombos, G. A. Ozin, "Periodic Mesoporous Organosilicas with Organic Groups inside the Channel Walls," *Nature* **1999**, *402*, 867-871.

[2] S. Inagaki, S. Guan, Y. Fukushima, T. Ohsuna, O. Teresaki, "Novel Mesoporous Materials with a Uniform Distribution of Organic Groups and Inorganic Oxide in Their Frameworks," *J. Am. Chem. Soc.* **1999**, *121*, 9611-9614.

[3] B. J. Melde, B. T. Holland, C. F. Blandford, A. Stein, "Mesoporous Sieves with Unified Hybrid Inorganic/Organic Frameworks," *Chem. Mater.* **1999**, *11*, 3302-3308.

[4] Q. H. Yang, J. Liu, J. Yang, M. P. Kapoor, S. Inagaki, C. Li, "Synthesis, Characterization, and Catalytic Activity of Sulfonic Acid-Functionalized Periodic Mesoporous Organosilicas," *J. Catal.* **2004**, *228*, 265-272.

[5] S. Hamoudi, S. Royer, S. Kaliaguine, "Propyl- and Arene-Sulfonic Acid Functionalized Periodic Mesoporous Organosilicas," *Micropor. Mesopor. Mater.* **2004**, *71*, 17-25.

[6] Q. H. Yang, M. P. Kapoor, S. Inagaki, N. Shirokura, J. N. Kondo, K. Domen, "Catalytic Application of Sulfonic Acid Functionalized Mesoporous Benzene-Silica with Crystal-Like Pore Wall Structure in Esterification," *J. Mol. Catal. A* **2005**, *230*, 85-89.

[7] K. Nakajima, I. Tomita, M. Hara, S. Hayashi, K. Domen, J. N. Kondo, "A Stable and Highly Active Hybrid Mesoporous Solid Acid Catalyst," *Adv. Mater.* **2005**, *17*, 1839-1842.

[8] Y. Wan, D. Q. Zhang, Y. P. Zhai, C. M. Feng, J. Chen, H. X. Li, "Periodic Mesoporous Organosilicas: A Type of Hybrid Support for Water-Mediated Reactions," *Chem. Asian J.* **2007**, *2*, 875-881.

[9] O. Olkhovyk, M. Jaroniec, "Periodic Mesoporous Organosilica with Large Heterocyclic Bridging Groups," *J. Am. Chem. Soc.* **2005**, *127*, 60-61.

[10] M. C. Burleigh, S. Dai, E. W. Hagaman, J. S. Lin, "Imprinted Polysilsesquioxanes for the Enhanced Recognition of Metal Ions," *Chem. Mater.* **2001**, *13*, 2537-2546.

[11] S. Dai, M. C. Burleigh, Y. H. Ju, H. J. Gao, J. S. Lin, S. J. Pennycook, C. E. Barnes, Z. L. Xue, "Hierarchically Imprinted Sorbents for the Separation of Metal Ions," *J. Am. Chem. Soc.* **2000**, *122*, 992-993.

[12] L. X. Zhang, W. H. Zhang, J. L. Shi, Z. L. Hua, Y. S. Li, J. N. Yan, "A New Thioether Functionalized Organic-Inorganic Mesoporous Composite as A Highly Selective and Capacious Hg^{2+} Adsorbent," *Chem. Commun.* **2003**, 210-211.

[13] J. Liu, J. Yang, Q. H. Yang, G. Wang, Y. Li, "Hydrothermally Stable Thioether-Bridged Mesoporous Materials with Void Defects in the Pore Walls," *Adv. Funct. Mater.* **2005**, *15*, 1297-1302.

[14] K. Z. Hossain, L. Mercier, "Intraframework Metal Ion Adsorption in Ligand-Functionalized Mesoporous Silica," *Adv. Mater.* **2002**, *14*, 1053-1056.

[15] B. D. Hatton, K. Landskron, W. Whitnall, D. D. Perovic, G. A. Ozin, "Spin-Coated Periodic Mesoporous Organosilica Thin Films - Towards a New Generation of Low-Dielectric-Constant Materials," *Adv. Funct. Mater.* **2005**, *15*, 823-829.

[16] Y. Lu, H. Fan, N. Doke, D. A. Loy, R. A. Assink, D. A. LaVan, C. J. Brinker, "Evaporation-Induced Self-Assembly of Hybrid Bridged Silsesquioxane Film and Particulate Mesophases with Integral Organic Functionality," *J. Am. Chem. Soc.* **2000**, *122*, 5258-5261.

[17] Ö. Dag, C. Yoshina-Ishii, T. Asefa, M. J. MacLachlan, H. Grondey, N. Coombs, G. A. Ozin, "Oriented Periodic Mesoporous Organosilica (PMO) Film with Organic Functionality Inside the Channel Walls," *Adv. Funct. Mater.* **2001**, *11*, 213-217.

[18] E. Besson, A. Mehdi, D.A. Lerner, C. Reyé, R. J. P. Corriu, "Photoresponsive Ordered Hybrid Materials Containing a Bridged Azobenzene Group," *J. Mater. Chem.* **2005**, *15*, 803-809.

[19] M. D. McInall, J. Scott, L. Mercier, P. J. Kooyman, "Super-Microporous Organic-Integrated Silica Prepared by Non-Electrostatic Surfactant Assembly," *Chem. Commun.* **2001**, 2282-2283.

[20] O. Dag, G. A. Ozin, "Organization of Bridging Organics in Periodic Mesoporous Organosilicas (PMOs) - Polarization Micro-Raman Spectroscopy," *Adv. Mater.* **2001**, *13*, 1182-1185.

[21] J. R. Matos, M. Kruk, L. P. Mercuri, M. Jaroniec, T. Asefa, N. Coombs, G. A. Ozin, T. Kamiyama, O. Terasaki, "Periodic Mesoporous Organosilica with Large Cagelike Pores," *Chem. Mater.* **2002**, *14*, 1903-1905.

[22] X. Y. Bao, X. S. Zhao, X. Li, P. A. Chia, J. Li, "A Novel Route toward the Synthesis of High-Quality Large-Pore Periodic Mesoporous Organosilicas," *J. Phys. Chem. B* **2004**, *108*, 4684-4689.

[23] X. Y. Bao, X. S. Zhao, "Morphologies of Large-Pore Periodic Mesoporous Organosilicas," *J. Phys. Chem. B* **2005**, *109*, 10727-10736.

[24] A. Sayari, S. Hamoudi, Y. Yang, I. L. Moudrakovski, J. R. Ripmeester, "New Insights into the Synthesis, Morphology, and Growth of Periodic Mesoporous Organosilicas," *Chem. Mater.* **2000**, *12*, 3857-3863.

[25] O. Muth, C. Schellbach, M. Fröba, "Triblock Copolymer Assisted Synthesis of Periodic Mesoporous Organosilicas (PMOs) with Large Pores," *Chem. Commun.* **2001**, 2032-2033.

[26] S. Inagaki, S. Guan, T. Ohsuna, O. Teresaki, "An Ordered Mesoporous Organosilica Hybrid Material with a Crystal-Like Wall Structure," *Nature* **2002**, *416*, 304-307.

[27] Q. H. Yang, Y. Li, L. Zhang, J. Yang, J. Liu, C. Li, "Hydrothermal Stability and Catalytic Activity of Aluminum-Containing Mesoporous Ethane-Silicas," *J. Phys. Chem. B* **2004**, *108*, 7934-7937.

[28] A. Sayari, S. Hamoudi, "Periodic Mesoporous Silica-Based Organic-Inorganic Nanocomposite Materials," *Chem. Mater.* **2001**, *13*, 3151-3168.

[29] G. Kickkelbick, "Hybrid Inorganic-Organic Mesoporous Materials," *Angew. Chem. Int. Ed.* **2004**, *43*, 3102-3104.

[30] B. Hatton, K. Landskron, W. Whitnall, D. Perovic, G. A. Ozin, "Past, Present, and Future of Periodic Mesoporous Organosilicas: The PMOs," *Acc. Chem. Res.* **2005**, *38*, 305-312.

[31] R. J. P. Corriu, A. Mehdi, C. Reyé, C. Thieuleux, "Mesoporous hybrid materials containing functional organic groups inside both the framework and the channel pores," *Chem. Commun.* **2002**, 1382-1383.

[32] M. A. Wahab, I. Kim, C. S. Ha, "Bridged Amine-Functionalized Mesoporous Organosilica Materials from 1,2-bis(triethoxysilyl)ethane and Bis[(3-trimethoxysilyl)propyl]amine," *J. Solid State Chem.* **2004**, *177*, 3439-3447.

[33] R. M. Grudzien, B. E. Grabicka, M. Jaroniec, "Adsorption and Structural Properties of Channel-like and Cage-like Organosilicas," *Adsorption* **2006**, *12*, 293-308.

[34] B. E. Grabicka, M. Jaroniec, "Microwave-Assisted Aynthesis of Periodic Mesoporous Organosilicas with Ethane and Disulfide Groups," *Micropor. Mesopor. Mater.* **2009**, *119*, 144-149.

[35] C. M. Li, J. Liu, L. Zhang, J. Yang, Q. H. Yang, "Mesoporous Organosilicas Containing Disulfide Moiety: Synthesis and Generation of Sulfonic Acid Functionality through Chemical Transformation in the Pore Wall," *Micropor. Mesopor. Mater.* **2008**, *113*, 333-342.

[36] R. M. Grudzien, S. Pikus, M. Jaroniec, "Periodic Mesoporous Organosilicas with *Im*3*m* Symmetry and Large Isocyanurate Bridging Groups," *J. Phys. Chem. B* **2006**, *110*, 2972-2975.

[37] D. Margolese, J. A. Melero, S.C. Christiansen, B. F. Chmelka, G. D. Stucky, "Direct Syntheses of Ordered SBA-15 Mesoporous Silica Containing Sulfonic Acid Groups," *Chem. Mater.* **2000**, *12*, 2448-2459.

[38] W. H. Zhang, X. N. Zhang, Z. L. Hua, P. Harish, F. Schroeder, S. Hermes, T. Cadenbach, J. L. Shi, R. A. Fischer, "Synthesis, Bifunctionalization, and Application of Isocyanurate-Based Periodic Mesoporous Organosilicas," *Chem. Mater.* **2007**, *19*, 2663-2670.

[39] C. M. Yang, B. Zibrowius, W. Schmidt, F. Schüth, "Consecutive Generation of Mesopores and Micropores in SBA-15," *Chem. Mater.* **2003**, *15*, 3739-3741.

[40] L. Gao, F. Wei, Y. Zhou, X. X. Fan, Y. Wang, J. H. Zhu, "Synthesis of Large-Pore Urea-Bridged Periodic Mesoporous Organosilicas," *Chem. Asian J.* **2009**, *4*, 587-593.

[41] K. Mortensen, J. S. Pedersen, "Structural Study on the Micelle Formation of Poly(ethylene oxide)-Poly(propylene oxide)-Poly(ethylene oxide) Triblock Copolymer in Aqueous Solution," *Macromolecules* **1993**, *26*, 805-812.

[42] B. L. Newalkar, S. Komarneni, "Control over Microporosity of Ordered Microporous-Mesoporous Silica SBA-15 Framework under Microwave-Hydrothermal Conditions: Effect of Salt Addition," *Chem. Mater.* **2001**, *13*, 4573-4579.

[43] A. M. Liu, K. Hidajat, D. Y. Zhao, "A New Class of Hybrid Mesoporous Materials with Functionalized Organic Monolayers for Selective Adsorption of Heavy Metal Ions," *Chem. Commun.* **2000**, 1145-1146.

[44] X. D. Feng, G. E. Fryxell, L. Q. Wang, A. Y. Kim, J. Liu, K. M. Kemner, "Functionalized Monolayers on Ordered Mesoporous Supports," *Science* **1997**, *276*, 923-926.

[45] J. Brown, R. Richer, L. Mercier, "One-Step Synthesis of High Capacity Mesoporous Hg^{2+} Adsorbents by Non-Ionic Surfactant Assembly," *Micropor. Mesopor. Mater.* **2000**, *37*, 41-48.

[46] L. Mercier, T. J. Pinnavaia, "Heavy Metal Ion Adsorbents Formed by the Grafting of a Thiol Functionality to Mesoporous Silica Molecular Sieves: Factors Affecting Hg(II) Uptake," *Environ. Sci. Technol.* **1998**, *32*, 2749-2754.

CHAPTER 6 Synthesis of Uniform PMO Hollow Spheres with Large-Pore Size and Efficient Encapsulation Capacity for Toluene and Large Biomolecules Bovine Serum Albumin

6.1 Introduction

Spheres with hollow interiors have attracted considerable attention over the past few years, as they can be used for immobilization and adsorption of large molecules by controlling framework properties [1-3]. Inorganic silica hollow spheres are interesting as host materials, and great efforts have been focused on the synthesis of hollow nanospheres [4, 5]. These include efforts to prepare mesocellular siliceous foams with continuous 3D pore system, by using new methods to synthesize siliceous foams with high pore volume. In this regard, Stucky and his co-workers [6] have synthesized mesoporous siliceous foams with uniformly sized cells and windows by using a sol–gel synthesis that involved a surfactant and an organic cosolvent. By using block-copolymer cooperative vesicle templating method, siliceous unilamellar vesicles and foams were prepared [7]. These nanofoams are proved to be useful in the immobilization of biomolecules, however, some inherent limitations exist in these materials: silica is the sole component and their adsorption capacity for biomolecules is not as high as expected. There is thus a need to further modify the material by introducing different functional groups [8].

PMO materials have attracted increasing research attention in materials science [9-11]. The high loading rate and uniform dispersion of organic moieties in the framework, as well as various surface properties imparted from different functional groups endow the PMO materials with unique advantages over mesoporous silica (MPS) and even their functionalized products [12]. PMOs with different morphologies [13-19] have been successfully synthesized. Among them, PMOs with hollow sphere morphology have been demonstrated to be good candidates for the immobilization of biomolecules and for efficient adsorption of small molecules through microwindows on the shell [20, 21]. Inspired by the synthesis of large-pore mesoporous organosilica using block copolymers as structure-directing agents, the

pore size was expanded which may be due to the increasing self-assembly interaction between the headgroups of triblock copolymer surfactant and the organosilane species by addition of inorganic salt [22, 23]. Park et al. [24] reported on the effect of inorganic salts on the synthesis of PMOs with hollow sphere morphology. More recently, Ha and co-workers synthesized PMOs with three different types of bridging organic groups in the framework by the co-condensation method, and examined the adsorption of lysozyme at different pH values [20]. Based on the co-condensation method, Liu *et al.* prepared organic-inorganic hybrid hollow nanospheres with microwindows, and used them for diffusion of small guest molecules into the hollow cavities [21]. It is noted that the limited microwindows of PMO hollow spheres may restrict their application in some areas where relatively large window sizes are in demand as for adsorption and immobilization of large biomolecules. Furthermore, there is no report on the synthesis of PMO hollow spheres via the low-temperature approach. Finally, the structure transformation from PMO hollow spheres to a cubic phase with the aid of cationic template has not been studied systematically.

Herein, we adopted a low-temperature approach to successfully prepare ethylene-bridged PMO hollow spheres with high pore volume (up to 2.5 $cm^3 \cdot g^{-1}$) by using triblock copolymer F127 as a template and 1,3,5-trimethylbenzene (TMB) as a swelling agent in the presence of inorganic salt [12, 25]. Further adjustment of the media acidity can increase the pore size to 15.1 nm. Most importantly, mesostructures can be tuned from hollow sphere to 3D cubic structure by adding cationic surfactant. It was found that these PMO hollow spheres show a strong affinity for toluene with a high adsorption capacity (703 $mg \cdot g^{-1}$). Using the protein bovine serum albumin (BSA) as a large probe molecule, an efficient adsorption of ~ 585 $mg \cdot g^{-1}$ and fast adsorption equilibrium were achieved, which shows promising properties for encapsulation or drug delivery.

6.2. Experimental

6.2.1 Synthesis of PMO hollow spheres

Large-pore PMO hollow spheres were prepared through a low temperature approach using Pluronic F127 as a template and BTSE as a silica source under acid conditions at 15 °C. Different contents of TMB, KCl and concentration of hydrochloric acid were adopted in batch experiments. A typical synthesis was carried out as follows: 0.335 g of Pluronic F127 and 0.88 g of KCl were dissolved in 20 mL of HCl (1.0 M). Then 0.40 g of TMB was added to the solution and the mixture stirred for 3 h at 15 °C. Then, 1.0 mL of BTSE was added to the solution and stirred for 24 h at the same temperature. The molar ratio of the reactants is F127 : BTSE : TMB : KCl : HCl : H_2O = 9.2×10^{-3} : 1 : 1.23 : 4.4 : 7.4 : 408. The solution along with the precipitate was then removed to an autoclave and put in the oven at 140 °C for 24 h and at 120 °C for another 24 h. After filtering, the sample was washed with water, and dried in air at 40 °C. The solid products were collected and then extracted with 80 mL of (99.0 %) ethanol and 2 mL of (37 wt %) HCl at 60 °C for 24 h in air to remove the F127 template. The final PMO products were collected after filtration, water washed and air dried at 40 °C. The resultant composites were denoted as PMO-F for PMO samples synthesized with only F127 template, and as PMO-F-C for PMO samples prepared with F127 and CTAB templates together.

In the syntheses using a mixture of F127 and CTAB as templates, four groups of template sources with different content of CTAB (0.02 ~ 0.16 g) were used, while keeping other conditions constant.

6.3 Results and discussion

6.3.1 Mesostructure

TEM images of the template-free PMO-F composites show uniform hollow spheres (Figure 6.1a and b). All the spheres are well dispersed. The diameters of the hollow interior measured from careful TEM measurements, are about ~ 13 nm. With an increase of the medium acidity, the diameter of the PMO hollow spheres increases

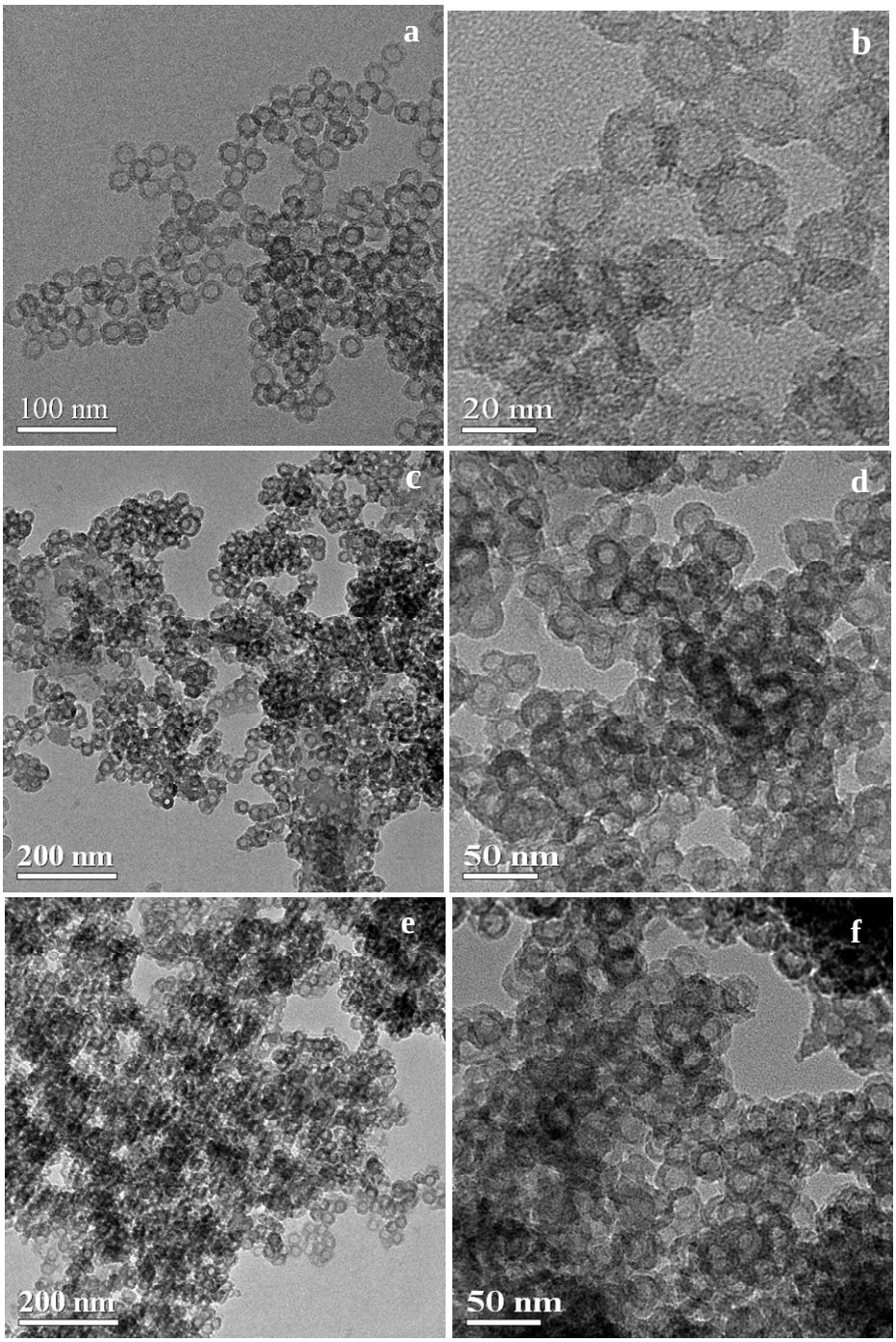

Figure 6.1. TEM images of the hollow spherical PMO-F composites synthesized by the low-temperature approach with 0.4 g of TMB, 0.88 g of KCl, 0.335 g of F127 and 0.958 g of BTSE at different HCl concentration: 1.0 M (a, b), 1.3 M (c, d) and 2.0 M (e, f).

-(Figure 6.1c and d). When the acidity of the solution increases to 2.0 M, uniform hollow spheres are also observed, and the diameter of the hollow mesopores is

roughly 14 ~ 16 nm (Figure 6.1e and f). These results clearly demonstrate that uniform and well dispersed PMO hollow spheres with large-pores can be synthesized by this low-temperature approach.

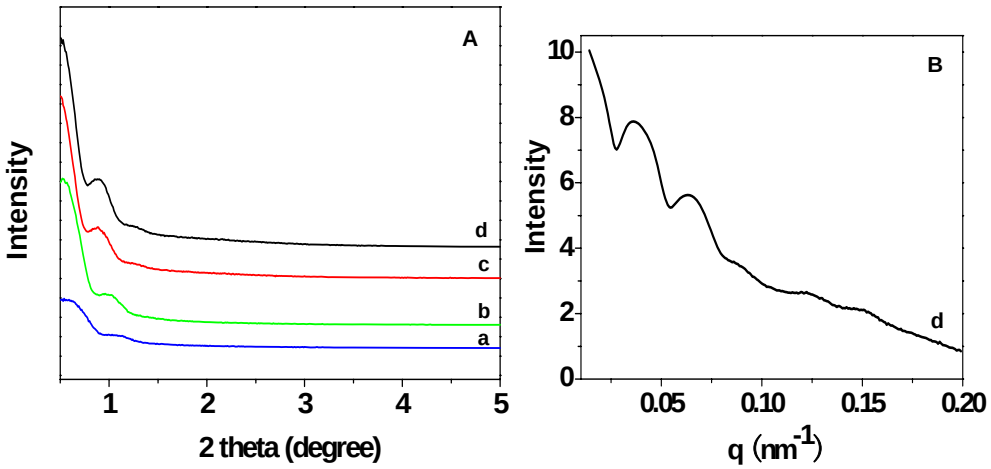

Figure 6.2. XRD patterns (A) of the template-free PMO-F composites synthesized from the low-temperature approach with different content of TMB at 1.0 M HCl: 0.1 g (a), 0.2 g (b), 0.3 g (c) and 0.4 g (d). The SAXS pattern (B) of the (d) sample is also provided.

Small-angle XRD patterns (Figure 6.2A) of the template-free PMO-F hollow spheres prepared with a high content of TMB under a low acid concentration (1.0 M) exhibit one broad diffraction peak (2θ = 0.88 °) with *d*-spacing value of 10.0 nm. Although the diffraction peak cannot be indexed into any plane of the known mesostructures, it is related to the scattering of monodispersed spheres [6]. The SAXS pattern shows more resolved scattering peaks (Figure 6.2B), which is very similar to the uniform mesoporous siliceous foams [6]. At least five resolved scattering peaks can be observed, the corresponding *d*-spacing values for the two higher order peaks are calculated to be 17.3 and 9.9 nm, where the latter is in agreement with that from the XRD pattern. According to the model and approximate simulation from the previous report [6], the *d*-spacing value of 17.3 nm for first order scattering corresponds to the cell diameter of the uniform spheres and 10.0 nm may be ascribed to the interior diameter. These values are similar to those (16 nm in diameter and 10 nm in pore size) from TEM and N_2 sorption measurements. So, the results clearly

indicate that the short-range periodicity of the closely packed hollow spheres is attributed to the small-angle XRD (SAXS) peak, further confirming that the particle size distribution is uniform based on the TEM images [21].

The nitrogen sorption isotherms (Figure 6.3A(a) and (b)) of the template-free PMO-F hollow spheres exhibit representative type-IV curves with two capillary condensation steps occurring in the high relative pressure range of 0.7 ~ 0.95, indicative of bimodal large nanopores. One condensation step occurs at a relative pressure of 0.7 ~ 0.8 and is not sharp. This corresponds to the pore diameter of the hollow interior after the removal of the template. Another condensation step at relative pressure range of 0.9 ~ 0.95 is sharp, which may be attributed to the voids from the aggregation or random packing of hollow spheres. Accordingly, a bimodal pore size distribution centered at 12.3 and 61.4 nm can be determined according to the BJH model, which coincides with the estimated size from TEM images. A large H2-type-hysteresis loop with delayed capillary evaporation at a relative pressure of 0.4 ~ 0.5 is observed, implying a cage-like mesopore with a window size smaller than 5.0 nm. The PMO-F hollow spheres prepared with a high content of TMB and a low acid concentration (1.0 M) has a BET surface area of 648 $m^2 \cdot g^{-1}$, and a pore volume of 2.50 $cm^3 \cdot g^{-1}$.

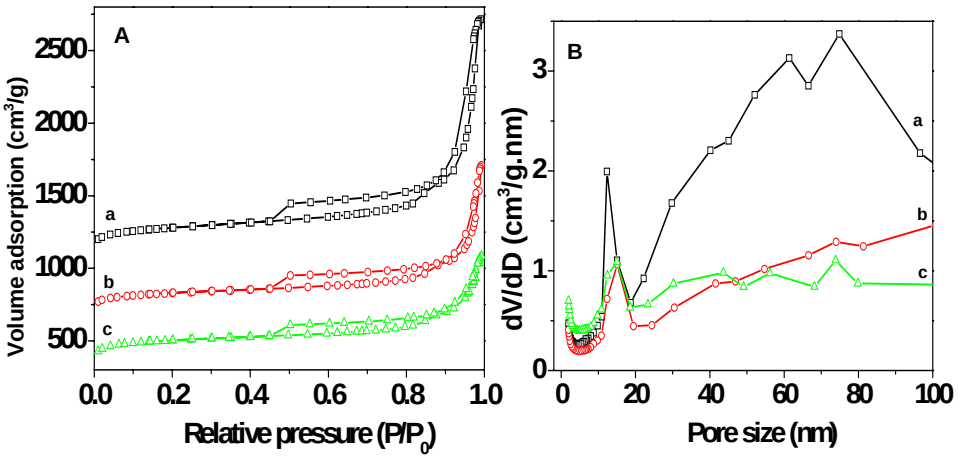

Figure 6.3. N_2 adsorption/desorption isotherms (A) and pore size distributions (B) for the template-free PMO-F composites synthesized by the low-temperature approach with different HCl concentration: 1.0 M (a), 1.3 M (b) and 2.0 M (c).

It is noted that upon increasing the HCl concentration (2.0 M), the nitrogen condensation in the adsorption branch shifts to higher relative pressure, indicating an increase of mesopore size (Figure 6.3). However, the pore volume decreases from 2.50 to 1.21 $cm^3 \cdot g^{-1}$, while the BET surface area shows no clear tendency when the acidity increases (Table 6.1). Thus increasing the HCl concentration has an effect on the pore diameter (increasing) and pore volume (decreasing) of PMO-F hollow spheres.

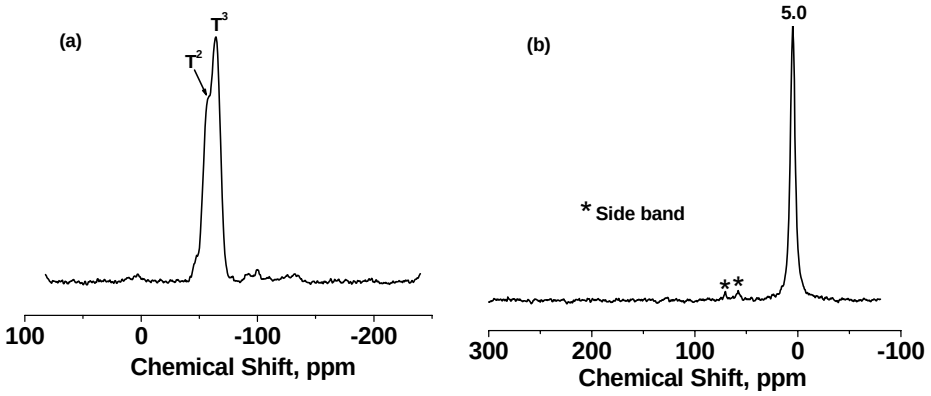

Figure 6.4. ^{29}Si-NMR (a) and ^{13}C-NMR (b) MAS NMR spectra for the template-free PMO-F composites synthesized by the low-temperature approach with 0.4 g of TMB, 0.88 g of KCl, 0.335 g of F127 and 0.958 g of BTSE at 1.0 M HCl.

6.3.2 Mesopore frameworks

^{29}Si MAS NMR spectrum (Figure 6.4a) of the template-free PMO-F hollow spheres prepared under the media acidity of 1.0 M shows two signals at -58.5, and -64.2 ppm, which can be assigned to T^2 [C-Si(OH)$(OSi)_2$] and T^3 [C-Si$(OSi)_3$] sites, respectively. The strong intensity for the T^2 and T^3 signals indicates an incorporation of the ethylene bridging groups into the pore walls, and the formation of highly condensed organosilicate hybrid frameworks [20]. The other two weak resonances around -90.9 and -99.5 ppm ascribed to Q^2 $(OH)_2Si(OSi)_2$, and Q^3 (OH)Si$(OSi)_3$ sites of silicates are also observed [26, 27], further suggesting that Si-C bonds are well-retained during the synthesis process. The ^{13}C CP-MAS NMR spectrum (Figure 6.4b) of the template-free sample PMO-F reveals a strong signal at about 5.0 ppm along with sidebands (denoted with asterisks), which is attributed to the carbons in the ethylene group

connected to Si atoms. It suggests that the silica framework is bonded covalently through the ethylene bridging groups. Additionally, no signal is observed for Pluronic F127, confirming that the template is completely removed by the organic solvent-extraction.

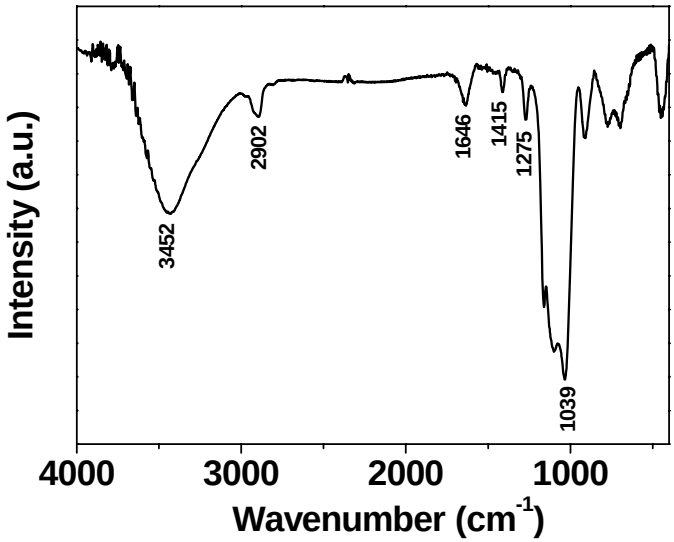

Figure 6.5. FT-IR spectrum of the template-free PMO-F composite synthesized by the low-temperature approach with 0.4 g of TMB, 0.88 g of KCl, 0.335 g of F127 and 0.958 g of BTSE at 1.0 M HCl.

The FT-IR spectrum (Figure 6.5) of the template-free PMO-F hollow spheres shows one intense band at 1646 cm^{-1}, which is attributed to the asymmetric ethylene (C-C) stretching modes. The peaks at 1275, 1415 and 2902 cm^{-1} are attributed to the bridging ethylene C-H vibration and stretching, respectively. These findings indicate the Si-C stability and the integrity of ethylene groups within the silica matrix during the synthesis and the solvent-extraction process. Furthermore, the sharp band at 1039 cm^{-1} from Si-O stretching confirms the formation of siloxane bonds. The band at 3452 cm^{-1} is from the Si-OH groups [28]. These results further reveal that the frameworks are inorganic-organic hybrid composites and composed of the ethylene bridging groups and silicate.

It is also worth mentioning that adding TMB into the F127 solution leads to hollow nanospheres with large-pores. All PMO-F composites prepared with different TMB contents (0.1 ~ 0.4 g) show similar broad XRD patterns (Figure 6.2). With decreasing

TMB content, the intensity of the diffraction peak tends to decrease, and the 2θ shifts to higher angle, indicating a decrease of the mesostructural diameter and periodicity, as listed in Table 6.1. Upon decreasing the TMB content, the nitrogen condensation shifts to lower relative pressure (P/P_0), indicating a decrease of the diameter of hollow spheres from 12.3 to 9.8 nm (Figure 6.6 and Table 6.1). However, the expansion of the pore size by the swelling of TMB is limited. These results are consistent with the decrease of intensity from the XRD data.

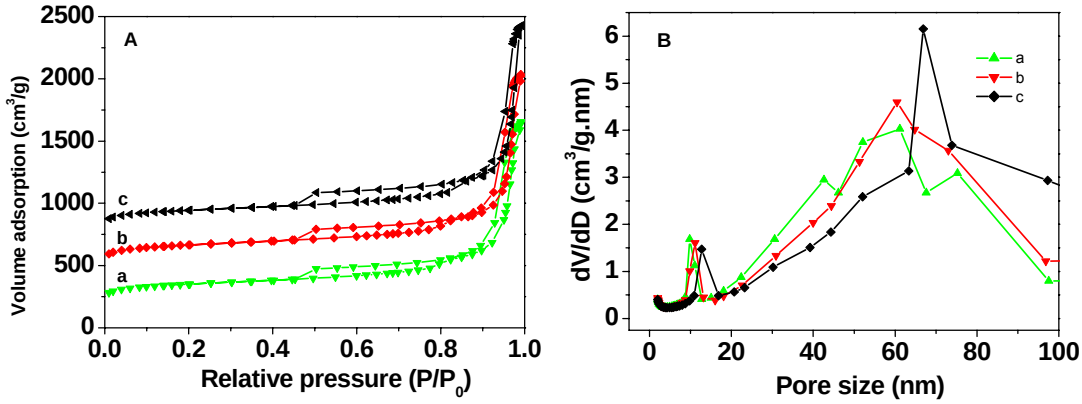

Figure 6.6. N_2 adsorption/desorption isotherms (A) and pore size distributions (B) for the PMO-F composites synthesized by the low-temperature approach with different content of TMB at 1.0 M HCl: 0.1 g (a), 0.2 g (b) and 0.3 g (c).

Similarly, all template-free PMO-F hollow spheres exhibit typical type-IV isotherms with pores larger than 6 nm synthesized with different KCl contents. Upon decreasing the KCl content, the nitrogen condensation varies a little at the relative pressure of 0.7 ~ 0.95, indicating no change of the diameter of hollow spheres of ~ 12 nm. In this work, the formation of large-pore hollow spheres can partly be attributed to the low solubility of micelles's solution by the addition of inorganic salt [24, 29].

Interestingly, when the content of CTAB was low, the TEM images of PMO-F-C composite (Figure 6.7a and b) also showed uniform and well dispersed hollow spheres. The diameter of the hollow pore was estimated to be about 10 nm. As CTAB content increases (to 0.10 g), wormlike disordered mesostructures are observed as a dominant phase throughout the sample (Figure 6.7c and d), suggesting the aggregation of the individual micelles, then cross-linking and self-assembly of

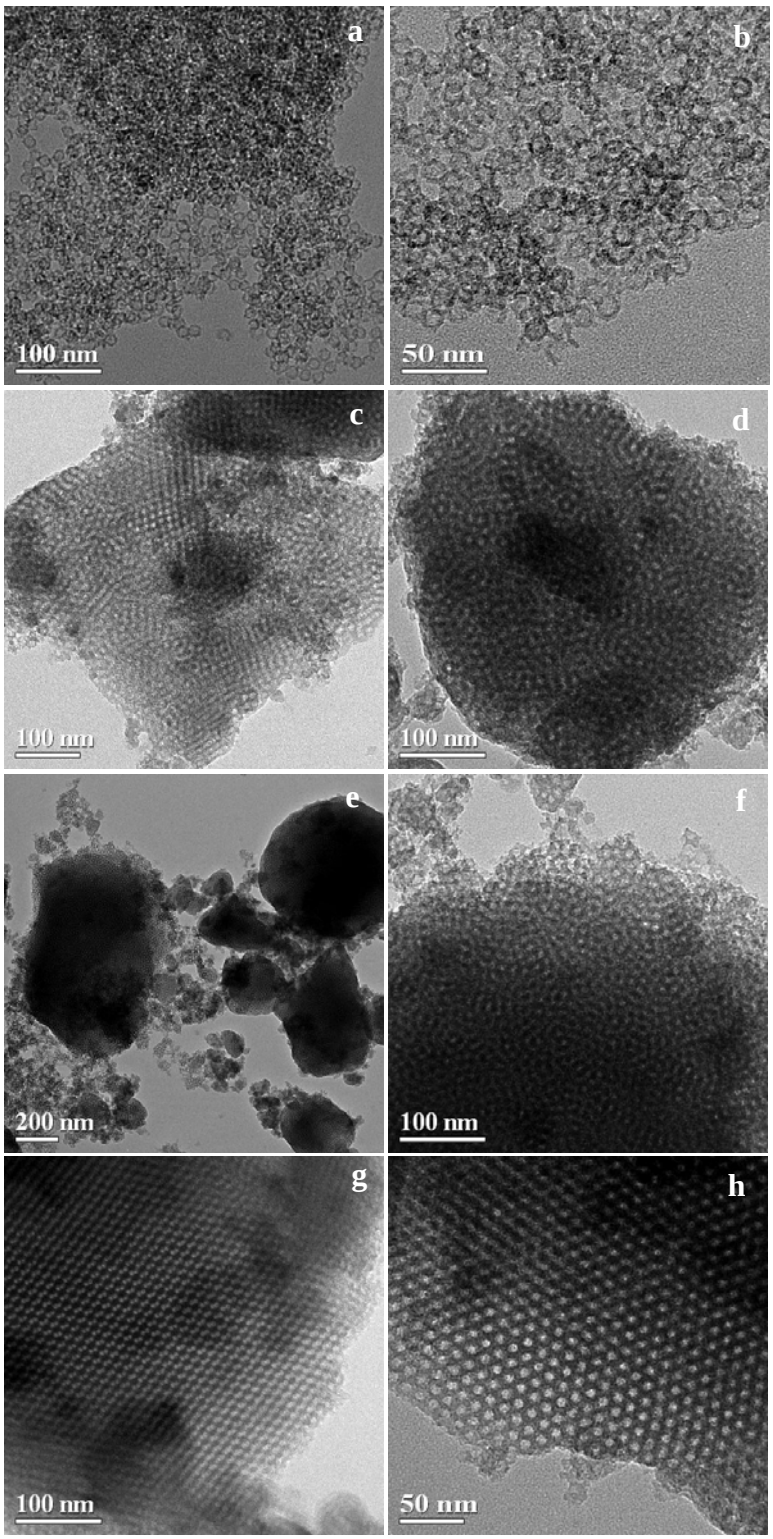

Figure 6.7. TEM images of the PMO-F-C composites synthesized by the low-temperature approach with different content of CTAB at 1.0 M HCl: 0.02 g (a, b), 0.10 g (c, d), 0.14 g (e, f), and 0.16 g (g, h), viewed along the [100] and [111] directions, respectively.

-hydrolyzed organosilica species. It implies that the structural transition from hollow spheres to wormlike structures occurs during this stage. When the content of CTAB is further increased, wormlike morphologies still exist (Figure 6.7e and f), indicating the further cross-linking of organosilica species. When the CTAB content is increased up to 0.16 g, an ordered mesostructure is obtained. Furthermore, the images exhibit typical [100] and [111] projection planes corresponding to the cubic *Im3m* mesostructue (Figure 6.7g and h). The pore size is ca. 8.0 nm. From these TEM results, the structural transformation as a function of CTAB content is apparent, i.e. the mesostructure of PMO-F-C composites gradually changes from a mesostructured hollow sphere via a wormlike structure to an ordered cubic mesophase with increasing the content of CTAB in the mixture gel.

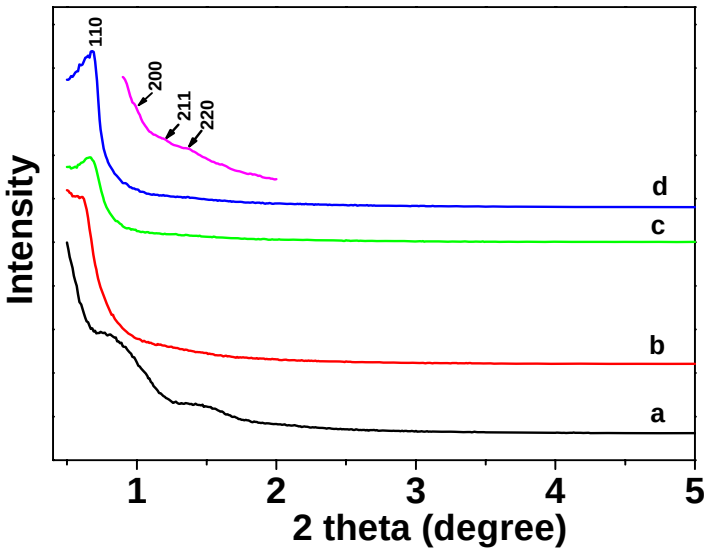

Figure 6.8. XRD patterns of the template-free PMO-F-C composites synthesized by the low-temperature approach with different content of CTAB at 1.0 M HCl: 0.02 g (a), 0.10 g (b), 0.14 g (c) and 0.16 g (d).

Small-angle XRD pattern (Figure 6.8a) of the template-free PMO-F-C composites prepared with a low CTAB content exhibits two broad diffraction peaks, suggesting a poor mesostructural regularity (worklike disordered mesostructure). When CTAB content increases (Figure 6.8b), one diffraction peak is observed. Although the peaks

cannot be indexed, it implies the appearance of organized mesostructures to some extent and the cross-linking occurs between individual micelles. With further increasing the CTAB content, more diffraction peaks are observed though they are quite broad and difficult to be indexed, which indicates the assembly of micelles and further cross-linking of organosilica species (Figure 6.8c). Finally, at least three resolved diffraction peaks can be observed with a high content of CTAB (Figure 6.8d). The four poorly-resolved diffraction peaks can be indexed to 110, 200, 211 and 220 reflections of the cubic mesostructure (space group *Im3m*), further confirmed by careful TEM observations (Figure 6.7g and h), implying that the structural transformations from hollow sphere via a wormlike mesostrucutre to a cubic mesostructure occurs with introducing CTAB into the synthesis system.

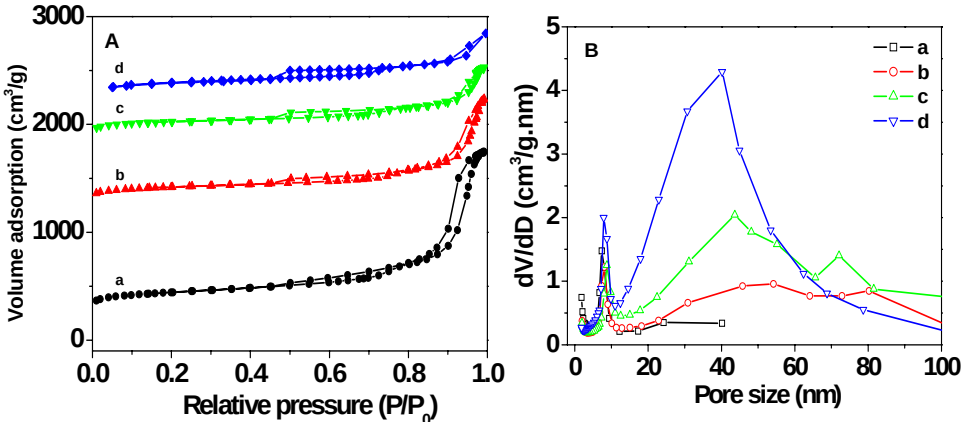

Figure 6.9. N_2 adsorption/desorption isotherms (A) and pore size distributions (B) for the PMO-F-C composites synthesized by the low-temperature approach with different content of CTAB at 1.0 M HCl: 0.02 g (a), 0.10 g (b), 0.14 g (c) and 0.16 g (d).

With increasing CTAB content (from 0.02 to 0.10 g), the sharp uptake of nitrogen by the PMO-F-C composite at a relative pressure at 0.80 ~ 0.99 shifts to lower relative pressures (P/P_0), which could be attributed to the decrease in particle packed pores, suggesting further cross-linking and assembly of organosilica species (Figure 6.9A(a)-(c)). The adsorption isotherms of the PMO-F-C composite prepared with a high content of CTAB (0.16 g) exhibit a typical type-IV with a H2 hysteresis loop, implying a large caged cubic mesostructure (Figure 6.9A(d)). The PMO-F-C

composite has a narrow pore size distribution, mainly centered at 7.3 nm. With increasing CTAB content, the total pore volume decreases from 2.50 to 0.97 $cm^3 \cdot g^{-1}$, while the BET surface area changes irregularly from 648 to 430 $m^2 \cdot g^{-1}$ (Table 6.1). These results suggest that the mesophase transformation occurs with increasing CTAB content.

6.3.3 Formation of mesostructures

Based on the above observations, we propose the formation of the PMO hollow spheres from an assembly of individual spherical micelles. At a low-temperature, as TMB is added to the F127 solution, the uniform droplets of TMB/F127 in water disperse and lead to the individual micelles. Subsequently, the added BTSE molecules hydrolyze and cross-link at the surface of the TMB/F127 micelle and then give the composite with spherical morphology. The salting-out effect also favours the formation of individual micelles, which could be attributed to the lower solubility of micelles's solution [24, 29]. As the hydrothermal temperature increases, the crosslinking and condensation of the organosilica species enhance, resulting in the formation of uniform PMO hollow spheres [6, 21]. Because of the individual micelle assembly, the obtained hollow spheres are well dispersed in the solution. However, it is expected that the dispersed spherical composites collide with each other in the solution, which induces silicate cross-linking on the interface between the colloidal spheres and results in the window-size pores of 3 ~ 4 nm observed from N_2 sorption isotherms (Table 6.1). The effects of low-temperature, inorganic salt and higher hydrothermal temperatures leading to large-pore and well dispersed PMO hollow spheres. The addition of cationic surfactant CTAB which has strong interaction with negative silicate oligomers can enhance crosslinking and condensation of interface silicates between individual spheres, further inducing packing and assembly of the PMO hollow spheres. Therefore, the successive mesophase transformation from hollow spheres via a wormlike mesostructure to cubic symmetry is achieved by increasing the content of cationic CTAB.

6.3.4 Adsorption of Toluene and large biomolecule BSA

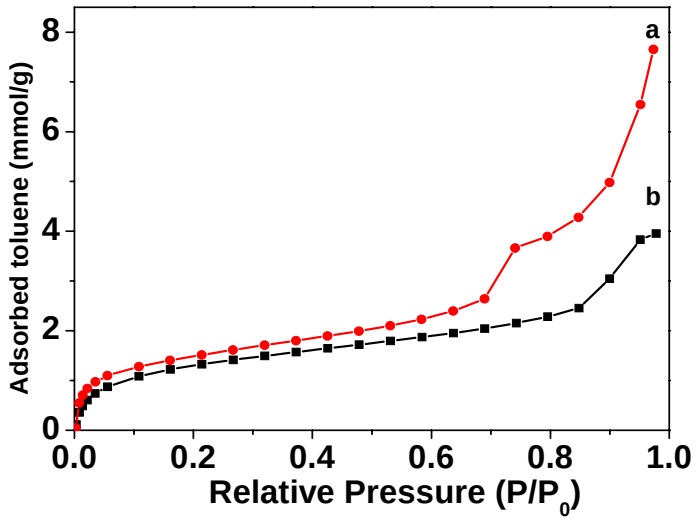

Figure 6.10. Adsorption isotherms of toluene vapour on the obtained PMO-F hollow spheres prepared with different content of KCl at 1.0 M HCl: 0.88 g (a) and 0.30 g (b) at 25 °C.

Toluene adsorption isotherms of the large-pore PMO-F hollow spheres with different pore volume show similar curves, which are nearly type-IV isotherms (Figure 6.10). A steep increase at a low relative pressure (< 0.04), corresponding to micropore filling, is observed. In the case of the PMO-F composite prepared with a high KCl content in a low acid medium (Figure 6.10a), after the micropores are partially saturated, a distinct increase is observed in the adsorption at relative pressure of 0.65 ~ 0.75 due to the filling of toluene in the mesopores. The mesopores can gradually take up gas molecules with the increase of pressure, thus showing a gradual adsorption increase in the isotherms. The large-pore PMO-F hollow spheres exhibit a high adsorption capability of volatile toluene up to 7.65 mmol·g^{-1} (703 mg·g^{-1}) at high pressure (P/P_0 ~ 0.97), due to its large-pore volume and pore size. It is clearly seen that the adsorbed amount of toluene over the PMO-F composite synthesized with low KCl content (Figure 6.10b) is significantly less than that of PMO-F composite prepared with high KCl content in the same acid medium, with toluene adsorption capacity amounting to 3.95 mmol·g^{-1} (363 mg·g^{-1}). With the decrease of pore volume, the adsorption capacity decreases. The high adsorption capacity for toluene could be

attributed to the hydrophobicity of the ethylene groups embedded inside the silica walls, which improves the affinity for toluene to a larger extent.

Table 6.1. Structure textural parameters of the mesoporous PMO-F and PMO-F-C composites synthesized by the low-temperature approach at different conditions.

HCl (M)	CTAB (g)	TMB (g)	KCl (g)	F127 (g)	BTSE (g)	Pore size[a1] (nm)	Window size[a2] (nm)	Surface area[b] ($m^2 \cdot g^{-1}$)	Pore volume[c] ($cm^3 \cdot g^{-1}$)	Micropore volume[d] ($cm^3 \cdot g^{-1}$)	Micropore area[d] ($m^2 \cdot g^{-1}$)
1.0	0	0.1	0.88	0.335	0.958	9.8/61.1	3.8	544	2.24	0.04	94
1.0	0	0.2	0.88	0.335	0.958	11.1/60.4	3.9	594	2.37	0.06	137
1.0	0	0.3	0.88	0.335	0.958	12.7/66.8	3.6	519	2.51	0.03	83
1.0	0	0.4	0.30	0.335	0.958	12.0/60.0	3.9	575	1.87	0.04	93
1.0	0	0.4	0.70	0.335	0.958	12.4/65.0	3.7	525	2.26	0.04	106
1.0	0	0.4	0.88	0.335	0.958	12.3/61.4	3.4	648	2.50	0.06	141
1.0	0	0.4	1.00	0.335	0.958	12.5/51.8	3.7	482	2.19	0.02	72
1.0	0.02	0.4	0.88	0.335	0.958	7.9/40.2	3.6	527	2.24	0	0
1.0	0.10	0.4	0.88	0.335	0.958	8.7/43.6	3.9	430	1.45	0.02	62
1.0	0.14	0.4	0.88	0.335	0.958	8.1/54.2	3.9	449	0.97	0.05	113
1.0	0.16	0.4	0.88	0.335	0.958	7.3	3.9	652	0.92	0.10	204
1.3	0	0.4	0.88	0.335	0.958	15.1/74.0	3.9	468	1.56	0.04	106
2.0	0	0.4	0.88	0.335	0.958	15.0/73.5	3.9	723	1.21	0.15	351

a1 derived from the adsorption branches of the isotherms based on the BJH model.

a2 derived from the desorption branches of the isotherms based on the BJH model.

b BET surface area calculated using experimental points at relative pressure of P/P_0 = 0.05 - 0.25.

c calculated by the N_2 amount adsorbed at the highest P/P_0 (~ 0.99).

d calculated by *t*-plot method using experimental points at relative pressure of P/P_0 = 0.10 - 0.20.

The encapsulation capacity for the large biomolecule BSA of the above two composites was further studied (Figure 6.11). The dimensions of BSA are 5.0 x 5.0 x 7.0 nm, whose cross section is close to the window size (~ 4.0 nm) of PMO-F hollow spheres [1]. It is noted that the adsorption equilibrium amount is significantly affected

by pH value of the buffer solution. The PMO-F composite prepared with high KCl content in a low acid medium exhibits a high adsorption capability of BSA up to 585 $mg \cdot g^{-1}$ at pH 4.7 buffer solution (same as the isoelectric point (pI) of BSA) [1], which is higher than the values reported previously [7]. Upon increasing the pH of the solution to 7.8, the adsorption capacity decreases to 290 $mg \cdot g^{-1}$. In contrast, the PMO-F composite synthesized with a low KCl content in the same acid medium shows lower BSA adsorption of 320 and 170 $mg \cdot g^{-1}$ at pH 4.7 and 7.8 buffer solution, respectively. Apparently the BSA adsorbed amount on the PMO-F hollow spheres is related with pore volume, surface area and the solution pH [1]. Though the cross section of BSAs dimensions is close to the window size, a fairly rapid adsorption was observed at 25 °C These results suggest that the large-pore PMO-F hollow spheres with high pore volume are good candidates for encapsulation and delivery of large biomolecules.

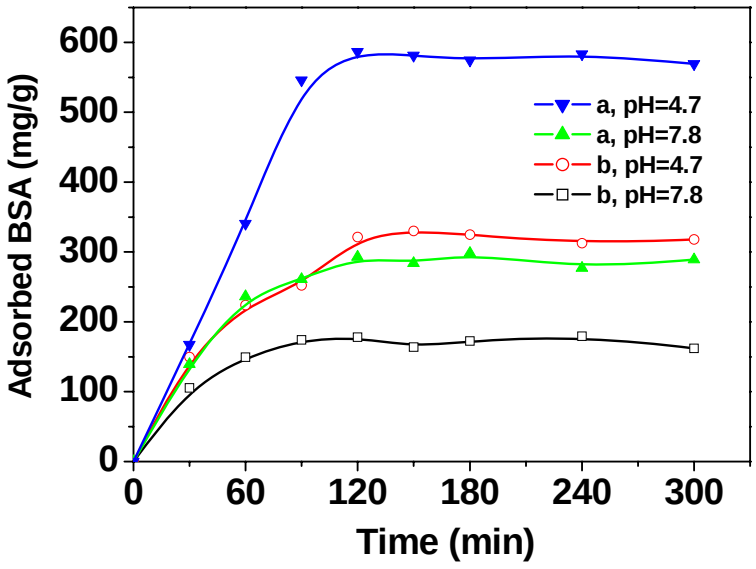

Figure 6.11. Adsorption amount of bovine serum albumin (BSA) in the PMO-F hollow spheres prepared with different content of KCl at 1.0 M HCl: 0.88 g (a) and 0.30 g (b) at 25 °C as a function of time in different pH value media (buffer).

6.4 Conclusions

Uniform PMO hollow spheres with large-pore sizes have been synthesized via a low-temperature approach by using Pluronic F127 as the template in the presence of

TMB and inorganic salt (KCl) at 15 °C. The obtained hollow spheres with controllable diameters of ~ 12-16 nm can be well dispersed in solution and a little aggregated in powder. By adjusting synthetic parameters, the pore size and structure can be simply tuned. The obtained PMO hollow spheres show a high pore volume (~ 2.5 $cm^3 \cdot g^{-1}$) and a large-pore size (up to 15.1 nm). The mesophase transformation from hollow sphere to wormlike disordered mesostructure to ordered cubic symmetry was achieved by the interaction of TMB/F127 micelles with a cationic template (CTAB). The presence of ethylene functional groups in the framework endows these materials with adsorption capacities of toluene up to 703 $mg \cdot g^{-1}$, and of protein BSA up to 585 $mg \cdot g^{-1}$, which indicates that the PMO hollow spheres are potential candidates for adsorption of organic compounds and biomolecules.

References

[1] M. Hartmann, "Ordered Mesoporous Materials for Bioadsorption and Biocatalysis," *Chem. Mater.* **2005**, *17*, 4577-4593.

[2] B. Tan, H. J. Lehmler, S. M. Vyas, B. L. Knutson, S. E. Rankin, "Fluorinated-Surfactant-Templated Synthesis of Hollow Silica Particles with a Single Layer of Mesopores in Their Shells," *Adv. Mater.* **2005**, *17*, 2368-2371.

[3] Z. X. Wang, L. M. Wu, M. Chen, S. X. Zhou, "Facile Synthesis of Superparamagnetic Fluorescent Fe_3O_4/ZnS Hollow Nanospheres," *J. Am. Chem. Soc.* **2009**, *131*, 11276-11277.

[4] R. K. Rana, Y. Mastai, A. Gedanken, "Acoustic Cavitation Leading to the Morphosynthesis of Mesoporous Silica Vesicles," *Adv. Mater.* **2002**, *14*, 1414-1418.

[5] Q. Y. Sun, P. J. Kooyman, J. G. Grossmann, P. H. H. Bomans, P. M. Frederik, P. C. M. M. Magusin, T. P. M. Beelen, "The Formation of Well-Defined Hollow Silica Spheres with Multilamellar Shell Structure," *Adv. Mater.* **2003**, *15*, 1097-1100.

[6] P. S. Winkel, W. W. Lukens Jr., D. Y. Zhao, P. D. Yang, B. F. Chmelka, G. D. Stucky, "Mesocellular Siliceous Foams with Uniformly Sized Cells and Windows," *J. Am. Chem. Soc.* **1999**, *121*, 254-255.

[7] H. N. Wang, "Siliceous Unilamellar Vesicles and Foams by Using Block-Copolymer Cooperative Vesicle Templating," *Adv. Funct. Mater.* **2007**, *17*, 613-617.

[8] L. Ji, A. Katiyar, N. G. Pinto, M. Jaroniec, P. G. Smirniotis, "Al-MCM-41 Sorbents for Bovine Serum Albumin: Relation between Al Content and Performance," *Micropor. Mesopor. Mater.* **2004**, *75*, 221-229.

[9] T. Asefa, M. J. MacLachlan, N. Coombos, G.A. Ozin, "Periodic Mesoporous Organosilicas with Organic Groups inside the Channel Walls," *Nature* **1999**, *402*, 867-871.

[10] S. Inagaki, S. Guan, Y. Fukushima, T. Ohsuna, O. Teresaki, "Novel Mesoporous Materials with a Uniform Distribution of Organic Groups and Inorganic Oxide in Their Frameworks," *J. Am. Chem. Soc.* **1999**, *121*, 9611-9614.

[11] B. J. Melde, B. T. Holland, C. F. Blandford, A. Stein, "Mesoporous Sieves with Unified Hybrid Inorganic/Organic Frameworks," *Chem. Mater.* **1999**, *11*, 3302-3308.

[12] X. F. Zhou, S. Z. Qiao, N. Hao, X. L. Wang, C. Z. Yu, K. L. Wang, D. Y. Zhao, G. Q. Lu, "Synthesis of Ordered Cubic Periodic Mesoporous Organosilicas with Ultra-Large Pores," *Chem. Mater.* **2007**, *19*, 1870-1876.

[13] Y.F. Lu, H.Y. Fan, N. Doke, D.A. Loy, R.A. Assink, D.A. LaVan, C.J. Brinker, "Evaporation-Induced Self-Assembly of Hybrid Bridged Silsesquioxane Film and Particulate Mesophases with Integral Organic Functionality," *J. Am. Chem. Soc.* **2000**, *122*, 5258-5261.

[14] S. Guan, S. Inagaki, T. Ohsuna, O. Terasaki, "Cubic Hybrid Organic-Inorganic Mesoporous Crystal with a Decaoctahedral Shape," *J. Am. Chem. Soc.* **2000**, *122*, 5660-5661.

[15] M. P. Kapoor, S. Inagaki, "Synthesis of Cubic Hybrid Organic-Inorganic Mesostructures with Dodecahedral Morphology from a Binary Surfactant Mixture," *Chem. Mater.* **2002**, *14*, 3509-3514.

[16] D. J. Kim, J. S. Chung, W. S. Ahn, G. W. Kam, W. J. Cheong, "Morphology Control of Organic-Inorganic Hybrid Mesoporous Silica by Microwave Heating," *Chem. Lett.* **2004**, *33*, 422-423.

[17] V. Rebbin, M. Jakubowski, S. Potz, M. Fröba, "Synthesis and Characterisation of Spherical Periodic Mesoporous Organosilicas (sph-PMOs) with Variable Pore Diameters," *Micropor. Mesopor. Mater.* **2004**, *72*, 99-104.

[18] M. P. Kapoor, S. Inagaki, "Synthesis of Phenylene Bridged Mesoporous Silsesquioxanes with Spherical Morphology in Ammonia Solution," *Chem. Lett.* **2004**, *33*, 88-89.

[19] S. Z. Qiao, C. Z. Yu, W. Xing, Q. H. Hu, H. Djojoputro, G. Q. Lu, "Synthesis and Bio-adsorptive Properties of Large-Pore Periodic Mesoporous Organosilica Rods," *Chem. Mater.* **2005**, *17*, 6172-6176.

[20] M. Park, S. S. Park, M. Selvaraj, D. Y. Zhao, C. S. Ha, "Hydrophobic Mesoporous Materials for Immobilization of Enzymes," *Micropor. Mesopor. Mater.* **2009**, *124*, 76-83.

[21] J. Liu, Q. H. Yang, L. Zhang, H. Q. Yang, J. S. Gao, C. Li, "Organic-Inorganic Hybrid Hollow Nanospheres with Microwindows on the Shell," *Chem. Mater.* **2008**, *20*, 4268-4275.

[22] W. P. Guo, J. Y. Park, M. O. Oh, H. W. Jeong, W. J. Cho, I. Kim, C. S. Ha, "Triblock Copolymer Synthesis of Highly Ordered Large-Pore Periodic Mesoporous Organosilicas with the Aid of Inorganic Salts," *Chem. Mater.* **2003**, *15*, 2295-2298.

[23] W. P. Guo, I. Kim, C. S. Ha, "Highly Ordered Three-Dimensional Large-Pore Periodic Mesoporous Organosilica with *Im*3*m* Symmetry," *Chem. Commun.* **2003**, 2692-2693.

[24] S. S. Park, B. An, Y. Kang, M. Park, I. Kim, C.-S. Ha, "The Effect of Inorganic Salt on the Synthesis of Large-Pore PMO with Aromatic Moieties in the Framework," *Stud. Surf. Sci. Catal.* **2006**, *165*, 421-424.

[25] J. Fan, C. Z. Yu, J. Lei, Q. Zhang, T. C. Li, B. Tu, W. Z. Zhou, D. Y. Zhao, "Low-Temperature Strategy to Synthesize Highly Ordered Mesoporous Silicas with Very Large Pores," *J. Am. Chem. Soc.* **2005**, *127*, 10794-10795.

[26] J. S. Beck, J. C. Vartuli, W. J. Roth, M. E. Leonowicz, C. T. Kresge, K. D. Schmitt, C. T. W. Chu, D. H. Olson, E. W. Sheppard, "A New Family of Mesoporous

Molecular Sieves Prepared with Liquid Crystal Templates," *J. Am. Chem. Soc.* **1992**, *114*, 10834-10843.

[27] W. H. Zhang, X. N. Zhang, Z. L. Hua, P. Harish, F. Schroeder, S. Hermes, T. Cadenbach, J. L. Shi, R. A. Fischer, "Synthesis, Bifunctionalization, and Application of Isocyanurate-Based Periodic Mesoporous Organosilicas," *Chem. Mater.* **2007**, *19*, 2663-2670.

[28] M. Cornelius, F. Hoffmann, M. Fröba, "Periodic Mesoporous Organosilicas with a Bifunctional Conjugated Organic Unit and Crystal-like Pore Walls," *Chem. Mater.* **2005**, *17*, 6674-6678.

[29] W. H. Zhang, L. Zhang, J. Xiu, Z. Shen, Y. Li, P. Ying, C. Li, "Pore size design of ordered mesoporous silicas by controlling micellar properties of triblock copolymer $EO_{20}PO_{70}EO_{20}$," *Micropor. Mesopor. Mater.* **2006**, *89*, 179-185.

CHAPTER 7 Synthesis of Ordered Meosporous Polymer-Organosilica and Carbon-Silica Nanocomposites by the Triconstituent Co-Assembly Method

7.1 Introduction

Much progress has been made in the preparation of a new class of organic-inorganic hybrid materials called periodic mesoporous organosilicas (PMOs) through surfactant-mediated synthesis by hydrolysis and condensation of bridged silsesquinoxanes $(RO)_3$-Si-R'-Si-$(RO)_3$ in the last decade [1-3]. The presence of organic functional groups in the framework is achieved in one step, which leaves pore voids, improves the smooth accessibility of functional sites [4], and thus promotes the use of PMOs for various potential applications such as catalysis [5-9], adsorption [10-14] and high-performance liquid chromatography [15]. Surfactant-directed organosilica mesophases are unique in that they can be used as a precursor to fabricate a wide range of mesostructured materials. A possibility for the transformation of PMOs into other mesoporous materials has been first reported by Pang *et al.* [16]. By heating a mesostructured phenyl-bridged PMO with crystal-like pore walls at 900 ºC in an atomosphere of nitrogen, they obtained mesoporous carbon/silica nanocomposites with pores walls uniformly constructed from carbon and silica units. Mesoporous carbon could be obtained *via* direct carbonation of phenyl-bridged organosilica/surfactant mesophases followed by removal of the silica components from the carbon/silica composites. However, the regular degree of mesoporous carbon was significantly lower, and no description on mesoporous silica fabricated from the carbon/silica composites. Following this work, Mokaya and co-workers [17] made some attempts to prepare mesoporous silica/carbon composites *via* carbonization of ethyl-bridged organosilica/surfactant mesophases. The well ordered mesoporous silica can be obtained by pyrolysis of the silica/carbon composites, while porous carbons with graphitic characteristics may be generated *via* silica etching of the composites. It is further demonstrated that PMO/surfactant mesophases can be used as a suitable precursor for the direct fabrication of versatile mesoporous silica/carbon composites, silica and carbon.

Recently, highly ordered mesoporous polymers have been reported by several research groups, which were synthesized from organic-organic assembly of block polymers and phenolic resins [18-22]. However, serious skeleton shrinkage arises during the high-temperature carbonization procedure. The incorporation of a rigid

constituent, for example silica, into organic polymeric networks can assist the organic polymers to organize into ordered mesostructures, which is an effective way for reduction of framework shrinkage [4, 23]. It is further shown that two or more phases can be combined together that historically have been viewed as very different and even incompatible. The resulting materials are more homogeneous than conventional hybrid materials and generate remarkable and complementary properties, which cannot be obtained in a single component [24-28]. For example, the mesoporous polymer-silica composites are considered as innovative materials, as the composites take advantage of the properties of both organic polymers and inorganic silica components. Similarly, mesoporous carbon/silica nanocomposites can also improve thermal, chemical, conductive, and mechanical properties [4].

Inspired by such one-pot fabrication of ordered mesoporous polymer-silica composites, it would be worthwhile to devote much effort to the synthesis of organic polymer frameworks with mesoporous organosilica/surfactant phases by manipulating polymerization [29], as the full potential of the mesophases as 'precursors' for the formation of these mesostructured materials with phenolic resins has not been fully explored. In particular, the preparation of mesoporous silica and carbon from as-synthesised mesoporous organosilica-polymer mesophases would offer a more direct route to these materials with a reduced number of synthesis steps compared to hard templating [17].

In this chapter, we report a triconstituent co-assembly approach to synthesize ordered hexagonal mesoporous polymer-organosilica and carbon-silica nanocomposites by using resols as a polymer precursor, BTSE as an organic silicate precursor, and triblock copolymer F127 as a template. The ordered 2D *p*6mm mesostructures of hybrid polymer-organosilica nanocomposites can be maintained, even when the BTSE content increases in the synthesis process. Our results clearly show that the organosilicates plays an important role in the reducing structural shrinkage during the calcination. After the removal of carbon by simple combustion or removal of silica by HF etching from carbon-silica composites, ordered mesoporous pure silica or carbon frameworks can be obtained. The ordered silica products have ordered 2D mesostructures with uniform pore sizes (5.6 ~ 8.8 nm). Furthermore, the adsorption properties of the obtained polymer-organosilica composite for benzene were also investigated.

7.2 Experimental

7.2.1 Preparation of resol precursors

The resol precursor (Mw < 500) was prepared according to the literature method [19]. In a typical procedure, 0.61 g of phenol was melted at 40 ~ 42 °C in a flask and mixed with 0.13 g of 20 wt % NaOH aqueous solution under stirring. After 10 min, 1.05 g of formalin (37 wt % formaldehyde) was added dropwise below 50 °C. Upon further stirring for 1 h at 70 ~ 75 °C, the mixture was cooled to room temperature and the pH value was adjusted to about 7.0 by HCl solution. After water was removed by vacuum evaporation below 50 °C, the final product was dissolved in ethanol (20 wt % ethanolic solution).

7.2.2 Synthesis of ordered mesoporous polymer-organosilica and carbon-silica nanocomposites

Mesoporous polymer-organosilica and carbon-silica nanocomposites were prepared by triconstituent coassembly of resols, oligomer silicates from BTSE, and triblock copolymer F127 template. In a typical preparation, 0.4 g of triblock copolymer F127 was dissolved in 2.0 g of ethanol with 0.037 g of 0.2 M HCl and stirred for 1 h at 40 °C to afford a clear solution. Next, 0.44 g of BTSE and 1.25 g of 20 wt % resols' ethanolic solution were added in sequence. After being stirred for 2 h, the mixture was transferred into dishes. It took 5 h at room temperature to evaporate ethanol and 24 h at 90 °C in an oven to thermopolymerize. The as-made products, flaxen and transparent films, were scraped from the dishes and ground into fine powders. Calcination was carried out in a tubular furnace at 350 °C for 3 h and at 900 °C for 2 h under N_2 flow to get mesoporous polymer-organosilica and carbon-silica composites, respectively, named as MP-COS-0.44BTSE and MP-CS-0.44BTSE. "MP-COS-xBTSE" and "MP-CS-xBTSE" denote the mesoporous polymer-organosilica and carbon-silica nanocomposite samples respectively, wherein x represents the weight of BTSE precursor during synthetics process. The heating rate was 1 °C/min for polymer-organosilica and 2 °C/min for carbon-silica nanocomposite, respectively.

Nanocomposites with different compositions (the mass ratios of polymer/BTSE) could be synthesized by adjusting the content of BTSE, while keeping the other parameters same during the synthesis. The typical samples denoted as MP-COS-0.22BTSE, -0.44BTSE, and -0.55BTSE are listed in Table 7.1.

7.2.3 Synthesis of ordered mesoporous carbon and silica from carbon-silica nanocomposites

After carbon-silica nanocomposites were immersed in 10 wt % HF solutions for 24 h, silicas were removed and mesoporous carbons were left. Calcination at 550 °C for 5 h in air could burn off carbons and generate mesoporous silica materials. The mesoporous pure carbon products were named as MP-C-0.22BTSE, -0.44BTSE, and -0.55BTSE respectively, and the mesoporous pure silica products were named as MP-Si-0.22BTSE, -0.44BTSE, and -0.55BTSE respectively, corresponding to their mother composites.

7.3 Results and discussion

7.3.1 Ordered mesostructured polymer-organosilica and carbon-silica nanocomposites

Mesostructured polymer-organosilica composites were prepared by triconstituent co-assembly of preformed resols, organosilica oligomers from acid-catalyzed hydrolysis of BTSE, and triblock copolymers F127 *via* the EISA approach [30] in ethanol solution. Here, we take the mesoporous nanocomposite MP-COS-0.44BTSE with the BTSE weight content of 0.44 g as an example. The as-made products are flaxen membranes without obvious macrophase separation.

The XRD pattern for as-made polymer-organosilica composite MP-COS-0.44BTSE (Figure 7.1a) shows one sharp diffraction peak, which is difficult to index. However, after calcination at 350 °C in nitrogen, the product turns brown and yields three well-resolved diffraction peaks (Figure 7.1b), associated with the 100, 110, and 200 reflections of 2D hexagonal symmetry with the space group of *p6mm* [31]. The unit cell parameter (a_0) is reduced from 15.4 to 13.4 nm upon the calcination (Table 7.1), reflecting a 13.0 % framework shrinkage. After being heated at 900 °C in nitrogen, the composite becomes black. The one diffraction peak indexed to the 100 reflection is still observed (Figure 7.1c), indicating that the ordered 2D hexagonal mesostructured composite is thermally stable. The a_0 is calculated to be 11.0 nm, reflecting minor framework shrinkage of 28.6 %. It is much smaller than that of C-FDU-15 (41.2 %) with the same *p6mm* symmetry but without silicates inside the framework after heating treatment at 900 °C. This phenomenon clearly demonstrates

that the presence of organosilica in the composite can efficiently reduce framework shrinkage as compared to pure polymer [4, 23, 31].

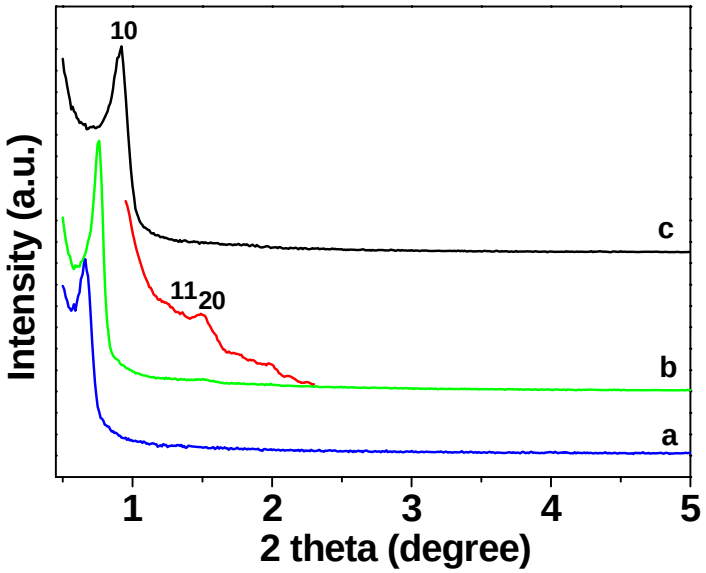

Figure 7,1. XRD patterns of mesoporous polymer-organosilica nanocomposites MP-COS-0.44BTSE: (a) as-made, (b) calcined at 350 °C, and (c) calcined at 900 °C in N_2.

TEM images of the template-free mesoporous MP-COS-0.44BTSE material calcined at 350 and 900 °C in N_2 show large domains of ordered hexagonal and stripe-like arranged arrays (Figure 7.2), clearly indicating an ordered 2D hexagaonal mesostructure with 1D pore channels, which can be retained after calcination at 900 °C. The unit cell parameter (a_0) is estimated from TEM images to be approximately 14.0 and 10.0 nm for the nanocomposites calcined at 350 and 900 °C, respectively, which is in good agreement with the values calculated from the XRD data.

Nitrogen sorption isotherms (Figure 7.3) of the mesoporous MP-COS-0.44BTSE composite calcined at 350 °C in N_2 exhibit representative type-IV curves with a sharp capillary condensation step at relative pressure range of 0.7 ~ 0.8, indicative of a large uniform mesopore. A H2-type-like hysteresis loop at a relative pressure of 0.4 ~ 0.5 is observed, implying imperfect cylinder mesochannels with a window size smaller than 5.0 nm. It may be caused by asymmetric shrinkage [32]. The polymer-organosilica composite MP-COS-0.44BTSE has a BET surface area of 696 $m^2 \cdot g^{-1}$, a pore volume of 0.67 $cm^3 \cdot g^{-1}$. The pore diameter is calculated according to the BJH model to be 6.9 nm. The above observations clearly demonstrates that the assembly between resol, organosilicates precursor and F127 is not easy to form the cubic mesostructure, as

synthesis is performed in non-aqueous solution by the EISA approach [4]. In our case, BTSE and resol are used as the silica and carbon sources, which contain hydrophobic organic group and makes the assembly of the organosilicate, resol species and F127 template different from that for TEOS or resol case. Therefore, it is reasonable that 2D hexagonal mesostructure is formed by using BTSE as a silica source, resol as carbon source and F127 as a template *via* an EISA method.

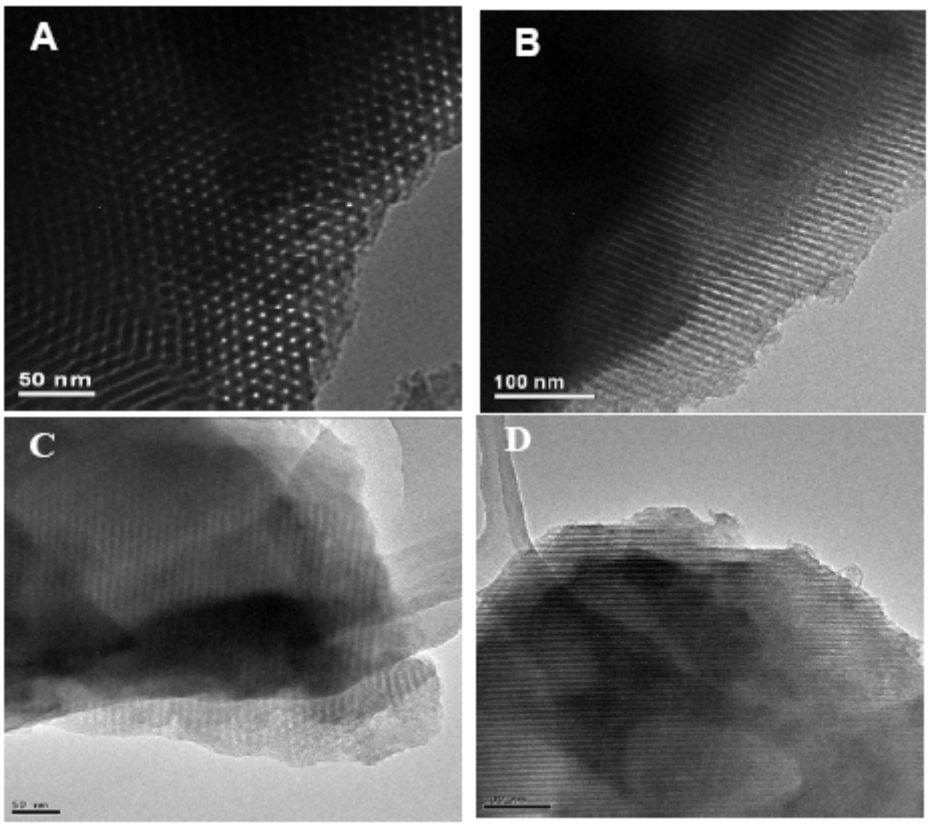

Figure 7.2. TEM images of mesoporous polymer-organosilica nanocomposites MP-COS-0.44BTSE calcined at 350 °C (A and B) and 900 °C (C and D) in N_2, viewed from the [001] (A and C) and [110] (B and D) directions.

Similarly, the composite MP-CS-0.44BTSE after calcination at 900 °C in N_2 also exhibits typical type-IV isotherms, but displays an H1-type hysteresis loop that is typical of mesoporous materials with cylindrical channels. The nitrogen condensation shifts to low relative pressure (P/P_0), indicating a decrease of mesopore size. These results are consistent with the decrease of unit cell parameters calculated from the XRD data. This phenomenon is accompanied by the change of cell unit parameters on account of framework shrinkage during the calcination. The pore size is 3.7 nm heated at 900 °C in N_2. The BET surface area and pore volume of the MP-CS-

0.44BTSE composite calcined at 900 °C are calculated to be 348 $m^2 \cdot g^{-1}$ and 0.29 $cm^3 \cdot g^{-1}$, respectively (Table 7.1).

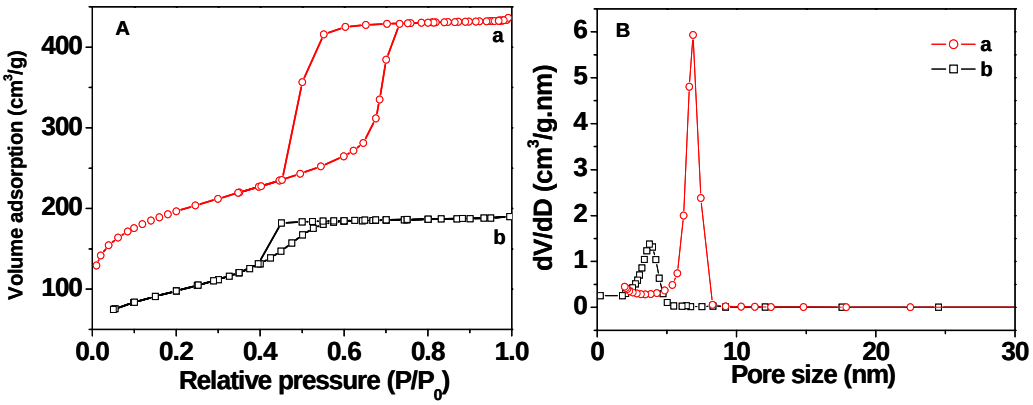

Figure 7.3. N_2 adsorption/desorption isotherm (A) and pore size distributions (B) for mesoporous composites (a) MP-COS-0.44BTSE calcined at 350 °C and (b) at 900 °C in N_2.

Table 7.1. Physicochemical properties of the mesoporous polymer-organosilica and carbon-silica nanocomposites prepared with different content of BTSE from triconstituent co-assembly via EISA Method.

Sample		a_0 (nm)	Pore size[a] (nm)	Surface area[b] ($m^2 \cdot g^{-1}$)	Pore volume[c] ($cm^3 \cdot g^{-1}$)	Micropore area[d] ($m^2 \cdot g^{-1}$)	Micropore volume[d] ($cm^3 \cdot g^{-1}$)
MP-COS-0.22BTSE	polymer-organosilica	11.7	6.2	794	0.88	138	0.06
MP-COS-0.44BTSE	polymer-organosilica	13.4	6.9	696	0.67	245	0.10
MP-COS-0.55BTSE	polymer-organosilica	14.0	7.3	619	0.61	209	0.09
MP-CS-0.22BTSE	carbon-silica	9.6	5.4	1417	1.39	622	0.28
MP-CS-0.44BTSE	carbon-silica	11.1	3.7	348	0.29	30	0.01
MP-CS-0.55BTSE	carbon-silica	10.1	5.1	288	0.29	56	0.02
MP-C-0.22BTSE	carbon	-	5.3	1423	1.01	310	0.12
MP-C-0.44BTSE	carbon	6.3	2.5	1398	1.13	0	0
MP-C-0.55BTSE	carbon	-	4.9	1491	1.02	102	0.03
MP-Si-0.22BTSE	silica	13.2	8.8	218	0.55	34	0.01
MP-Si-0.44BTSE	silica	9.9	5.9	350	0.58	7	0
MP-Si-0.55BTSE	silica	9.8	5.6	411	0.54	9	0

a derived from the desorption branches of the isotherms based on the BJH model.

b BET surface area calculated using experimental points at relative pressure of $P/P_0 = 0.05 - 0.25$.

c calculated by the N_2 amount adsorbed at the highest P/P_0 (~ 0.99).

d calculated by *t*-plot method using experimental points at relative pressure of $P/P_0 = 0.10 - 0.20$.

^{29}Si MAS NMR spectrum (Figure 7.4a) of the template-free mesoporous polymer-organosilica MP-COS-0.44BTSE composite calcined at 350 °C shows one signal at -61.8 ppm, which can be assigned to T^3 [C-Si(OSi)$_3$] site. The strong intensity for T^3 signal indicates a corporation of the ethylene bridged groups into the pore walls, and the formation of highly condensed organosilicate frameworks [33]. Another weak resonance around -101.0 ppm ascribed to Q^3 (OH)Si(OSi)$_3$ sites of silicate is also observed [34, 35], further suggesting that Si-C bonds are well-retained during the synthesis process. The ^{13}C CP-MAS NMR spectrum (Figure 7.4b) of the template-free sample MP-COS-0.44BTSE further reveal that the polymer-organosilica framework is bonded covalently through the ethylene and resin polymer. The occurrence of a strong signal at about 5 ppm is attributed to the carbons in the ethylene group connected to Si atoms. The signals at 15, 34, 63, 129 and 151 ppm are assigned to the polymer phenolic resins, except the weak signal at ~ 63 ppm is related to Si-O-C bonds, suggesting the presence of resin polymeric frameworks in the polymer-organosilica nanocomposite [36]. The signal at about 71 ppm is due to the main-chain carbons of ethylene oxide (EO) and propylene oxide segments of Pluronic F127, suggesting a partial residue of the surfactant template, which gives evidence on almost complete decomposition of F127 template during reaction process [37].

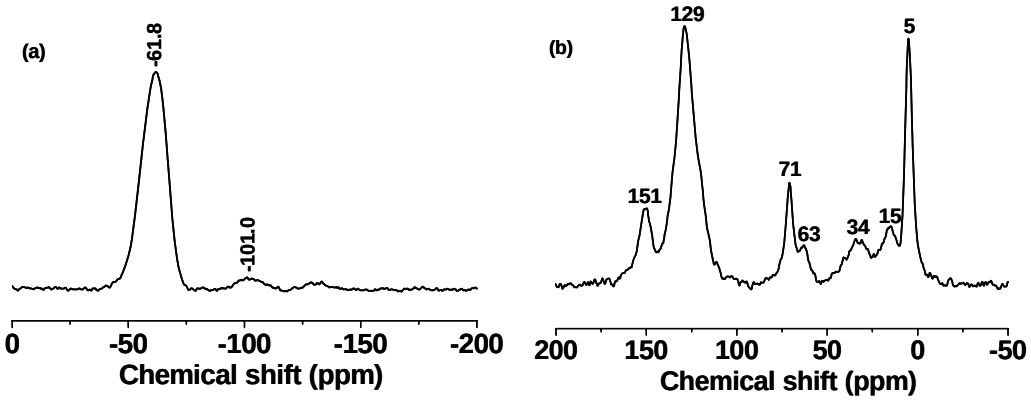

Figure 7.4. ^{29}Si-NMR (a) and ^{13}C-NMR (b) MAS NMR spectra for template-free mesoporous polymer-organsilica nanocomposite MP-COS-0.44BTSE calcined at 350 °C in N_2.

FT-IR spectra (Figure 7.5a) of the MP-COS-0.44BTSE composite calcined at 350 °C under nitrogen shows one intense band 1623 cm^{-1}, which is attributed to the asymmetric ethylene (C-C) stretching modes. The bands at 1270, 1480 and 2931 cm^{-1}

are attributed to the bridging ethylene C-H vibration and stretching, respectively. These findings indicate that Si-C stability and the integrity of ethylene groups within the silica matrix in the synthetic and calcination process. Furthermore, the sharp band at 1098 cm^{-1} from Si-O-Si vibration confirms the formation of siloxane bonds. The bands at 2931 and 1098 cm^{-1} are also attributed to the C-H and C-O stretching of triblock copolymer F127 [37] and the overlap with Si-O-Si vibration [38]. The band at 3446 cm^{-1} is from the Si-OH groups [39]. A broad band at 3446 cm^{-1} and one at 1623 cm^{-1} are assigned to the characteristic stretching modes of phenolic resins [40, 41], indicating that highly cross-linking phenol resin polymer networks are preserved well. And the absorbance at 803 cm^{-1} ascribed to Si-OH vibration is observed. These results further reveal the coexistence of polymer and silicate solids with ethylene bridging groups. After calcination at 900 °C in N_2, the characteristic vibration bands of phenolic resins disappear and those of silicates are retained as shown in Figure 7.5b. The decreasing intensity of bands at around 2931 cm^{-1} for the composite calcined at 900 °C under nitrogen further suggests completely decomposition of F127 template [37].

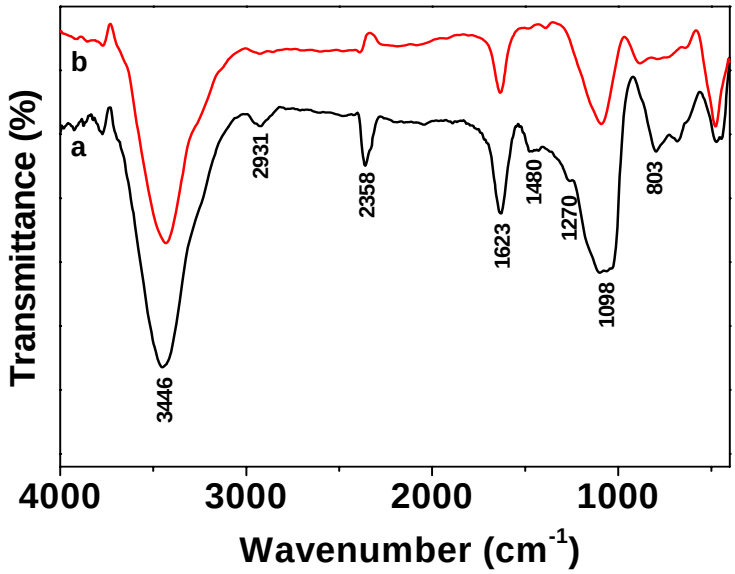

Figure 7.5. FT-IR spectra of the mesoporous nanocomposites: (a) MP-COS-0.44BTSE calcined at 350 °C in N_2 and (b) MP-CS-0.44BTSE calcined at 900 °C in N_2, respectively.

The TGA curve of the composite MP-COS-0.44BTSE after calcination at 350 °C in N_2 (Figure 7.6A(b)) displays an obvious weight loss of 40 wt % in the temperature

range of 300 to 400 °C under nitrogen for as-made MP-COS-0.44BTSE composite. Correspondingly, 98.5 wt % loss of pure triblock copolymer F127 occurs at the same temperature range (Figure 7.6A(a)), which suggests that most templates can be removed at 350 °C in N_2. A weight loss of 22 wt % can be observed at 400 ~ 900 °C, corresponding to dehydrogenation and polymerization of phenolic resins and silicate species in the composite. Similarly, the TGA curve of the MP-COS-0.44BTSE composite after calcination at 350 °C in N_2 (Figure 7.6B(c)) shows a weight loss of 55 wt % in air between 350 and 600 °C, which is attributed to the combustion of organic phenolic resins and ethylene bridging groups. The composition can then be given as organics of 55 wt % and silica of 45 wt %. It may fluctuate a bit because condensation of silicate species may also contribute to the weight loss [31]. After the calcination at 900 °C in N_2, the characteristic weight loss of the MP-COS-0.44BTSE composite in the temperature range from 500 to 600 °C is 45 wt %, and the weight residue is 55 wt % (Figure 7.6B(d)). They are attributed to carbon compound and silica, respectively.

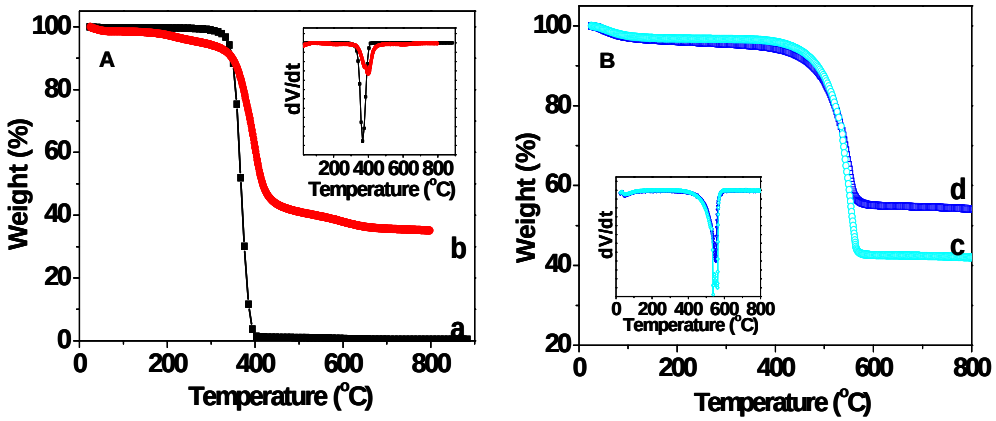

Figure 7.6. TG and DTG curves (inset) recorded in N_2 (A) and air (B) of triblock copolymer F127 (a), the as-made mesoporous nanocomposite MP-COS-0.44BTSE, (b), MP-COS-0.44BTSE calcined at 350 °C (c) and 900 °C in N_2 (d).

The ratios of polymer/organosilica in the polymer-organosilica composites can be tuned by varying the mass of BTSE in tri-constituent co-assembling process, while keeping the other synthetic parameters unchanged. Compartively, the other two composites with different content of BTSE after calcination at 350 and 900 °C in N_2 show one sharp diffraction peak, which could be attributed to 2D hexagonal mesostructure (Figure 7.7). As BTSE contents increases, the mesostructure regularity

varies a little to some extent. These results also suggest that the mesoporous polymer-organosilica and carbon-silica composites are thermally stable.

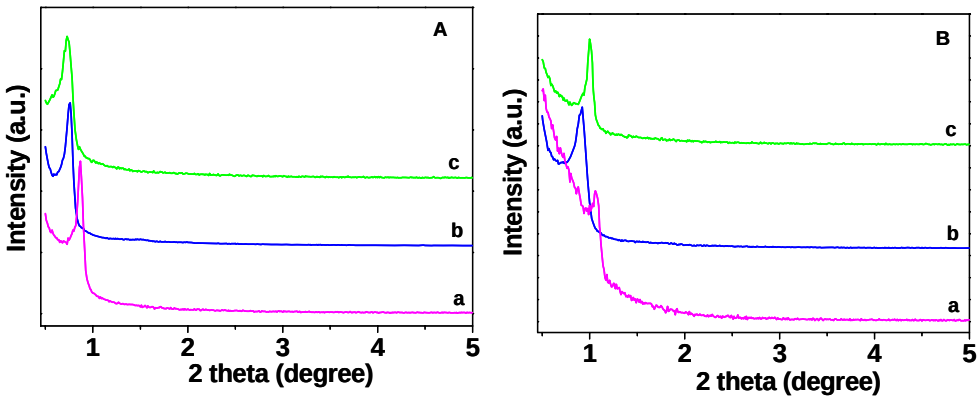

Figure 7.7. XRD patterns of the mesoporous nanocomposites prepared with different contents of BTSE calcined at 350 °C (A) and 900 °C in N_2 (B). In both (A) and (B), (a) MP-COS-0.22BTSE, (b) MP-COS-0.44BTSE and (c) MP-COS-0.55BTSE.

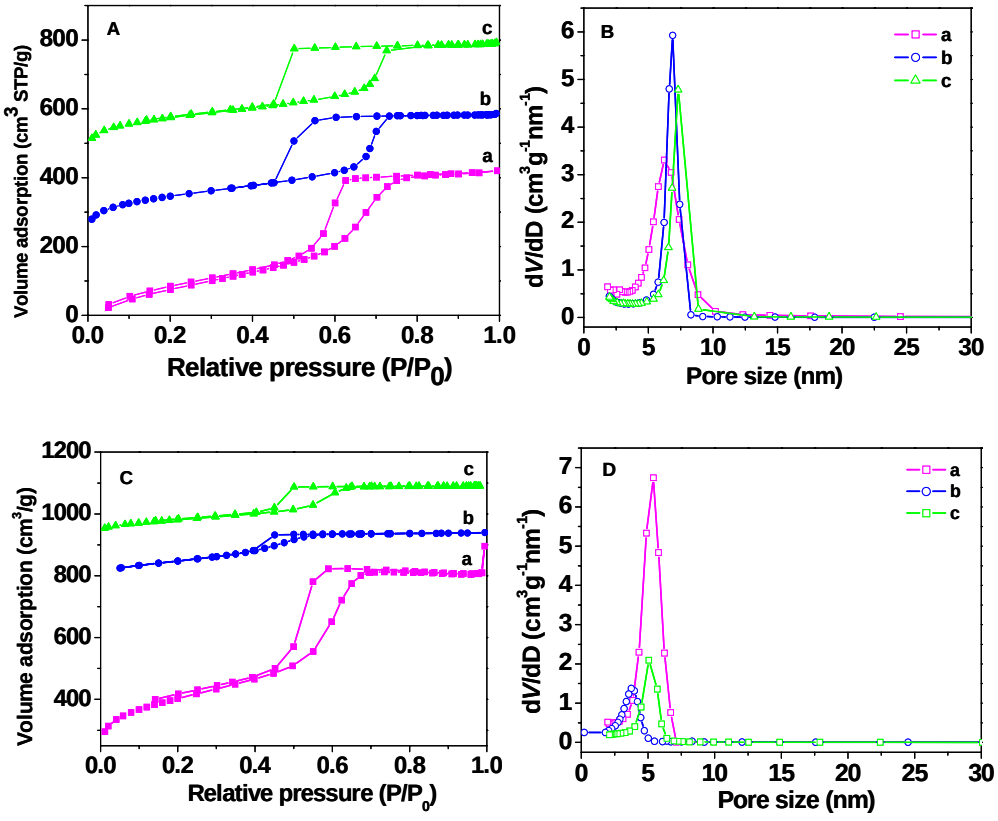

Figure 7.8. N_2 sorption isotherms (A and C) and pore size distribution curves (B and D) of the mesoporous nanocomposites calcined at 350 °C (A and B) and 900 °C in N_2 (C and D). In all figures, a, b, and c correspond to the polymer-organosilica and carbon-silica nanocomposites of MP-COS-0.22BTSE, (b) MP-COS-0.44BTSE, and (c) MP-COS-0.55BTSE, respectively.

All composites exhibit type-IV curves with distinct capillary condensation steps, suggesting narrow mesopore size distributions. It is coincident with their ordered mesostructures, confirmed by the XRD results. When BTSE contents are low, ideal H1 hysteresis can be observed for polymer-organosilica composites (Figure 7.8A(a)), suggesting well-ordered cylinder mesopore channels [31]. When BTSE contents are high, obvious H2 hysteresis can be seen for the polymer-organosilica composites (Figure 7.8A(b, c)) after calcination at 350 °C in N_2, suggesting caged pore mesostructure. It further suggests that the composites have roughly cylindrical pore channels, probably resulting from the different shrinkage between organosilicates and phenolic polymer resins [32]. This implies local component nonuniformity.

The BET surface area decreases with increasing the content of BTSE in the synthesis of polymer-organosilica composites, while the mean pore sizes are similar at range of 6 ~ 7 nm regardless of BTSE contents (Figure 7.8B). All carbon-silica nanocomposites after calcination at 900 °C in N_2 show H1 hysteresis (Figure 7.8C), suggesting uniform mesopore channels. As BTSE contents increase in carbon-silica composites, both BET surface areas and pore volumes decrease sharply. And the mean pore sizes also decrease from 5.4 to 3.7 nm (Figure 7.8D).

7.3.2 Mesoporous carbon and silica materials from carbon-silica nanocomposites

The integrated frameworks with ordered 2D hexagonal mesostructure have been synthesized by triconstituent co-assembly *via* the one-step EISA approach, composed of organosilicas and polymer resins or silicas and carbons. Some interactions may occur on the interface between the polymer and organosilica or carbon and silica, and affect the structures and networks. To understand the structures of carbon (polymer) and organosilica in the composites is critical for the control of triconstituent co-assembly, and thus it is necessary to investigate the resultants of carbon and silica separately. Carbon-silica composites are used as the parents. Etching with HF solution or combustion of composites in air can remove silica or carbon, leaving carbon or silica phases [4].

7.3.2.1 Mesoporous carbon materials

The XRD pattern (Figure 7.9A) of the mesoporous carbon material (MP-C-0.44BTSE) shows one diffraction peak with unit cell parameters of about 6.3 nm, indicative of a disordered mesostructure. Only one weak diffraction peak or none can

be detected in the XRD pattern (Figure 7.9A). There are two possible reasons. One is that the carbon mesostructure has been destroyed during a large amount of silica removal. The other may be a low XRD contrast due to voids caused by copious silica removal and small residue of carbon.

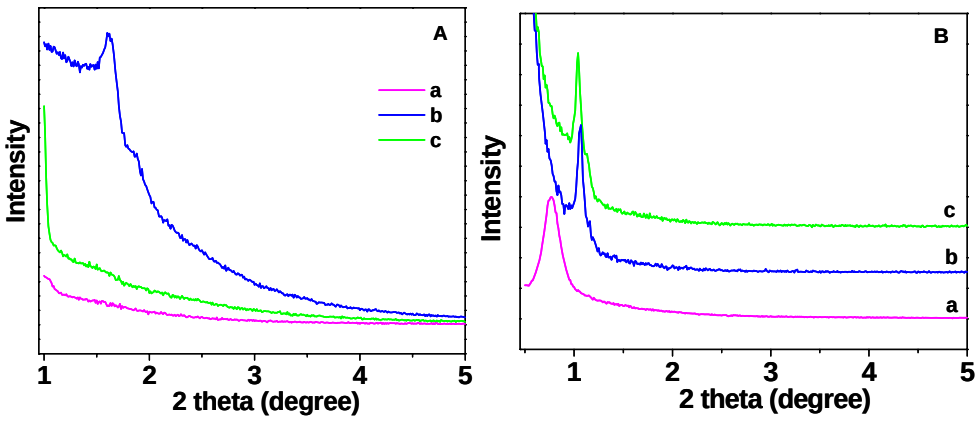

Figure 7.9. XRD patterns of the mesoporous carbon (A) and silica (B) samples obtained from the corresponding omposites with different contents of BTSE calcined at 900 °C in N_2 (B). In both (A) and (B), (a) MP-CS-0.22BTSE, (b) MP-CS-0.44 BTSE, and (c) MP-CS-0.55 BTSE.

Representative TEM images of the mesoporous carbon (MP-C-0.44BTSE) derived from the mother ocomposite MP-CS-0.44BTSE viewed from the [001] and [110] directions, respectively (Figure 7.10A, B), further confirm a 2D hexagonal *p6mm* mesostructure.

N_2 sorption isotherms were measured on the mesoporous carbon materials to evaluate their textural properties, as shown in Figure 7.11A. Mesoporous carbons exhibit similar type-IV isotherms with distinct capillary condensation steps occurring at relative pressures of 0.5 ~ 0.7, corresponding to narrow pore size distributions of mesopores at range of 2.5 ~ 5.3 nm. The pore sizes are close to those of their mother composites. These mesopores are, therefore, inherited from carbon-silica composites due to the degradation of triblock copolymer F127 and can retain comparative large values due to small contraction. Remarkably, a distinctly increased sorption in the isotherm curves at relative pressure of P/P_o of 0.1 ~ 0.3 is observed for mesoporous carbons (Figure 7.11B), suggesting smaller pores with a wide distribution near 2.5 nm (Figure 7.11B). The smaller pores are inside the pore walls caused by the removal of silicas from the carbon-silica composites. It implies that carbon and silica phases are separated and “homogeneously” distributed inside pore walls on nanoscale.

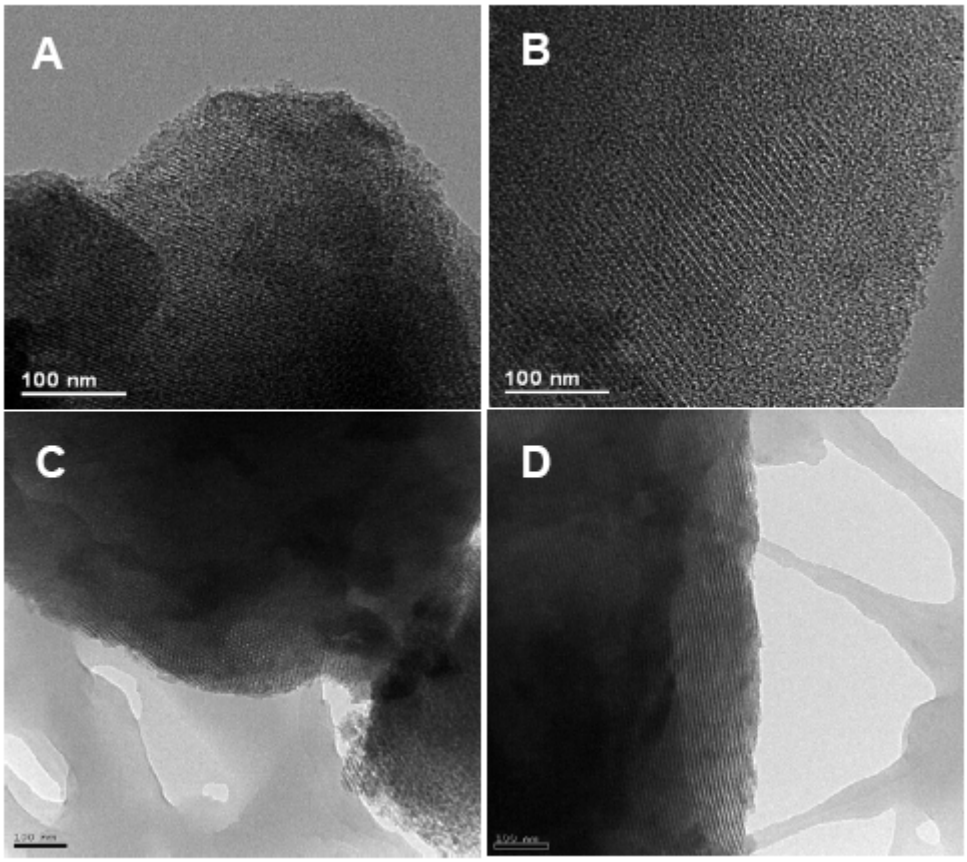

Figure 7.10. TEM images of the products from the MP-COS-0.44BTSE nanocomposite calcined at 900 °C in N_2: mesoporous carbon MP-C-0.44BTSE (A and B) and mesoporous silica MP-Si-0.44BTSE (C and D). The TEM images were recorded along the [001] (A and C) and [110] (B and D) directions.

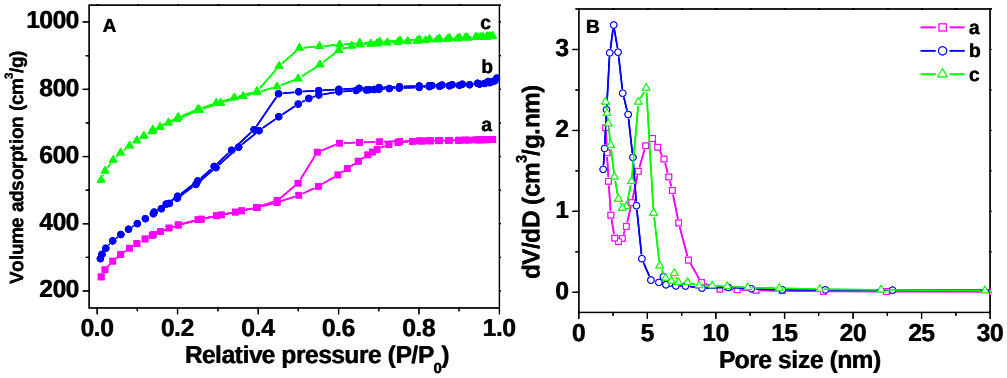

Figure 7.11. N_2 adsorption/desorption isotherms (A) and The pore-size distribution (B) of the mesoporous carbon from the carbon-silica composite: (a) MP-C-0.22BTSE, (b) MP-C-0.44BTSE, and (c) MP-C-0.55BTSE obtained after the removal of silica. The isotherms (A) of MP-C-0.44BTSE and MP-C-0.55BTSE composites are offset vertically by 100 and 300 cm^3/g, respectively.

The wide-angle XRD patterns (Figure 7.12) for all mesoporous carbon-silica composites show a broad amorphous silica peak at 2θ of about 23 °, together with a broad diffraction peak at ~ 43 °, corresponding to the 101 reflection of graphitic carbon materials. These results give evidence for amorphous carbon frameworks, which may be related to the carbon precursors of phenolic resins and the low calcination temperature [4, 18].

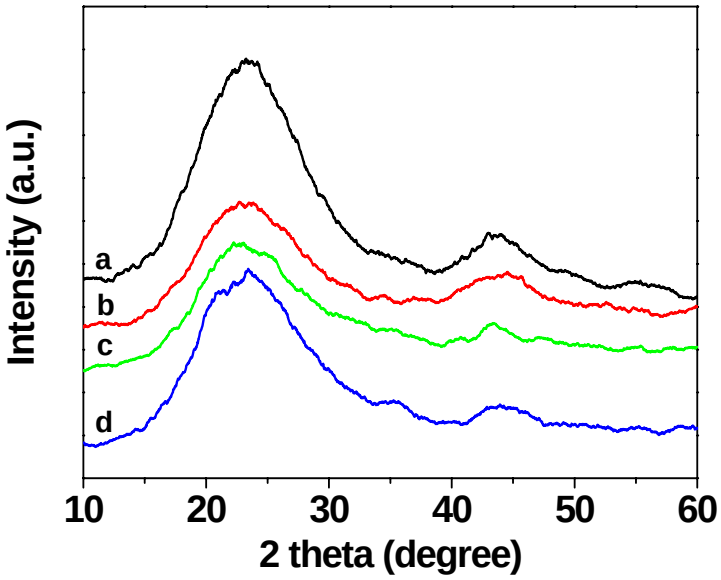

Figure 7.12. XRD patterns of mesoporous carbon-silica nanocomposites after calcination at 900 °C in N_2 of (a) MP-CS-0.22BTSE, (b) MP-CS-0.44BTSE, and (c) MP-CS-0.55BTSE, respectively.

7.3.2.2 Ordered mesoporous silica materials

Burning the carbon-silica composite MP-CS-0.44BTSE at 550 °C in air brings about the corresponding ordered mesoporous silica materials, as evidenced by characteristics of one sharp diffraction peak in the XRD pattern (Figure 7.9B(b)) and typical TEM images (Figure 7.10C, D) with 2D hexagonal *p6mm* symmetry. The unit cell parameters of the ordered mesoporous silicas is higher than that of the mesoporous carbons, and decreases a little as BTSE contents increase in their mother composites (Figure 7.9B and Table 7.1). Similarly, as BTSE content increases, only one diffraction peak can be detected for the mesoporous silica composites (Figure 7.9B). It is analogous to their mother carbon-silica nanocomposites (Table 7.1).

Type-IV N_2 sorption isotherms with capillary condensation steps at a relative pressure of 0.55 – 0.75 are observed for all mesoporous silica materials derived from the carbon-silica composites by simple combustion at 550 °C in air (Figure 7.13A),

suggesting a uniform pore size distribution. On comparison with their mother carbon-silica nanocomposites, the pore sizes calculated from adsorption branches for ordered mesoporous silicas are a little larger (Table 7.1). These mesoporous silica materials have BET specific surface areas and pore volumes ranging from 218 to 411 $m^2 \cdot g^{-1}$ and from 0.54 to 0.58 $cm^3 \cdot g^{-1}$ (Table 7.1), respectively, which are much lower than their mesoporous carbon counterparts. The low BET surface areas may be related to the preparation method. The removal of carbon in the carbon-silica composite was rigorous by calcination at 550 °C in air. It may eliminate the small pores in silica walls left by removal of carbons and condense silica frameworks [4].

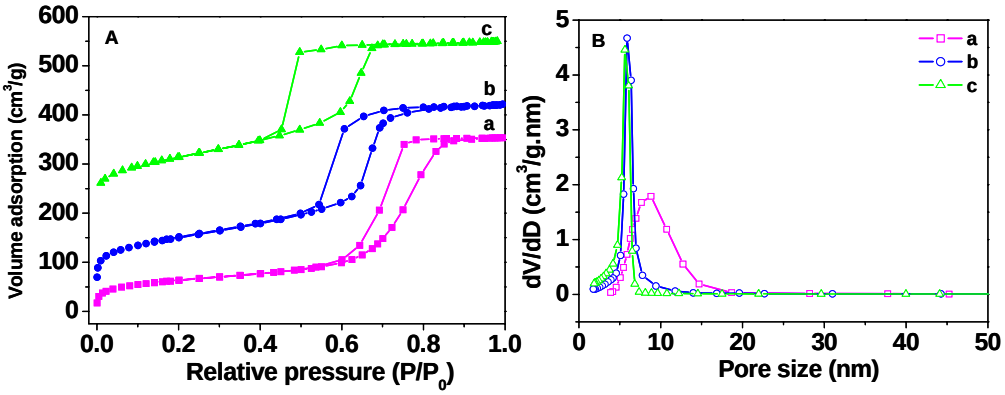

Figure 7.13. N_2 adsorption/desorption isotherms (A) and the pore-size distribution (B) of Mesoporous silica from carbon-silica composite: (a) MP-Si-0.22BTSE, (b) MP-Si-0.44BTSE, and (c) MP-Si-0.55BTSE obtained after the removal of carbon. The isotherm (c) of MP-Si-0.55BTSE composite is offset vertically by 200 $cm^3 \cdot g^{-1}$.

7.3.3 Adsorption of volatile benzene

All the benzene isotherms of the mesoporous polymer-organosilica composites prepared with different BTSE contents show similar curves, which are nearly type IV isotherms (Figure 7.14). A steep increase at low relative pressure (< 0.05), corresponding to micropore filling, is observed. After the micropores are partially saturated, it exhibits a sharp uptake at a relative pressure of 0.25 ~ 0.40 due to capillary condensation of benzene in the mesopores. The mesopores can gradually take up gas molecules with the increase of pressure, thus showing the gradual adsorption increase in the isotherms. This may be due to the silicate layers of the organosilicate frameworks are hydrophilic, while the polymer and ethylene groups inside the pore walls are hydrophobic in the polymer-organosilica composite. When the pressure is high, the interaction of benzene molecules with the ethylene- and

phenyl- bridging groups in the polymer-organosilica framework is dominant in the adsorption, which attributes to an increase of the adsorption.

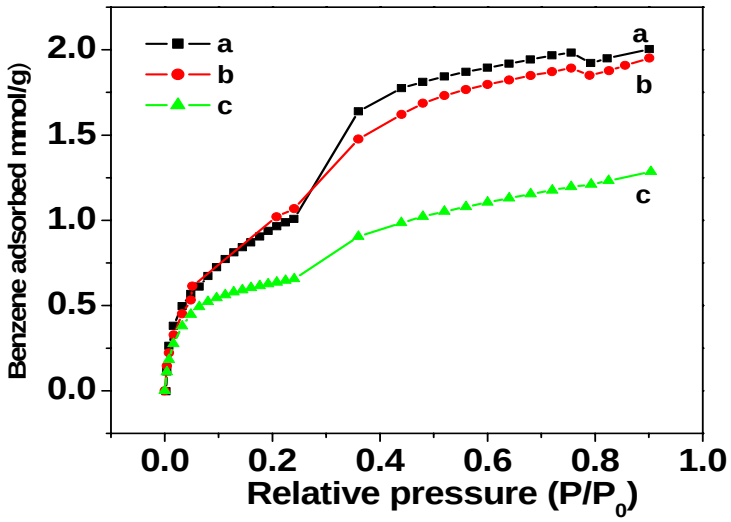

Figure 7.14. Adsorption isotherms of volatile benzene on the obtained polymer-organosilica composites (a) MP-COS-0.22BTSE, (b) MP-COS-0.44BTSE and (c) MP-COS-0.55BTSE at 25 °C.

The mesoporous MP-COS-0.22BTSE material exhibits a high adsorption capability of volatile benzene up to 2.0 mmol·g^{-1} at a high relative pressure ($P/P_0 \sim 0.90$), due to its large surface area. With the decrease of surface area, the adsorption capacity decreases. The mesoporous polymer-organosilica MP-COS-0.55BTSE composite shows the lowest benzene adsorption of 1.28 mmol·g^{-1}, suggesting that the capability is also related to BTSE content as well as the low surface area. As more BTSE introduced, the packing of ethylene- and phenyl- bridging groups in the polymer-organosilica framework tends to be denser and disordered, which does not favor interaction with benzene rings by the π-π stacking, resulting in a decrease of the amount of adsorption. It is found that there is a little fluctuation of adsorption curves at a high relative pressure for the MP-COS-0.22BTSE and MP-COS-0.44BTSE composites, which may arise from the equipment errors.

7.4 Conclusions

Ordered mesoporous polymer-organosilica and carbon-silica nanocomposites have been synthesized through a triconstituent co-assembly strategy using resols and prehydrolyzed BTSE as two organic precursors and triblock copolymer F127 as templates *via* the EISA approach. The resultant polymer-organosilica nanocomposites

show ordered 2D hexagonal mesostructures with uniform pore size (6.2 ~ 7.3 nm), suitable surface areas (619 ~ 794 $m^2 \cdot g^{-1}$) and pore volumes (0.61 ~ 0.88 $cm^3 \cdot g^{-1}$). With increasing BTSE content, the BET surface area and pore volume reduce for the polymer-organosilica composites. The mesoporous polymer-organosilica nano-composites have homogeneous interpenetrating frameworks, in which both polymer and organosilica synergistically support the ordered mesostructure. After burning out the carbon in the carbon-silica nanocomposites, resultant mesoporous silicas have ordered 2D hexagonal mesostructures. The presence of phenyl-bridging groups from resin polymer and ethylene groups in the framework endows these materials with the adsorption capacity of benzene up to 2.0 $mmol \cdot g^{-1}$, which suggests that they are a potential candidates for adsorption of organic compounds.

References

[1] T. Asefa, M. J. MacLachlan, N. Coombos, G.A. Ozin, "Periodic Mesoporous Organosilicas with Organic Groups inside the Channel Walls," *Nature* **1999**, *402*, 867-871.

[2] S. Inagaki, S. Guan, Y. Fukushima, T. Ohsuna, O. Teresaki, "Novel Mesoporous Materials with a Uniform Distribution of Organic Groups and Inorganic Oxide in Their Frameworks," *J. Am. Chem. Soc.* **1999**, *121*, 9611-9614.

[3] F. Hoffmann, M. Cornelius, J. Morell, M. Fröba, "Silica-Based Mesoporous Organic-Inorganic Hybrid Materials," *Angew. Chem. Int. Ed.* **2006**, *45*, 3216-3251.

[4] R. L. Liu, Y. F. Shi, Y. Wan, Y. Meng, F. Q. Zhang, D. Gu, Z. X. Chen, B. Tu, D. Y. Zhao, "Triconstituent Co-assembly to Ordered Mesostructured Polymer-Silica and Carbon-Silica Nanocomposites and Large-Pore Mesoporous Carbons with High Surface Areas," *J. Am. Chem. Soc.* **2006**, *128*, 11652-11662.

[5] Q. H. Yang, J. Liu, J. Yang, M. P. Kapoor, S. Inagaki, C. Li, "Synthesis, Characterization, and Catalytic Activity of Sulfonic Acid-Functionalized Periodic Mesoporous Organosilicas," *J. Catal.* **2004**, *228*, 265-272.

[6] S. Hamoudi, S. Royer, S. Kaliaguine, "Propyl- and Arene-Sulfonic Acid Functionalized Periodic Mesoporous Organosilicas," *Micropor. Mesopor. Mater.* **2004**, *71*, 17-25.

[7] Q. H. Yang, M. P. Kapoor, S. Inagaki, N. Shirokura, J. N. Kondo, K. Domen, "Catalytic Application of Sulfonic Acid Functionalized Mesoporous Benzene-Silica

with Crystal-Like Pore Wall Structure in Esterification," *J. Mol. Catal. A* **2005**, *230*, 85-89.

[8] K. Nakajima, I. Tomita, M. Hara, S. Hayashi, K. Domen, J. N. Kondo, "A Stable and Highly Active Hybrid Mesoporous Solid Acid Catalyst," *Adv. Mater.* **2005**, *17*, 1839-1842.

[9] Y. Wan, D. Q. Zhang, Y. P. Zhai, C. M. Feng, J. Chen, H. X. Li, "Periodic Mesoporous Organosilicas: A Type of Hybrid Support for Water-Mediated Reactions," *Chem. Asian J.* **2007**, *2*, 875-881.

[10] S. Dai, M. C. Burleigh, Y. H. Ju, H. J. Gao, J. S. Lin, S.J. Pennycook, C. E. Barnes, Z. L. Xue, "Hierarchically Imprinted Sorbents for the Separation of Metal Ions," *J. Am. Chem. Soc.* **2000**, *122*, 992-993.

[11] M. C. Burleigh, S. Dai, E. W. Hagaman, J. S. Lin, "Imprinted Polysilsesquioxanes for the Enhanced Recognition of Metal Ions," *Chem. Mater.* **2001**, *13*, 2537-2546.

[12] K. Z. Hossain, L. Mercier, "Intraframework Metal Ion Adsorption in Ligand-Functionalized Mesoporous Silica," *Adv. Mater.* **2002**, *14*, 1053-1056.

[13] L. X. Zhang, W. H. Zhang, J. L. Shi, Z. L. Hua, Y. S. Li, J. N. Yan, "A New Thioether Functionalized Organic-Inorganic Mesoporous Composite as a Highly Selective and Capacious Hg^{2+} Adsorbent," *Chem. Commun.* **2003**, 210-211.

[14] J. Liu, J. Yang, Q. H. Yang, G. Wang, Y. Li, "Hydrothermally Stable Thioether-Bridged Mesoporous Materials with Void Defects in the Pore Walls," *Adv. Funct. Mater.* **2005**, *15*, 1297-1302.

[15] V. Rebbin, R. Schmidt, M. Fröba, **"**Spherical Particles of Phenylene-Bridged Periodic Mesoporous Organosilica for High-Performance Liquid Chromatography," *Angew. Chem. Int. Ed.* **2006**, *45*, 5210-5214.

[16] J. B. Pang, V. T. John, D. A. Loy, Z. Z. Yang, Y. F. Lu, "Hierarchical Mesoporous Carbon/Silica Nanocomposites from Phenyl-Bridged Organosilane," *Adv. Mater.* **2005**, *17*, 704-707.

[17] Z. X. Yang, Y. X. Xia, R. Mokaya, "Periodic Mesoporous Organosilica Mesophases are Versatile Precursors for the Direct Preparation of Mesoporous Silica/Carbon Composites, Carbon and Silicon Carbide Materials," *J. Mater. Chem.* **2006**, *16*, 3417-3425.

[18] C. D. Liang, K. L. Hong, G. A. Guiochon, J. W. Mays, S. Dai, "Synthesis of a Large-Scale Highly Ordered Porous Carbon Film by Self-Assembly of Block Copolymers," *Angew. Chem. Int. Ed.* **2004**, *43*, 5785-5789.

[19] Y. Meng, D. Gu, F. Q. Zhang, Y. F. Shi, H. F. Yang, Z. Li, C. Z. Yu, B. Tu, D. Y. Zhao, "Ordered Mesoporous Polymers and Homologous Carbon Frameworks: Amphiphilic Surfactant Templating and Direct Transformation," *Angew. Chem. Int. Ed.* **2005**, *44*, 7053-7059.

[20] S. Tanaka, N. Nishiyama, Y. Egashira, K. Ueyama, "Synthesis of Ordered Mesoporous Carbons with Channel Structure from an Organic-Organic Nanocomposite," *Chem. Comm.* **2005**, 2125-2127.

[21] F. Q. Zhang, Y. Meng, D. Gu, Y. Yan, C. Z. Yu, B. Tu, D. Y. Zhao, "A Facile Aqueous Route to Synthesize Highly Ordered Mesoporous Polymers and Carbon Frameworks with *Ia*-3*d* Bicontinuous Cubic Structure," *J. Am. Chem. Soc.* **2005**, *127*, 13508-13509.

[22] Y. Meng, D. Gu, F. Q. Zhang, Y. F. Shi, L. Cheng, D. Feng, Z. X. Wu, Z. X. Chen, Y. Wan, A. Stein, D. Y. Zhao, "A Family of Highly Ordered Mesoporous Polymer Resin and Carbon Structures from Organic-Organic Self-Assembly," *Chem. Mater.* **2006**, *18*, 4447-4464.

[23] Y. Wei, D. L. Jin, C. C. Yang, G. Wei, "A Fast Convenient Method to Prepare Hybrid Sol-Gel Materials with Low Volume-Shrinkages," *J. Sol.-Gel Sci. Technol.* **1996**, *7*, 191-201.

[24] Y. Wei, D. L. Jin, C. C. Yang, M. C. Kels, K. Y. Qiu, "Organic-Inorganic Hybrid Materials: Relations of Thermal and Mechanical Properties with Structures," *Mater. Sci. Eng., C* **1998**, *6*, 91-98.

[25] R. K. Nagarale, G. S. Gohil, V. K. Shahi, R. Rangarajan, "Organic-Inorganic Hybrid Membrane: Thermally Stable Cation-Exchange Membrane Prepared by the Sol-Gel Method," *Macromolecules* **2004**, *37*, 10023-10030.

[26] M. Chen, S. X. Zhou, B. You, L. M. Wu, "A Novel Preparation Method of Raspberry-like PMMA/SiO_2 Hybrid Microspheres," *Macromolecules* **2005**, *38*, 6411-6417.

[27] M. Choi, F. Kleitz, D. N. Liu, H. Y. Lee, W. S. Ahn, R. Ryoo, "Controlled Polymerization in Mesoporous Silica toward the Design of Organic-Inorganic Composite Nanoporous Materials," *J. Am. Chem. Soc.* **2005**, *127*, 1924-1932.

[28] B. J. Scott, G. Wirnsberger, G. D. Stucky, "Mesoporous and Mesostructured Materials for Optical Applications," *Chem. Mater.* **2001**, *13*, 3140-3150.

[29] Y. P. Zhai, B. Tu, D. Y. Zhao, "Organosilane-Assisted Synthesis of Ordered Mesoporous Poly(furfuryl alcohol) Composites," *J. Mater. Chem.* **2009**, *19*, 131-140.

[30] Y. F. Lu, R. Ganguli, C. A. Drewien, M. T. Anderson, C. J. Brinker, W. L. Gong, Y. X. Guo, H. Soyez, B. Dunn, M. H. Huang, J. I. Zink, "Continuous Formation of Supported Cubic and Hexagonal Mesoporous Films by Sol-Gel Dip-Coating," *Nature* **1997**, *389*, 364-368.

[31] D. Y. Zhao, J. L. Feng, Q. S. Huo, N. Melosh, G. H. Fredrickson, B. F. Chmelka, G. D. Stucky, "Triblock Copolymer Syntheses of Mesoporous Silica with Periodic 50 to 300 Angstrom Pores," *Science* **1998**, *279*, 548-552.

[32] D. H. Chen, Z. Li, Y. Wan, X. J. Tu, Y. F. Shi, Z. X. Chen, W. Shen, C. Z. Yu, B. Tu, D. Y. Zhao, "Anionic Surfactant Induced Mesophase Transformation to Synthesize Highly Ordered Large-Pore Mesoporous Silica Structures," *J. Mater. Chem.* **2006**, *16*, 1511-1519.

[33] M. Park, S. S. Park, M. Selvaraj, D. Y. Zhao, C. S. Ha, "Hydrophobic Mesoporous Materials for Immobilization of Enzymes," *Micropor. Mesopor. Mater.* **2009**, *124*, 76-83.

[34] J. S. Beck, J. C. Vartuli, W. J. Roth, M. E. Leonowicz, C. T. Kresge, K. D. Schmitt, C. T. W. Chu, D. H. Olson, E. W. Sheppard, S. B. McCullen, J. B. Higgins, J. L. Schlenker, "A New Family of Mesoporous Molecular Sieves Prepared with Liquid Crystal Templates," *J. Am. Chem. Soc.* **1992**, *114*, 10834-10843.

[35] W. H. Zhang, X. N. Zhang, Z. L. Hua, P. Harish, F. Schroeder, S. Hermes, T. Cadenbach, J. L. Shi, R. A. Fischer, "Synthesis, Bifunctionalization, and Application of Isocyanurate-Based Periodic Mesoporous Organosilicas," *Chem. Mater.* **2007**, *19*, 2663-2670.

[36] M. F. G. Loustalot, S. Larroque, P. Grenier, "Phenolic Resins: 5. Solid-State Physicochemical Study of Resoles with Variable F/P Ratios," *Polymer* **1996**, *37*, 639-650.

[37] C. M. Yang, B. Zibrowius, W. Schmidt, F. Schüth, "Consecutive Generation of Mesopores and Micropores in SBA-15," *Chem. Mater.* **2003**, *15*, 3739-3741.

[38] D. H. Sun, R. Zhang, Z. M. Liu, Y. Huang, Y. Wang, J. He, B. X. Han, G. Y. Yang, "Polypropylene/Silica Nanocomposites Prepared by in-Situ Sol-Gel Reaction with the Aid of CO_2," *Macromolecules* **2005**, *38*, 5617-5624.

[39] M. Cornelius, F. Hoffmann, M. Fröba, "Periodic Mesoporous Organosilicas with a Bifunctional Conjugated Organic Unit and Crystal-like Pore Walls," *Chem. Mater.* **2005**, *17*, 6674-6678.
[40] K. A. Trick, T. E. Saliba, "Mechanisms of the Pyrolysis of Phenolic Resin in a Carbon/Phenolic Composite," *Carbon* **1995**, *33*, 1509-1515.
[41] J. Kim, J. Lee, T. Hyeon, "Direct Synthesis of Uniform Mesoporous Carbons from the Carbonization of As-Synthesized Silica/Triblock Copolymer Nanocomposites," *Carbon* **2004**, *42*, 2711-2719.

CHAPTER 8 Conclusions and Outlook

8.1 Conclusions

As stated in the research motivation above, one important scientific issue in this field is the control of the constitution and pore size for PMOs materials to improve the adsorption performance of these mesoporous materials. This research project therefore mainly consists of two parts, one is the synthesis and characterization of large-pore PMOs with functional organic groups, and another part is the testing and understanding of their performances on adsorption with different adsorbent. Therefore, the conclusions are centred on these two aspects.

(1) The large-pore (~ 9.9 nm) phenyl-bridged PMOs were facilely synthesized by evaporation-induced self-assembly of 1, 4-bis(triethoxysily)benzene and triblock copolymer Pluronic F127 as a template under acid conditions combined with a mixed-solvothermal treatment. N_2 adsorption/desorption isotherms reveal imperfect mesopore channels with high surface areas (up to 1150 $m^2 \cdot g^{-1}$) and thick pore walls (up to 7.7 nm). The mesopores can be expanded with the decrease of acidity, as well as the increase of F127 content. A mixed-solvothermal treatment in N, N-dimethylformamide (DMF) and water at 100 °C was first used to improve the periodicity of the mesopore walls, as well as increase the wall thickness. The composites exhibit efficient adsorption capacities (2.06 $mmol \cdot g^{-1}$) for benzene, suggesting a potential adsorbent for removal of volatile organic compounds.

(2) The well-ordered 2D hexagonal PMOs with high content of disulfide groups have been successfully prepared by a simple metal-ion assisted amphiphilic surfactant P123 templating process under a strong acid condition. The content of disulfide functional groups is up to 20 % (BTSPDS molar content in the initial silane mixture) incorporated into the framework. The obtained ordered mesoporous DS-PMO materials have relatively high BET surface area (~ 580 $m^2 \cdot g^{-1}$), large uniform pore size (up to 6.3 nm) and thick pore walls (thickness up to 7.1 nm), because of the long-chain disulfide bridges. The disulfide-bridged PMO materials exhibit excellent hydrothermal stability in boiling water for 5 days, probably due to the thick pore walls. Excellent adsorption efficiency (~ 716 $mg \cdot g^{-1}$) for Hg^{2+} ions is observed,

suggesting a potential application in removal of heavy metal ions in wastewater.

(3) The large-pore PMO hollow spheres with controllable pore size and high pore volume (2.5 $cm^3 \cdot g^{-1}$) were successfully synthesized at a low temperature (~ 15 °C) in the presence of inorganic salt (KCl). The PMO hollow spheres are uniform and well dispersed, and the composites have a large wall thickness. The pore size (9.8 ~ 15.1 nm) of the hollow spheres can be gradually expanded by increasing TMB content together with a relatively high acidity. By controlling the content of CTAB, successive structural transformation from hollow sphere to wormlike mesostructure and eventually to ordered body-centered cubic (*Im*3*m*) mesostructure is observed. The composites exhibit efficient adsorption capacity (703 $mg \cdot g^{-1}$) for toluene, suggesting they are a potentially useful adsorbent for removal of volatile organic compounds. The PMO hollow spheres also show superior encapsulation capacity (~ 585 $mg \cdot g^{-1}$) of bovine serum albumin (BSA) molecules over other porous materials.

(4) Ordered mesoporous polymer-organosilica and carbon-silica nanocomposites have been synthesized through a triconstituent co-assembly strategy using resols and prehydrolyzed BTSE as two organic precursors and triblock copolymer F127 as templates *via* the EISA approach. The resultant polymer-organosilica nanocomposites show ordered 2D hexagonal mesostructures with uniform pore size (6.2 ~ 7.3 nm), suitable surface areas (619 ~ 794 $m^2 \cdot g^{-1}$) and pore volumes (0.61 ~ 0.88 $cm^3 \cdot g^{-1}$). With increasing BTSE content, the BET surface area and pore volume reduce for the polymer-organosilica composites. The mesoporous polymer-organosilica nanocomposites have homogeneous interpenetrating frameworks, in which both polymer and organosilica synergistically support the ordered mesostructure. After burning out the carbon in the carbon-silica nanocomposites, resultant mesoporous silicas have ordered 2D mesostructures. The presence of phenyl-bridging groups from resin polymer and ethylene groups in the framework endows these materials with the adsorption capacity of benzene up to 2.0 $mmol \cdot g^{-1}$, which suggests that they are a potential candidates for adsorption of organic compounds.

8.2 Outlook

Since its first synthesis, PMO materials have attracted increasing research attention in materials science because these materials can organize a wide number of chemical units inside silica matrices with almost no limitation. The high loading rate and uniform dispersion of a broad spectrum of organic and organometallic groups in their frameworks endow PMO materials with unique advantages over pure mesoporous silica, thus new materials with potential applications in non-linear optics, chemical sensing, electro- and photocatalysis, chemical delivery, filtration, and chromatography may arise.

There are a few key areas that should be pursued in order to expand upon and enrich what we currently know about PMOs. A goal in the coming years will be to convert the acquired knowledge into technical applications.

From the point of syntheses, four aspects should be considered as follows:

(1) Expanding the synthetic approach to elemental compositions beyond organosilicas, for example, semiconductiong mesoporous organotin sulfides could arise from the condensation of $(EtO)_3Sn\text{-}R\text{-}Sn(OEt)_3$ precursors with sulfide-based reagents.

(2) The pore size effects on the adsorption should be investigated for PMOs with different functional groups, which will provide more information about the possibility of large molecule adsorption.

(3) Morphology control of PMOs as fibers, films, spheres, monoliths and patterns.

(4) Measuring the mechanical and physical properties of the PMOs as a function of their organic components. Further investigations of the reactivity, chemistry, thermal stability, and transformations of PMO materials.

From the point of applications, six aspects should be considered as follows:

(1) One of the interesting characteristics of PMOs is that their polarity, that is, their hydrophobicity or hydrophilicity, can be tuned within a certain range by the choice of the organic component, and hence their ability to adsorb other materials can at least be partly controlled. The adsorption systems and conditions should be considered according to the functional groups of obtained PMOs materials. As the phenyl-bridged PMOs materials exhibit

hydrophobic properties, the simulation test may be conducted in atmosphere or water, which is an important real system.

(2) It is possible to use chiral organic bridges. Thus, it is conceivable that new materials based on PMOs for enantioselective chromatography and new catalysts for heterogeneous catalysis will be developed.

(3) The formation of PMOs with molecular periodicity in their walls advances the development of molecular nanotechnology and nanoscience. Pioneering research in controlling molecular self-organization would allow the use of nanostructured materials in diverse applications and nanodevices.

(4) If host-guest interactions based on organically functionalized mesoporous silica phases are considered, the possibility arises to construct anisotropic systems with interesting properties, especially with PMOs-their ability to adsorb host-guest species that impart interesting properties should be exploited: If organic bridges with a permanent dipole are used and care taken that they are anchored within the pore walls with uniform orientation, they could be the basis of quite novel materials with NLO properties. In a broad sense, the functionalized PMOs are promising candidates as molecular switchable porous materials and optical-electro transformers.

(5) Particularly promising is the work of drug delivery systems that react to an external stimulus by releasing an active compound (stimulus-response behavior).

(6) Investigation on the adsorption mechanism of PMOs materials with functional groups could be considered so as to finely control the preparation of these materials which in turn would give controlled adsorption capacity. The mechanisms could be used to instruct the preparation of adsorbents. That may be why even the same materials from different sources do not give even similar adsorption performance. And it could be useful to understand the relationship between structure, function and application.

Certainly, research on PMOs is still in its early stages. In view of the interdisciplinary nature of the topics, the growing number of research groups involved, and the diversity of the building blocks deployed, it is difficult to predict which expansions of this field must be reckoned with. A fundamental question that regards to PMOs, it must not be forgotten that the synthesis of the precursors and SDAs is laborious and costly, in particular on an industrial scale.

These are just a few of many topics that could play a role in the future. Finally, various challenges still remain; however, we look ahead with excitement on the further development of this field of research and will endeavor to make a contribution to this development.

List of Publications

Referred Journal Articles:

1. **Na Hao**, Yunxia Yang, Huanting Wang, Paul A. Webley, Dongyuan Zhao, "Synthesis of Large-Pore Phenyl-Bridged Mesoporous Organosilica with Thick Walls by Evaporation-Induced Self-Assembly for Efficient Benzene Adsorption," *J. Colloid Interface Sci.* **2010**, *346*, 429-435.

2. **Na Hao**, Lu Han, Yunxia Yang, Huanting Wang, Paul A. Webley, Dongyuan Zhao, "A Metal-Ion-Assisted Assembly Approach to Synthesize Disulfide-Bridged Periodical Mesoporous Organosilicas with High Sulfide Contents and Efficient Adsorption," *Appl. Surf. Sci.* **2010**, *256*, 5334-5342.

3. **Na Hao**, Huanting Wang, Paul A. Webley, Dongyuan Zhao, "Synthesis of Uniform Periodic Mesoporous Organosilica Hollow Spheres with Large-Pore Size and Efficient Encapsulation Capacity for Toluene and the Large Biomolecule Bovine Serum Albumin," *Micropor. Mesopor. Mater.* **2010**, *132*, 543-551.

4. **Na Hao**, Zhangxiong Wu, Paul A. Webley, Dongyuan Zhao, "Synthesis of Ordered Mesostructured Polymer-Organosilica by the Triconstituent Co-Assembly Method," *Mater. Lett.* **2011,** *65*, 624-627.

5. Haifeng Bao, **Na Hao**, Yunxia Yang, Dongyuan Zhao, "Biosynthesis of Biocompatible Cadmium Telluride Quantum Dots Using Yeast Cells," *Nano Research*, **2010**, *3*, 481-489.

6. Zhangxiong Wu, **Na Hao**, Gongkui Xiao, Liying Liu, Paul A. Webley, Dongyuan Zhao, "One-pot Generation of Mesoporous Carbon Supported Nanocrystalline Calcium Oxides Capable of Efficient CO_2 Capture at a Wide Range of Temperatures," *Phys. Chem. Chem. Phys.*, **2011,** *13*, 2495-2503.

7. Winston Duo Wu, Ria Amelia, **Na Hao**, Cordelia Selomulya, Yu-Lung Chiu, Dongyuan Zhao, Xiaodong Chen, "Assembly of Uniform Photoluminecent

Microcomposites Using a Novel Micro-Fluidic-Jet-Spray-Dryer," *AIChE J.,* **2010**. DOI: 10.1002/aic.12489.

8. Xinyi Zhang, Wei Lu, Jiyan Dai, Laure Bourgeois, **Na Hao**, Huanting Wang, Dongyuan Zhao, Paul A. Webley, "Ordered Hierarchical Porous Platinum Membranes with Tailored Mesostructures," *Angew. Chem. Int. Ed.* **2010**, *49*, 10101-10105.

9. Xufeng Zhou, Shizhang Qiao, **Na Hao**, Xinglong Wang, Chengzhong Yu, Lianzhou Wang, Dongyuan Zhao, Gao Qing Lu, "Low Temperature Synthesis of Ordered Cubic Periodic Mesoporous Organosilicas with Ultra Large Pores," *Chem. Mater.*, **2007**, *19*, 1870-1876.

10. Ying Wan, Dieqing Zhang, **Na Hao**, Dongyuan Zhao, "Organic Groups Functionalized Mesoporous Silicates," *Int. J. Nanotechnology,* **2006***, 4*, 66-99.

11. Dan Li, Jianfeng Yao, Huanting Wang, **Na Hao**, Dongyuan Zhao, Kyle R. Ratinac, Simon P. Ringer, "Organic-Functionalized Sodalite Nanocrystals and Their Dispersion in Solvents," *Micropor. Mesopor. Mater.* **2007**, *106*, 262-267.

Conference paper:

1. Winston Duo Wu, Sean Xu Qi Lin, Cordelia Selomulya, **Na Hao**, Xiao Dong Chen, "In Vitro Release of Vitamin B12 from Uniform Non-agglomerated Silica Microparticles Produced by a Novel Micro-Fluidic-Jet Spray dryer," *The Proceedings of the 4th Nordic Drying Conference*, Reykjavik, Iceland, Oral Presentation, **2009**.

ADDENDUM

p 5 line 23: Insert “One cartoon illustration of the different porous structures”:

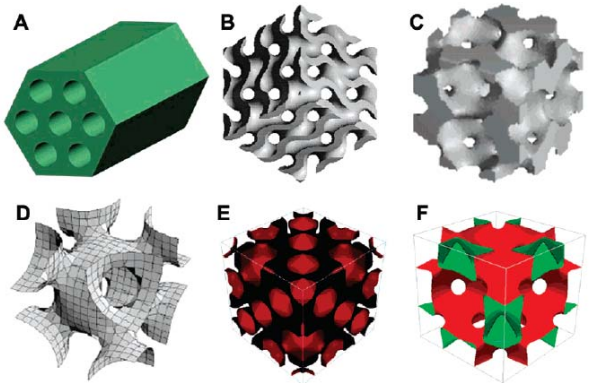

Figure 1.2. Pore models of mesostructures with symmetries of (A) *p*6*mm*, (B) *Ia*3*d*, (C) *Pm*3*n*, (D) *Im*3*m*, (E) *Fd*3*m*, and (F) *Fm*3*m*, as ref [17, 38, 42, 60, 61, 70, 76].

p 43 and p 44: Add “The detailed sample preparation procedures for SAXS, XRD and NMR” at the end of line 23 and line 24, respectively:

“Prior to the experiments, the samples were grinded to fine powder, and placed into a holder. Care must be taken to create a flat upper surface”.

“Before NMR measurements, the ground powder sample was put into a rotor”.

p 54 Figure 4.1D: “theat” for “theta”.

p 55: Add “the methods for calculating the structure parameters, such as d_{100}, a_0, and V_{micro}” as footnotes at the end of Table 4.1:

d_{100}: the interplanar spacing, was calculated by the formula of $2d\sin\theta = \lambda$ (λ = 0.15418 nm).

a_0: the unit cell parameter, was determined from the interplanar spacing of the (100) plane using the formula of $a_0 = 2\, d_{100}/\sqrt{3}$.

V_{micro}: the micropore volume, was calculated by *t*-plot method using experimental points at relative pressure of P/P_0 = 0.10 - 0.20.

p 57, Figure 4.3, p 97 Figure 6.4, p 106 Figure 6.11: The figure captions with units blocked are corrected without blockage.

p 58 line 24 ~ 26: Add “However, the surface area and pore volume nearly follow the decreasing tendency with lowering F127 content.”

p 60 Figure 4.6: Cause of “the oddity for Ph-PMO-0.3-0.2 composite” in TGA:

Firstly, this oddity is due to the acid concentration. It is related to a fast condensation and cross-linking of silicates. The phenyl-bridging organosilica has a faster rate of condensation at higher acid concentration, and accelerate cross-linking of silicates, which could lead to the more phenyl groups incorporated into the framework.

Secondly, the stability of mesoporous materials depends on their inherent wall properties. The oddity of Ph-PMO-0.3-0.2 composite could be attributed to the thick pore walls and the hydrophobic surface of the framework.

p 61 para 3: Comment on “the benefit of the mixed-solvothermal treatment”: In our case, the water-DMF mixed-solvothermal treatment may provide a proper micro-environment to improve the structural arrangement of organic-inorganic composites.

Comment on “the improved molecular periodicity”: In the point of phenyl-bridged PMOs, the molecular periodicity is important to be mentioned. The molecular periodicity in the pore walls could enhance the functionalities of PMOs in electronic, optical, and sensors.

p 61 para 3: Comparison of “benzene adsorption capacity of Ph-PMO with other available VOC adsorbing materials”:

As reference “*Res. Chem. Intermed.*, **2008**, *34*, 743-753.” reported, the benzene adsorption amount at 30 °C for SBA-15 was ~ 0.13 mmol·g^{-1}, titanium addition into SBA-15 resulted in the enhancement of benzene adsorption capacity, up to ~ 0.19 mmol·g^{-1}; As reference “*Energy & Fuels*, **1998**, *12*, 1051-1054.” stated, the adsorption capacity of benzene on MCM-41 was ~ 2.5 mmol·g-1 at P/P_0 = 0.10 and 22 °C.

So based on the above mentions, the phenyl-bridged PMO materials with the adsorption capacity of benzene up to 2.06 mmol·g^{-1} could be a potential candidate for adsorption of organic compounds.

p 63: Comment on “the difference of using benzene and N_2 as the probe molecules to investigate the adsorption properties of the Ph-PMO samples”: (1) the molecular size of benzene and N_2 is different. (2) the characterization temperature for adsorption capacity is different, with using benzene performed at 298 K (25 °C) and N_2 tested at 77 K. (3) The N_2 sorption isotherms exhibit typical type IV curves with a sharp capillary condensation step at a relative pressure range of 0.6 ~ 0.8, while the benzene isotherms show nearly type IV curves with a steep increase at a low relative pressure (< 0.04) and a sharp uptake at a relative pressure of 0.24 ~ 0.36 due to capillary condensation of benzene molecules in the mesopores. At high relative pressure, as benzene molecules have interaction with the phenyl-bridging groups, so an increase of the adsorption occurs, on the contrary, N_2 molecules have no interaction as that of benzene, so it exhibits even lines at a high relative pressure.

p 72 para 2: Comment: The content of S (%) in the mesoporous framework here means the molar ratio of thioether organic groups to TEOS, so the content of S (%) has no unit, and it was already mentioned in line 18 on page 72.

p 74: Comment: In our case, the upper limit of the amount of disulfide incorporated for ordered mesostructures is about 20 %, and disordered disulfide-bridged PMO materials structures (Figure attached below) containing nearly 25 % BTSPDS could be obtained by this metal-ion assisted method.

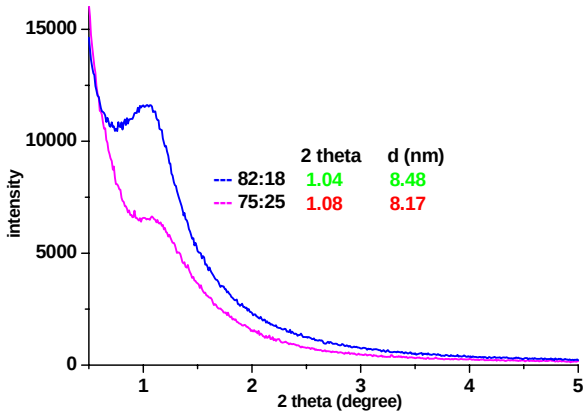

p 79 line 9: "4.0 ~ 8.7 wt %" for "1.25 ~ 3.37 mmol·g^{-1}" which is consistent with that in Table 5.2 on p 79.

p 80: Reason for "DS-PMO-20 not included in the stability study": In this chapter, the main target is to increase the content of disulfide organic groups in the framework as well as keep the ordered mesostructures. The XRD results showed that up to 20 % of organic groups could be introduced by metal-ion assistant method. That was the key point of this chapter. So not all the samples, three of four were selected for the stability study, which could have a general idea of the stability of the disulfide-bridged PMO materials.

p 84: Comment on "comparison of different porous materials for Hg^{2+} adsorbing": As listed in Table 5.2, the DS-PMO materials exhibit a high adsorption capability of heavy metal Hg^{2+} ions up to 716 mg·g^{-1}, compared with other mesoporous materials listed in reference [45-47].

Comment on "the advantage of the ordered porous structure in terms of adsorption": In the case of disulfide-bridged PMOs with long alkyl chains, with more organic groups introduced into the framework, the ordered porous structure could provide more space or extra binding sites for the adsorbates. On the contrary, the disordered or wormlike pores could be blocked, which is not benefit for the adsorption of large guest molecules. Therefore, it is important to develop the new pathway to synthesize ordered porous mesostructure with long-chain organic groups.

p 93: Comment on "characterization of the dispersity of the hollow spheres": Dispersity means the state or the degree of materials' dispersion, which could be characterised by TEM technique. And one should measure the particle size distribution by DLS (dynamic light scattering) technique, and compare the results with TEM images.

p 95, line 1: "Figure 6.11e and f" for "Figure 6.1 e and f".

p 103: Comment on "the existence of 'windows' around the hollow spheres": The speculation on the existence of "windows" around the hollow spheres was based on three references [20], [21], [24] in Chapter 6, although not many data were provided to confirm the existence of "window" on the shell of the hollow spheres. Such "windows" could also be called "smaller mesopores or micrpores" or "secondary pores" of the hollow spheres, which can be confirmed sufficiently by N_2 adsorption-desorption, TEM, HRTEM, ^{129}Xe NMR, adsorption of guest molecules with different molecular sizes on hollow spheres.

p 106: Comment on "the BSA adsorption, how can we tell the proteins are not just adsorbed on the outer surface of the hollow spheres": Currently, it is not confirmed that the guest molecules have been loaded in the hollow cores or only in the pore channels. The adsorption capacity on PMO hollow spheres is determined by several factors, such as pore volume, surface area, the solution pH and electrostatic interaction between PMO surface and guest molecules. In our work, some primary adsorption results of PMO hollow spheres were presented, and the detailed research should be done in future.

p 126: Comment on "the VOC adsorption capacity of the mesoporous carbon materials": As reference "*Adsorption*, **2009**, *15*, 123-132." reported, the adsorption capacity of xylene isomers on FDU-15-900 carbon is up to 2.40 mmol·g^{-1} at 25 °C. The carbon adsorbent has a non polar surface and the polarity of the adsorbate may play an important role for such high adsorption capacity. In our study, the samples MP-C-0.22BTSE and MP-C-0.44BTSE have much higher surface area compared to that of FDU-15-900 carbon composite. It is a very interesting. So the further study for the adsorption comparison of the mesoporous carbon materials would be done in future.